Phosphate Based Glass in Developing Anti-Scale Devices with Antimicrobial Properties

A thesis submitted to the University College London in fulfilment of the requirements for the Degree

Doctor of Philosophy by

Song Yi Baek

University College London

2021

UCL Eastman Dental Institute

Biomaterials and Tissue Engineering Research Division

University College London

Declaration

I, Song Yi Baek confirm that the work presented in this thesis is my own. Where information has been derived from other sources, I confirm that this has been indicated in the thesis.

Signature: Date: 31st December 2021

Acknowledgements

First, I would like to thank my primary supervisor Professor Jonathan Knowles, for his encouragement and support throughout this PhD, without his guidance it would not have been possible. I would also like to thank my secondary supervisor Professor Anne Young for her support.

I would also like to show my appreciation to everyone at UCL, Eastman Dental Institute, Dr Graham Palmer, Dr George Georgiou and Dr Nicola Mordan for their training and technical guidance and would also like to extend my gratitude at friends at UCL, Chemistry Department especially Dr Sanjayan Sathasivam for his technical assistance and Professor Clare Carmalt and Professor Ivan Parkin for their help also.

Special thanks to Dr Nazanin Owji, Dr Mayda Arshad, Dr Alaa Aldaadaa, Zalike Keskin and to all present and past friends at Eastman Dental Institute BTE group who made the research and time so fun and academically productive.

I would also like to thank Dr Patricia Silva and everyone at Dyson Ltd. and EPSRC for the funding of the thesis.

To my parents, Eui Sung Baek and Kyung Ae Lee whom I am grateful for their support with prayers and patience, and my brother Seung Hyun Baek whom he knows well our journey was not so easy.

Finally, I would like to praise and thank God, Jesus Christ for the wisdom and strength and determination to pursue this PhD.

Abstract

Previous study allowed us to focus on the most effective anti scaling glass composition of $50P_2O_5 \cdot 10Na_2O \cdot 40CaO$ (mol%) showing the best anti scaling property with the controlled release of the desired $P_3O_9^{3-}$ and $P_3O_{10}^{5-}$ phosphates. Achieving anti scaling properties with an increase of more than 1000% in humidifier running time using hard water (*ca*. 320 ppm), previously broken due to scale formation within 2 months.

Primary studies carried out was glass dissolution, where tap and deionized water was used to observe dissolution and ion release in water with presence and absence of ions. Followed by dynamic and static tests to understand how the flow of liquid will effect dissolution and ion release. Extreme temperature and humidity experiments were carried out to test the glass' durability trying to understand how the condition in which the glasses are kept will affect its overall performance. Glass and its following results were characterized with thermal gravitational analysis (TGA), differential thermal analysis (DTA), scanning electron microscopy (SEM), energy dispersive x-ray (EDX), x-ray photoelectron spectroscopy (XPS) and ^{31}P nuclear magnetic resonance (NMR) with dissolution properties analysed using ion chromatography, inductively coupled plasma-optical emission spectroscopy (ICP-OES).

The glass chosen by this thesis showed great durability in extreme temperatures and humidity. Finally, extending on its controlled ion release and anti scaling property; the addition of copper showed antimicrobial property with $50P_2O_5 \cdot 10Na_2O \cdot 20CaO \cdot 20CuO$ (mol%) showing best performance. Addition of copper decreased $P_3O_9^{3-}$ and increased $P_3O_{10}^{5-}$ phosphate release showing

change in glass bulk structure with addition of Cu^{2+}, making the glass more ideal as it allows for the glass not to excessively release phosphates whilst achieving antimicrobial property. The glass was also pulled into fibres with its possible application into cooperation into filters also showing excellent antimicrobial property.

In conclusion, the glasses studied exhibited steady release of anti scaling phosphates in all conditions making it an excellent candidate for industrial uses in all hard water environments with effective antibacterial and antiviral property.

Impact Statement

This thesis outlines the details of ternary and quaternary phosphate glass exposed in different wet and humid environments for its controlled ion release applications. Its uses ranges from scale inhibition by the release of phosphates in hard water environments to antimicrobial application with release of copper ions in environments prone to bacteria and viruses.

There is great potential for its use in both academia and in industry, hence its support from Dyson Ltd. In light of the recent COVID 19 it shows its potential use in antimicrobial use as glass discs as well as its possible use in filters for air and water. Benefiting not only academic research but to general public health.

Table of Content

Table of Contents

List of Tables

List of Figures

Publications

1. Z. Lim, D. G. Smith, J. Kolanowski, R. L. Mattison, J. C. Knowles, S. Y. Baek, W. Chrzanowski and E. J. New. A reversible fluorescent probe for monitoring Ag(I) ions. *Journal of The Royal Society Interface*. 15(144). 2018

2. M. J. Powell, B. A. D. Williamson, S. Y. Baek, J. Manzi, D. B. Potter, D. O. Scanlon and C. J. Carmalt. Phosphorous Doped SnO_2 Thin Films for Transparent Conducting Oxide Applications: Synthesis, Optoelectronic properties and Computational Models. *Chemical Sciences*. 9(41). 2018

3. E. A. About Neel, A. Kiani, S. P. Valappil, N. Mordan, S. Y. Baek, K. M. Z. Hossain, R. Felfel, I. Ahmed, K. Divakarl, W. Chrzanowski and J. C. Knowles. Glass microparticle-verses microsphere-filled experimental dental adhesives. *Journal of Applied Polymer Science*, 136(2), 2019

4. D. Carta, F. Foroutan, J. McGuire, P. Gupta, A. Nikolaou, B. Kyffin, N. L. Kelly, J. V, Hanna and J. Gutierrez. Antibacterial Copper-Doped Calcium Phosphate Glasses for Bone Tissue Regeneration. *ACS biomaterials Science and Engineering*. 2019

Chapter 1

Introduction

1 Chapter 1

1.1 Problem Statement

Hard water is well known to cause domestic, economic, and environmental issues. Occurring naturally as rain and water passes through limestone and chalk. When the levels of calcium carbonate in water is above *ca.*200 ppm, that water is considered hard. The presence of ions such as calcium and magnesium in large amounts cause deposits of its oxides in appliances causing overheating, mechanical failure and corrosion.

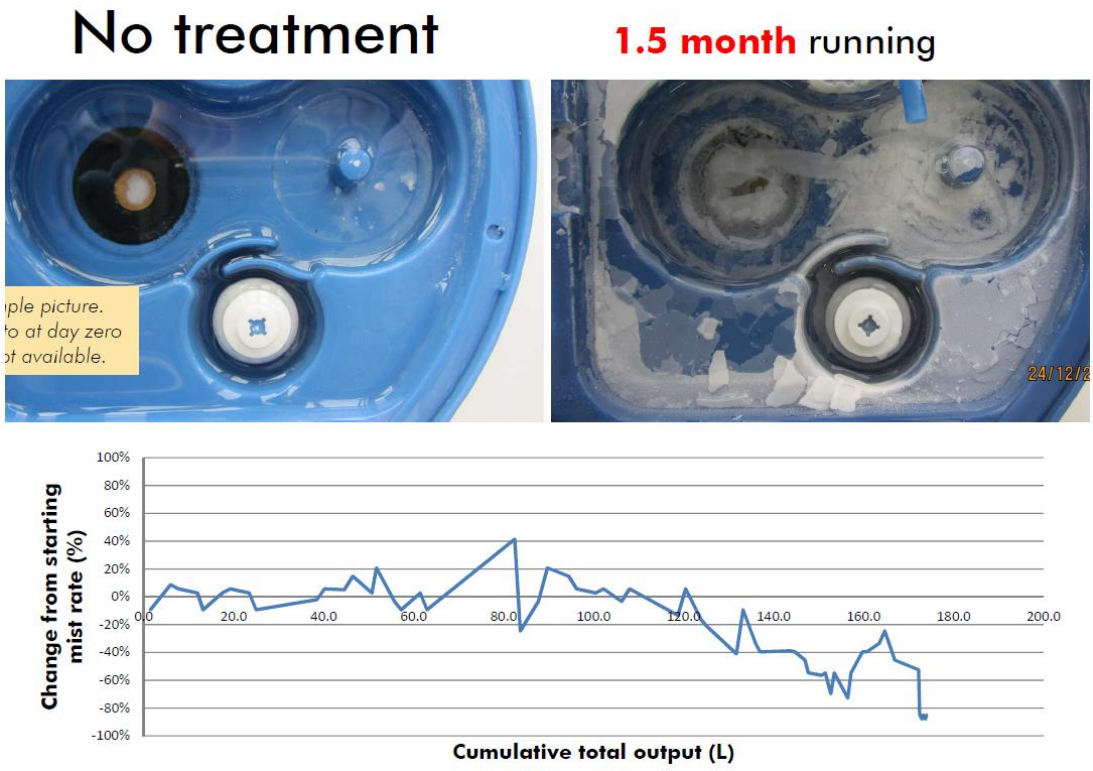

Figure 1. Image of a Honeywell Humidifier breaking down due to calcite build up after 1.5 months of continual usage, no treatment used. Data provided by Dyson Ltd.

Figure 1 shows the build-up of solid white precipitates or scale in an ultrasonic mist generating humidifiers using tap water. Within a period of 1.5 months the percentage change in mist rate decreased to as low as -90% until the appliance stopped working as the cumulative total output reached 180 litres. The solid precipitates eventually caused the humidifiers to stop working requiring manual removal of the solids. This is only one example of the common problems hard water. Apart from physical blockage, more domestically, deposits of scale on heating elements in appliances such as boilers acts as an insulator decreasing the efficiency of heat transfer, causing overheating and failure.[1,2]

The glass developed by previous and this research at UCL showed significant scale inhibition as seen in Figure 2. The use of P50Ca40Na10 glass composition allowed the humidifier to run with the same tap water for more than 22 months with only *ca.* -40% decrease in mist rate with more than 1800 litres of tap water. This increase of more than 1000% of operating time of the humidifier and the clear visible decrease in scale formation shows that our glass is highly effective and has extensive research values on its possible scale inhibiting material.

Chemical and physical methods are available to treat hard water, but current methods involve large instalments, regular replacement of filters and overall, not effective nor efficient to use in common everyday appliances.

This thesis has concentrated on glass dissolution property of this specific composition of glass and how humidity and different wet environment will have an impact on its dissolution and physical property, ultimately understanding its

durability and effectiveness in all exposed conditions. This research also extends its understanding into copper doped ternary phosphate glass for possible antimicrobial effect.

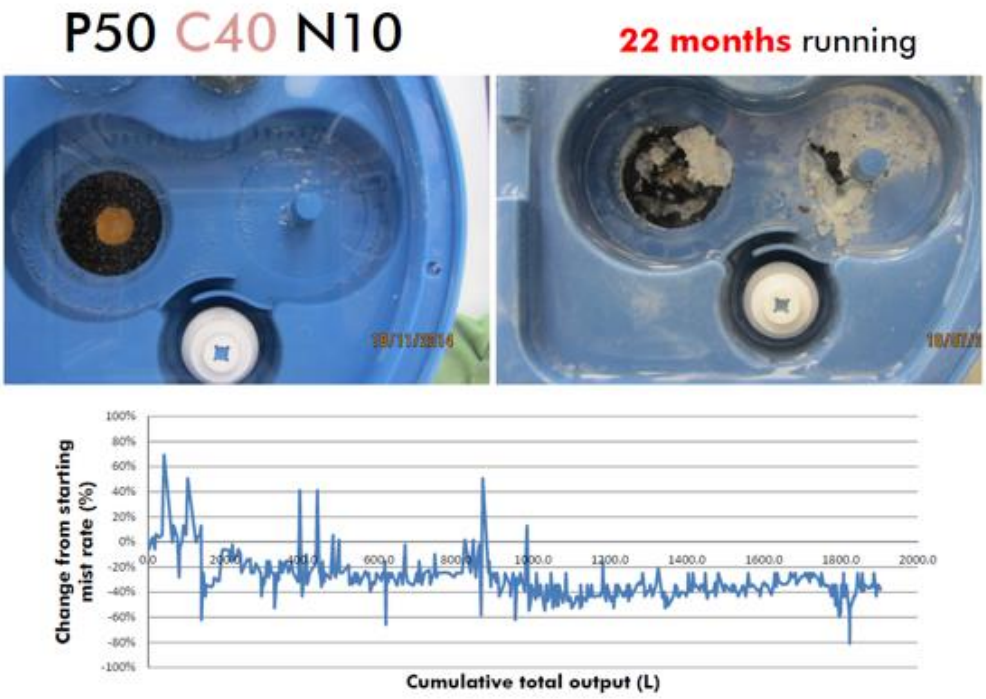

Figure 2. Image of Honeywell Humidifier before and after 22 months continual usage with phosphate glass used provided by this research. Data provided by Dyson Ltd.

1.2 Introduction

1.2.1 Introduction to glass

Glass has many definitions such as an amorphous non-crystalline material, a solid material obtained by quenching a liquid and a material showing glass transition nature when heated back to its liquid state. A material appearing to be a solid but over a long time continuously relaxes towards a liquid state. Glass occurs naturally in various forms: volcanic magma known as obsidian, from meteorite impact known as impactite, from lightening striking sand known as fulgurites and so on.[3] Glass has been used by mankind for centuries and its synthesis can even be dated back to Mesopotamia, approximately 4000 BC.[4] It would be very difficult to imagine the lives we live today without glass, it takes part in everyday life from the windows we see thorough to the transparent conducting oxides we have on our phone screens to the bioactive glass for enamel reconstruction on our teeth. This inert and tuneable properties of glass make it such an ideal material to use. With so much research into silicon-based glass allows us to endeavour into phosphate-based glass a whole different branch of glass.

1.2.2 Different glass compositions

Although almost any compound when cooled fast enough can form glassy state only the following four oxides are considered able to form glass on its own: B_2O_3, SiO_2, P_2O_5 and GeO_2 known as “glass-formers”.[5] These oxides provide the backbone to form numerous combinations of glass. Glass formed from two oxides are known as binary systems and with three oxides a ternary

and with four oxides a quaternary system. The coordination number of boron, silicon and phosphorous are 4 with boron often forming 3.

Amorphous non-crystalline glass has three main components: 1. Network forming oxides; SiO_2, P_2O_5 and B_2O_3. These are the primary oxides which are mainly found in group 4 and 5 of the periodic table. However other oxides can act as network forming oxides: GeO_2, Bi_2O_3, As_2O_3, Sb_2O_3, TeO_2, Al_2O_3, Ga_2O_3 and V_2O_5. 2. Network modifying oxides: all oxides given in 1 and 3 can act as modifying oxides. 3. Intermediate oxides: (Al, Ga, Ti, C, V, Bi, Mo, W, S, Se, Te). Depending on the network forming oxides we obtain silicate based or phosphate-based glasses.

Soda-lime glass has compositions of 70-75 wt% SiO_2, 12-16 wt% of Na_2O and 10-15 wt% of CaO and counts for more than 90% of the glass manufactured. Commonly used for windows and glass jars and bottles, they are inexpensive and can be reused numerous times. Composed of mainly SiO_4 tetrahedral structure connected via oxygen atoms (Figure 3) they have very strong chemical bonds, making them durable. In soda-lime silica glass, the glass network is disrupted by the addition of soda, or sodium carbonate (Na_2CO_3) and lime, calcium oxide (CaO). Since pure silica glass softens around 1200 °C the addition of soda forms a lower energy ionic bond, Na_2O as the sodium donates an electron to the oxygen. The oxygen then binds to the silicon hence preventing the formation of silicon bridges, reducing the melting point to a more workable 700 °C.[6] However, the addition of sodium makes the glass more soluble, where the lime is added to make the glass more durable, giving the soda-lime glass structure as seen in Figure 4. Therefore, increase in

sodium or group 1 alkali metal content reduces the melting point and increases the viscosity in these glasses.

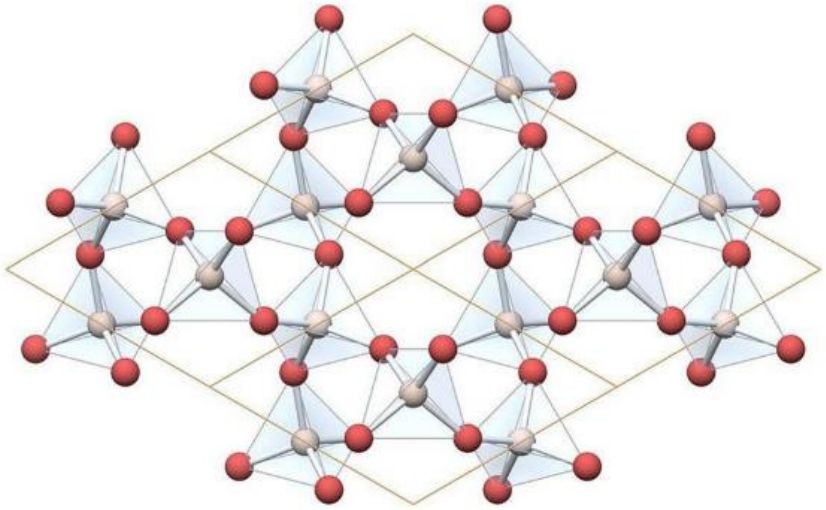

Figure 3. Adjacent SiO4 tetrahedral-type unit cell. [7]

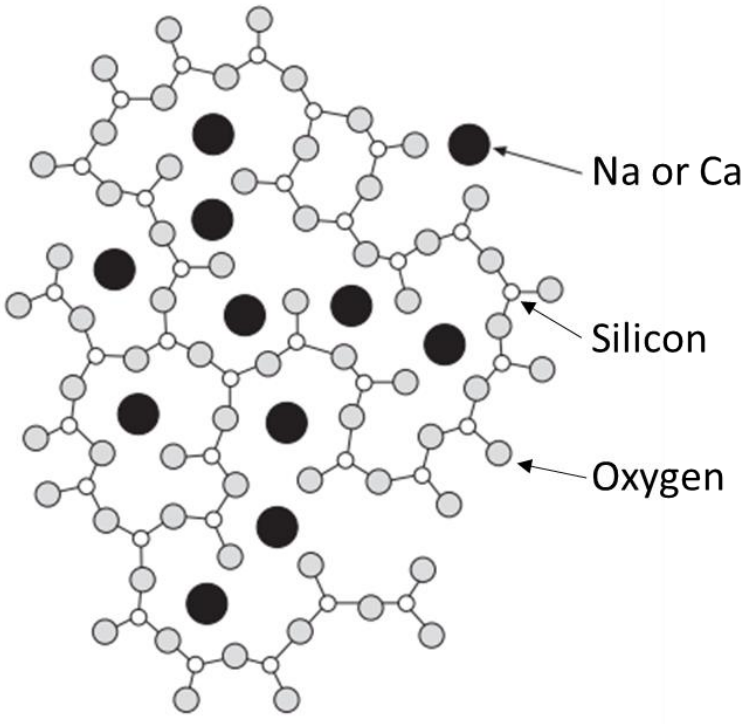

Figure 4. Structure of soda lime glass.[6]

Borosilicate glass is another common glass with high Silica (SiO_2) content typically of 70-80 wt% with 7-13 wt% of B_2O_3, 4-8 wt% Na_2O or K_2O and 2-8 wt% of Al_2O_3. Borosilicate glass are highly durable and resistant to chemical, moisture and thermal attack, which is why they are used as laboratory glassware, cooking (thermal expansion of borosilicate glass is only one third of the soda lime glass) and even for nuclear waste immobilisation.[8] Varied amount of boric anhydride (B_2O_3) gives different glass properties with low B_2O_3 content glass used in chemical apparatus and lamps to high B_2O_3 content glass used for stationary media in chromatography.[9]

In borosilicate glass the network is irregular with bond angles of Si-O-Si ranging from 120° to 180° with network modifiers with 6 or higher coordination numbers. These form weaker bonds with oxygen than network formers leading to bond breaking and with non-bonding oxygen (NBO) SiO^- ions localised to modifying ions as see in Figure 6.[10] The boron atoms can be present as BO_3 triangles and BO_4 tetrahedra and in some conditions they can combine to form superstructural units such as boroxol rings. This shows how versatile the glass can be.[11,12]

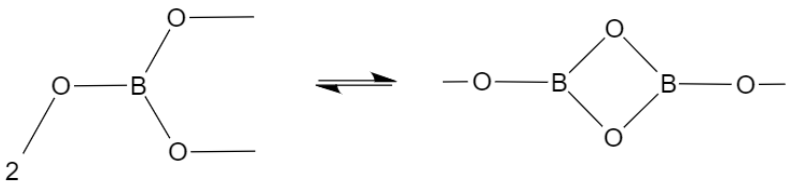

Figure 5. Borate coordination from three to four.

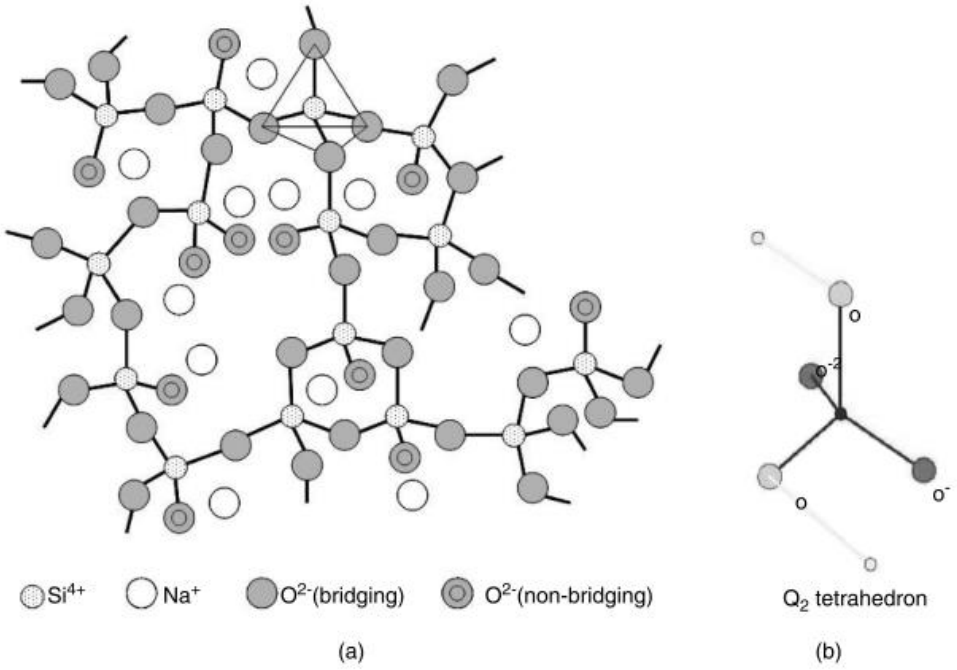

Figure 6. (a) Structure of alkali-silicate glasses; (b) a Q_n structural unit: Q_2 comprises two bridging oxygen atoms and two NBO.[10]

Glass compositions that contain phosphates are readily available such as Bioglass® made of 45.0 wt% SiO_2, 24.5 wt% CaO, 24.5 wt% Na_2O and 6.0 wt% P_2O_5. These glass has bone regeneration and clinical applications although there are questions to its long term effects.[13,14] Glass containing network forming phosphates has potential uses as activated glass since their composition are similar to some body tissues.

Pure P_2O_5, readily used as drying agents in laboratories has been used to make glass compositions but has been very limited due to its hygroscopic nature,[15] its reactiveness arise discrepancies when trying to produce consistent and reproducible results as crystalline P_2O_5 has three polymorphic forms: hexagonal, orthorhombic and tetragonal. With varying melting times the

structure can change from tetrahedra to forming rings.[16] As discuss previously, other oxides are incorporated into silicon oxide in order to manipulate the glass easier since pure SiO_2 glass has very strong bonds. With phosphate glass since P_2O_5 are so reactive, other oxide are added to decrease its reactivity making it more durable.

Phosphate glasses on their own are formed by tetrahedral phosphate anion[17], the Q^i terminology are used to classify these structures, where "*I*" represents the number of bridging oxygens. The P-tetrahedra structure is formed by sp^3 hybrid orbitals by the P outer electrons. Fifth electron from phosphorous is promoted to a 3d orbital where it forms a strong pi-bonding molecular orbital with oxygen 2p electron.[18,19] Sodium oxide and calcium oxides are introduced to form binary phosphate glasses. Addition of these modifying oxides forms non-bridging oxygens at the expense of bridging oxygens which results in the depolymerisation of the phosphate network.[20]

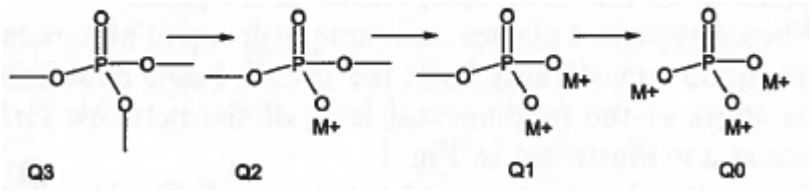

Figure 7. Effect of monovalent ion addition to P_2O_5 network.[20]

Figure 7 illustrates the three main building blocks, the end unit Q^1, the middle unit Q^2 and the branching unit Q^3. Depending on the ratio of phosphorous pentoxide and M_2O they can be classified as orthophosphates, pyrophosphates, metaphosphates and ultraphosphate as can be seen in Figure 8 below.

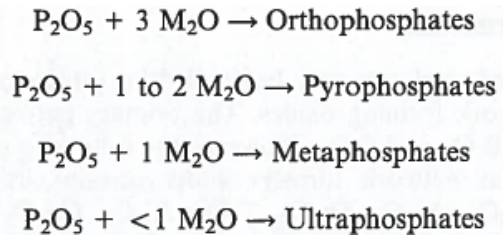

Figure 8. Naming of phosphates.[20]

Ternary phosphate glasses very much like the binary are mainly composed of Na_2O-CaO-P_2O_5 system and in particular the $(Na_2O)_{0.55-x}$-$(CaO)_x(P_2O_5)_{0.45}$ due to their dissolution characteristics. The amount of CaO determines the dissolution times which can vary from several hours to several months. As their dissolution rate can be controlled they have potential as resorbable materials since their constituent atoms are biocompatible with the natural bone.[21] Ternary phosphate glass can incorporate other metal ions such as titanium and strontium to form quaternary and quintenary glass to alter their dissolution and ion releasing property to be used much more widely in orthopaedic tissue engineering and medical uses.[22] This adaptable nature of phosphate glass makes it an ideal material to begin with for research.

1.2.3 Glass properties

Glass shows three distinct natures when heated. As seen in Figure 9 it displays glass transition T_g, glass crystallisation T_c and glass melting temperature T_{me}. Glass transition temperature (T_g) which is always lower than the glass melting temperature (T_{me}) which is located at the mid-point of the curve.

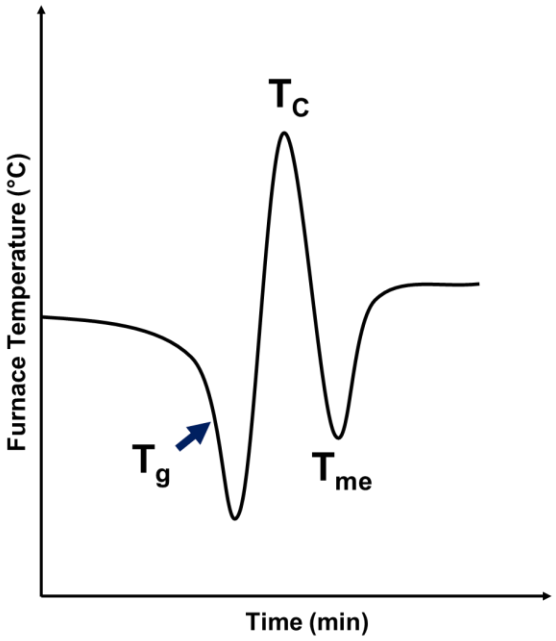

Figure 9. Graph plot to show the different transition temperatures (T_g/T_c/T_{me}) observed when glass is heated during analysis such as DTA (Differential Thermal Analysis)

When hot liquid cools it undergoes contraction until it reaches the point of solidification, also known as the T_f (glass formation temperature) the liquid either undergoes crystallisation or the liquid goes into a supercooled state. When crystallised, it continues to contract as it cools but with the supercooled liquid it also contracts with a coefficient identical to the original liquid (Figure

10 (a)) and at T_g, the cooling curve suddenly decreases to that of the crystalline solid (Figure 10 (b)).[4]

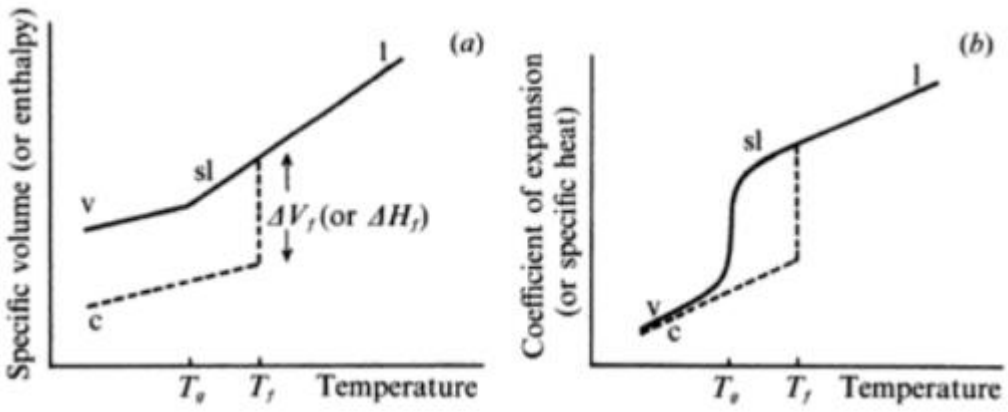

Figure 10. Definition of the glass transition temperature T_g. (a) Variation of the specific volume (or the enthalpy *H*) with temperature (l: liquid, s.l: supercooled liquid, c: crystal, v: glass). (b) Variation of derivative quantities: coefficient of expansion α (or specific heat C_p).[4]

Glass transition temperature helps determine various flexible and rigid applications for a material. Crystallisation temperature as by its name is at the highest peak, temperature required to crystallise glass. Glass melting temperature is the critical temperature above which the crystalline regions are able to flow.[23]

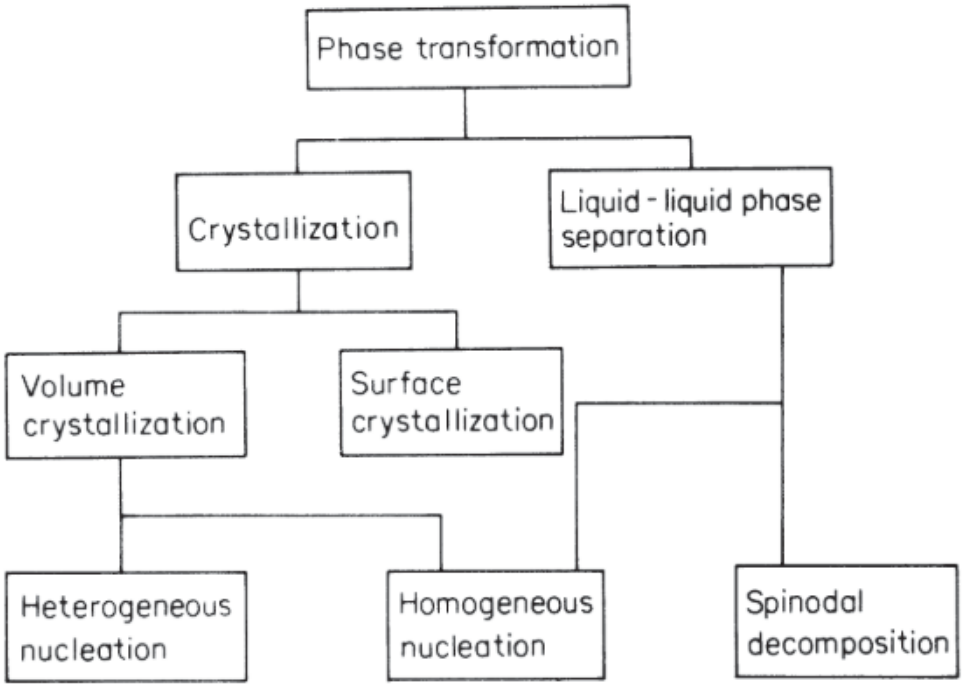

Figure 11. Phase transformation usually observed in glass.[24]

Figure 11 shows the common phase transformation observed in glass. Crystallisation can happen on surface or in volume. The difference is the site of nucleation origin, either from the glass-atmosphere interface in surface or from the bulk media of the material. Heterogeneous nucleation is when the nucleation begins from a foreign material to the bulk where homogeneous nucleation is the same material to the bulk. Liquid-liquid phase separation happens in a multi-component system where there is a growth of non-crystalline phase different in composition to the original phase.

1.2.3.1 Glass dissolution

Dissolution and diffusive process in glass has been studied for soda-lime, borosilicate and phosphate glass. Since one's chemical durability is one of the key factors determining suitability for its application. Glass surface structure, presence of hydration layer and the transformation of it greatly determines the dissolution rate of the glass.

Soda-lime silicate glass without alumina dissolved at a faster rate than with alumina which dissolved about the same rate as vitreous silica (glass consisting of almost pure amorphous SiO_2). Pyrex borosilicate glass dissolved *ca.* 100 times faster than the commercial soda-lime glass with alumina but not as fast as soda-lime without alumina.[25] With soda-lime glass, sodium ion are released first into the solution compared to borosilicate glass, increasing the pH of the solution further causing the glass to dissolve faster. The difference with and without alumina is thought to be due to greater proportion of the non-alumina-containing hydrated layers causing a phase separating of the layers into silica rich and open phases causing more rapid ionic transport[26] making it easier for water to penetrate into the surface, reacting with silicon-oxygen lattice and forming Si-O-H bonds.[27] With borosilicate glass, it is thought that there is a phase separation into a near pure silica matrix and regions with sodium borosilicate spheres increasing the porosity of the glass. This allowing more water to penetrate and effectively increasing the dissolution rate.[28,29]

Similar to silicate glass, phosphate glass dissolution is thought to undergo two steps: hydration followed by network breakage (Equation 1 and Equation 3).

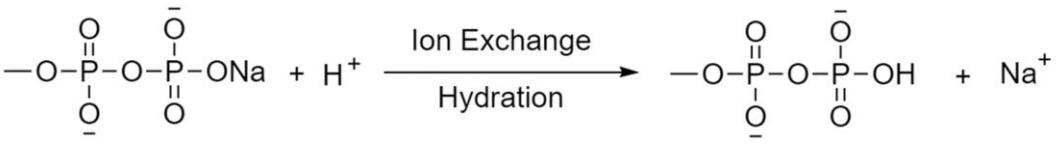

Equation 1. Equation of hydration reaction where Na+ and H+ are exchanged and forms a hydrated layer on the glass surface.[30]

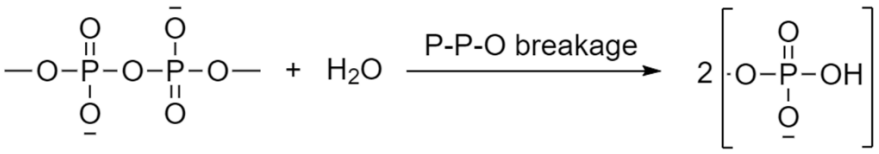

Equation 2. Equation showing network breakage, where the proton from water breaks the P-O-P bond in the hydrated layer breaking the glass network to release different polymerised phosphates.[30]

Phosphate glass dissolve much faster than those of silicate glass and their dissolution highly depends on the phosphate and calcium ion concentration in the glass, solution pH and temperature. Bunker *et al.*[31] conclude that the ion exchange is the dominating reaction in the dissolution process of phosphate glass whilst Liu *et al.*[32] proposed that the network breaking reaction is the domination one by saying that the ion exchange merely provides the moist hydration layer to initiate the network breaking process. Hou *et al.*[33] suggested that the aqueous media attributes to an enhancement effect, accelerating dissolution leading to roughness of glass after prolonged leaching. Extensive mechanism study by Gao *et al.*[30] talks about the process in four stages. Mass transfer in hydration layer, formation and development of the hydrated layer, network breakage and chelating effect.

Gao *et al.* describes the formation of hydration when glass is in contact with water brings about the previously mentions Na^+ dissociation from the $[PO_4]$ units in the middle of change and exchange with H^+. Within the hydration later the ion exchange is not the dominating reaction as the ion exchange happen immediately meaning the diffusion of water molecules becomes the limiting step. Phosphate glass with calcium oxide, the Ca^{2+} with greater charge and polarisation will bond with the non-bridging oxygen on $[PO_4]$, this is why we observe increase in durability as CaO is increased.

As the hydration layer becomes thicker, the P-O-P network bond breakage becomes the dissolution rate determining step. This is as water molecules have difficulty in penetrating into the glass. Since H^+ ion increases the network breaking reaction, the lower the pH the dissolution rates are increased with increase release of phosphates. The presence of CaO or other divalent cations also has significant effect. Depending on the concentration of polyphosphate in media the CaO can either prevent further penetration or increase in penetration, but general high concentration of divalent ions will lead to deposition in the glass network forming protective film over the hydrated later, preventing further diffusion into bulk glass.

1.2.4 Water and scale

Association of domestic tap water and its health impact has been widely investigated by global NGO organisations such as WHO[34] providing guidelines for safe drinking water and researches on how the presence of fluoride[35], manganese[36] and microorganisms[37] may have health impacts on both children

and adults. There is a wide divide in the discussion of whether water hardness has negative health related impact such as eczema[38], urinary concretion[39], growth and general well-being[40] compared to potential cardiovascular benefits and overall better for the body than softened water.[41–43]

Naturally sourced water contains alkaline metal cations such as Ca^{2+}, Ba^{2+} and Mg^{2+} and anions such as carbonates, bicarbonates, sulphate, silicate, phosphates and many more. These occur naturally as water passes through limestone and rock compositions of the area picking up these minerals. Water that has been deionised can also contain ions when left out for prolonged period as gases such as CO_2 dissolve into the water forming carbonate ions. Water is considered soft, moderately hard, hard and very hard when there is <50, 50-150, 150-300 and >300 $mg.L^{-1}$ as $CaCO_3$ respectively.[44] Hard waters form white precipitates of calcium carbonates, known as calcite. Calcium Carbonate is formed when Calcium ion (Ca^{2+}) and Carbonate ion (CO_3^{2-}) ionically bond to form solid Calcium Carbonate ($CaCO_3$) as in Equation 3. Carbonate and Bicarbonate ions are formed when Carbon Dioxide (CO_2) gas dissolves and dissociates in water and is summarised in Equation 4.

$$Ca^{2+} + CO_3^{2-} \rightarrow CaCO_3$$

Equation 3. Formation of Calcium Carbonate

$$CO_2.H_2O/H_2CO_3 \leftrightarrow H^+ + HCO_3^- \leftrightarrow 2H^+ + CO_3^{2-}$$

Equation 4. Equilibrium of Bicarbonate and Carbonate Ions Present in Water

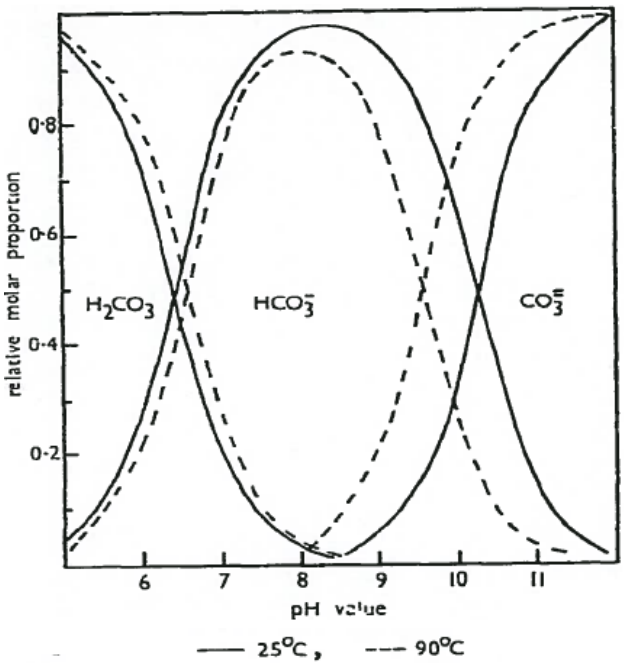

Figure 12. Carbonic acid distribution diagram.[45]

Calcium carbonate exists in six polymorphic forms: calcite, aragonite, vaterite, amorphous $CaCO_3$ and two hydrated crystalline phases, calcium carbonate monohydrate and hexahydrate.[46] Calcite is the most thermodynamically stable and hence is the form we observe in domestic appliances.

Since carbonate ions are involved in dynamic equilibrium when aqueous, the position of the equilibrium depends strongly on pH and temperature. Figure 12 shows the relative molar proportion of these ions over pH 5-12 and at 25 and 90 °C. At pH below 6 carbonic acid and dissolved carbon dioxide are predominant and between pH 6.5-9.5 bicarbonate is predominant and above pH 10 carbonate is the most predominant.[45] Comparing the predominance at 25 and 90 °C, at higher temperature the graph shifts to the left to show carbonate ions to be more predominant. Therefore, at high pH and high temperatures more carbonate ions are present, leading to increase in bonding

with calcium ions to precipitate out as calcium carbonate also more commonly known as lime scale. This is the reason to why white calcium carbonate deposits are readily observed in kettles, taps and washing machines in hard water areas, as calcium carbonate precipitates outs at higher temperature.

Orthophosphates, zinc orthophosphates, polyphosphates along with other blends of phosphates are used in more than half of the water treatment utilities in the United States.[47] The use of these phosphates prevents calcium carbonate deposition by removing calcium and inhibiting precipitation to control pipe corrosion. It has been widely researched that orthophosphate inhibit calcite growth even at very low concentrations, which was later found to be due to the competition between carbonate and phosphate ions to bind to the available calcium;[46] active crystal sites are blocked as the phosphate adsorb onto the surface. This inhibition process is dependent on the pH, which suggests that certain phosphate species are predominant at interacting with the calcite surface and this was found to be $CaHPO_4$ by *Lin et al*., $CaHPO_4$ underwent a chemisorption process with endothermic adsorption reaction driven by the entropy change.[48]

Current product for scale inhibition includes Siliphos® which contains polyphosphate silicate spheres which dissolves in water and provides threshold scale inhibition by stabilising the water to prevent calcium carbonate from forming. Polyphosphate is able to form a protective layer in presence of iron and calcium by forming calcium iron phosphate which separates water and oxygen in water from the metal pipes to prevent corrosion.[15] However, this product is not ideal for domestic use due to excessive release in

phosphate ions which releases nutrients which can cause bacterial build-up and hence requires the need for slow phosphate releasing material.

Chapter 2

Literature Review

2.1.1 Water softening

There are various methods used in water softening but most can be separated into either chemical and / or physical methods. Water softening is key when preventing scale deposition causing thermal, mechanical and hydraulic problems. Addition of lime is a well-known method used to treat hard water.[49] Known more commonly as carbonate conditioning, lime [$Ca(OH)_2$] and soda ash [Na_2CO_3] are added to react with magnesium and calcium ions to precipitate out in cold water by producing solid calcium carbonate and magnesium hydroxide as seen in equations below.[50] This essentially prevents deposition of $CaSO_4$ and forms loose $CaCO_3$ which can be more easily removed than $CaSO_4$.

$$2CO_2 + Ca(OH)_2 \rightarrow Ca(HCO_3)_2 \quad (1)$$

$$H_2CO_3 + Ca(OH)_2 \rightarrow CaCO_3 + {}_2H_2O \quad (2)$$

$$[Ca^{2+} + 2HCO_3^-] + Ca(OH)_2 \rightarrow 2CaCO_3(s) + 2H_2O \quad (3)$$

$$[Mg^{2+} + 2HCO_3^-] + 2Ca(OH)_2 \rightarrow 2CaCO_3 + Mg(OH)_2(s) + 2H_2O \quad (4)$$

Lime and soda ash to soften water is effective and has the ability to treat wide range of water quality and the following clarification system step after lime addition can happen simultaneously with other treatment process. There are disadvantages to using this method such as precipitates formed must be

removed before further treatment meaning increase in labour costs, disposing of the chemical sludge also increase costs, bulk storage of chemicals and its handling is unpleasant and costly and ultimately cannot achieve complete softness as addition of the alkaline materials causes increase in pH which must be controlled before reaching the tap.[49,51]

Ion exchange softening is another method in softening water, an external treatment unlike other internal treatment. It essentially removes calcium and magnesium ions from the water by replacing them with other ions such as sodium. Ion exchange materials include zeolites and polymeric resins and synthetic materials. The effectiveness of this method depends on the porosity, mobility and ion size, exposure time to hard water and the effectiveness of the ion exchange method.[52–54] This method is very effective and can achieve ultrapure water standard and can have in-house applications. However, its disadvantages include increase in sodium levels in water, threshold limit of iron content of water, not suitable for turbid water and bulk storage is required.[49]

As explained above the common methods of water softening is not suitable for small scale applications and therefore the development and research into glass with the ability of controlled phosphate release, especially orthophosphate is an attractive and effective solution.

Phosphates are widely used as antiscalants in drinking water in the methods commonly known as phosphate conditioning. The mechanism of which phosphate prevent calcite build up is known as threshold scale inhibition first proposed by Raistick *et al*. in 1949.[55] The molecular dimension of the

polyphosphate chain being very similar to those of calcite lattice Raistick suggested that as calcium carbonate started to form from the supersaturated solution, the polyphosphate would be adsorbed onto the surface and since PO_3^- having one less negative charge than CO_3^{2-}. The structure's net charge will then become positive, preventing further Ca^{2+} depositions. Making the crystals small, or sub-microscopic and negligible in size. Whilst Elliot[56] suggested that polyphosphates would provide site of crystal growth due to its similarities in structure, forming countless small crystals preventing stable precipitate formation.[45,57,58] However both agrees with the idea of phosphate and carbonate interaction forming smaller nuclei preventing growth of $CaCO_3$.

Study of phosphate adsorption on different $CaCO_3$ structures of vaterite and calcite has been carried out by Sawada *et al*.[59] and Suzuki *et al*.[60] They say how the magnitude if the retardation depends on the polymorph of the calcium carbonate, i.e. calcite, argonite or vaterite.[61] The $Ca^{2+} \cdot PO_4^{3-}$ formation on surface accounts to the positive charge on the surface on vaterite and neutral species formation of $(Ca^{2+})_3(PO_4^{3-})_2$ and $(Ca^{2+})(HPO_4^{2-})$ on calcite. This irreversible adsorption in blocking active crystal growth sites, $>CaCO_3^-$ and $>CO_3^-$ suggested by Lin and Singer[48] via an endothermic reaction driven by entropy change likely driven by dehydration process on calcite surface, preventing large $CaCO_3$ build up. The presence of pyrophosphates and other polyphosphates are very important in threshold scale inhibition as orthophosphate (PO_4^{3-}) alone would not be efficient in scale prevention as it may prevent calcium carbonate formation but is likely to form highly insoluble calcium phosphate or apatite.[62] Therefore the presence of multiple polyphosphate is crucial in scale inhibition.

Although there are different mechanisms explaining how phosphates inhibit calcite growth, there is no doubt that phosphate is very effective at calcite inhibition, even by looking at the results in Chapter 1 Figure 2. However there are concerns of excessive phosphate in water leading to eutrophication and damages to environment[63–70] therefore there is a need for material having the ability to release sufficient phosphate to prevent calcite but not excessive to cause adverse effect to nature and other possible unknown consequence.

2.1.2 Antimicrobial properties of metals

Prevention and treatment of disease is an area researched extensively as it is an area directly related to life and death. The establishment of the World Health Organization (WHO) in 1945 was prompted by numerous life threatening events such as the outbreaks of the Spanish flu in 1918 and cholera pandemics killing millions of people in early 1800s including the current ongoing COVID-19. These wide spread of bacteria and viruses has highlighted the ever more importance of utilising antimicrobial materials in killing and prevention of spreading of disease, being more effective than treatment.

In the recent two years the use of antimicrobial copper films has been widely utilised on surfaces such as door handles and buttons on an elevator.[71,72] It has been researched that the spread of disease via public surfaces significantly increase the risk as bacterial contamination between people. [73] Metals and its oxides has been used in antimicrobial applications in solids, fluids and tissues for centuries.[74,75] Metals that are potentially toxic to living

and non-living cells are classified into four groups based on health impact. A) Essential: Cu, Zn Co, Mn and Fe; B) Non-essential: Ba, Al and Li; C) Less toxic: Sn and Al and D) Highly toxic Hg, Cd,As.[76] Essential metals are toxic when taken in excess of requirements such as more than 140 mcg/dL of copper, 2589 ppm of silver and 50 mg of zinc;[77–79] but at controlled amounts are used as antimicrobial agents since antiquity.[80] Commonly used and well known for their antibacterial properties include silver, gold, copper, titanium, zinc and magnesium oxides. Many of these metals have been researched in many forms such as nanoparticles to be incorporated in polymers or coatings, nanorods and nanofibers used in drug delivery, phototherapy and water filtration and nanomats such as nanosheets and films of 1-100 nm.[81] They have shown great antibacterial properties as seen in Figure 13. This section will explore different candidates of metals as dopants in glass composition for antimicrobial effect.

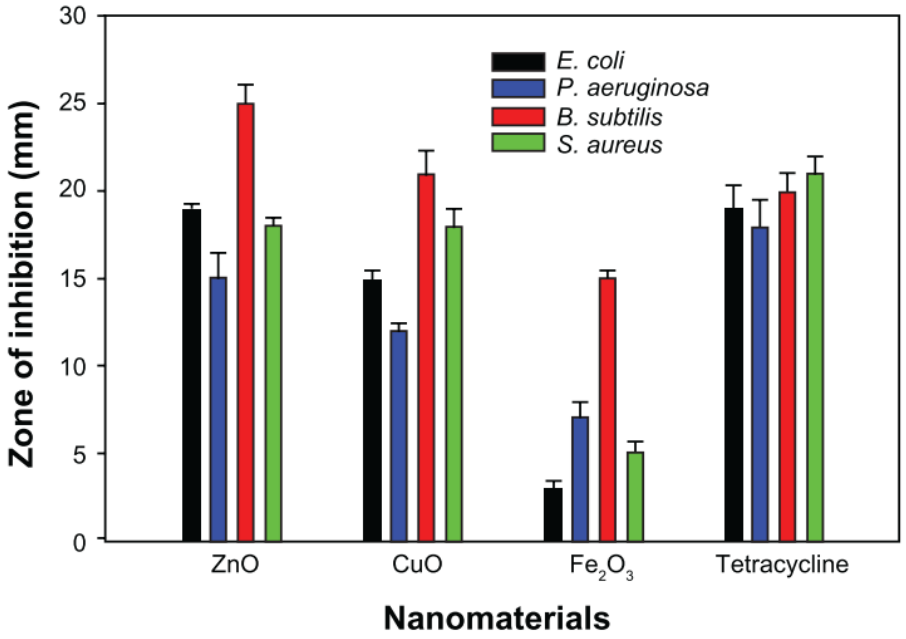

Figure 13. Bar graphs showing zone of inhibition introduced by different metal oxides again various microorganisms.[82]

2.1.2.1 Copper

Copper is a metallic element essential to human health and considered safe to humans with prolonged use in copper intrauterine devices.[83] Copper is known to kill microorganisms via 'contact killing' method due to its ability to kill 99.9% of pathogenic bacteria within 2 hours. Although not fully understood it is known that no micro-organism survived with prolonged exposure and incubation on copper surfaces.[84]

Vincent *et al*.[85] reviewed copper's contact killing properties and compared antibacterial, antifungal and antiviral properties of copper surface and particle. Extensive research is carried out in antibacterial properties of copper showed that copper was most effective in higher temperatures and at higher copper content. Copper kill both gram negative and positive bacteria. With the size of

the copper nanoparticle being one key factor contributing to its antimicrobial activity.[86,87] Copper was also an effective antifungal showing similar to of bacterial species and antiviral with its ability to kill influenza, norovirus and human immunodeficiency virus (HIV).[88–90] Copper was able to kill bacteria suspended in water and showed its potential as water purifying material.[91] Figure 17 shows how copper damages microorganisms. The contact killing is initiated when copper ions catalyse the production of highly reactive hydroxyl radicals damaging membranes followed by DNA degradation.[92,93]

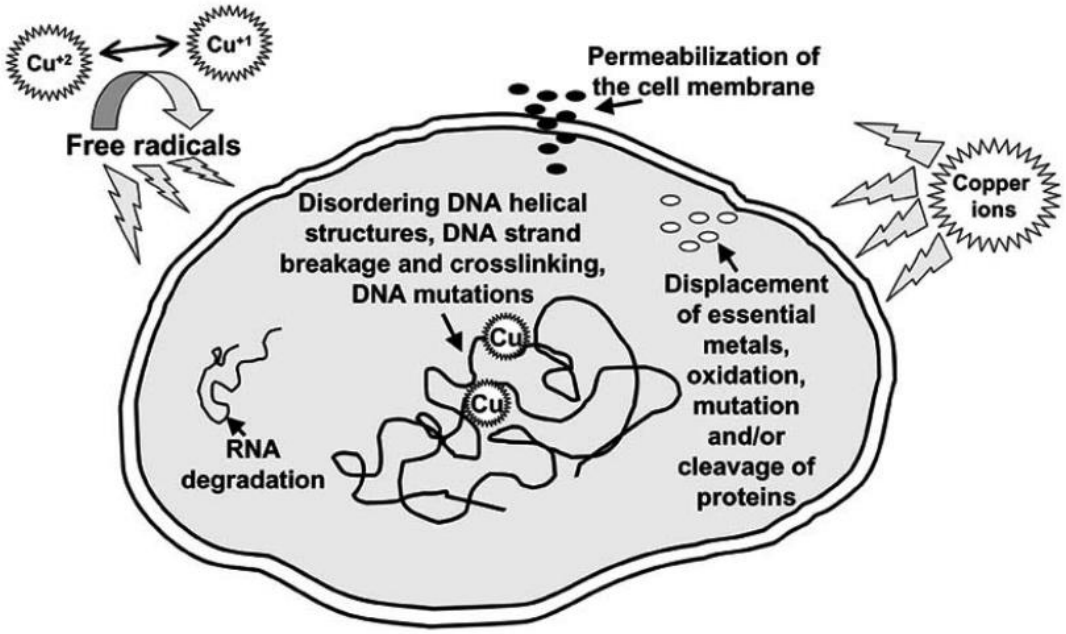

Figure 14. Mechanism of toxicity of copper to microorganisms.[91]

Copper has been incorporated to thin film membranes to improve biofouling in reverse osmosis (RO) will 80-95% decrease in the number of live bacteria attached to the film.[94] Copper incorporated into bioactive scaffolds was not only able to significantly enhance hypoxia-like tissue reaction with Cu^{2+}

incorporation, it significantly inhibited the viability of the bacteria showing its use as a multifunctional material.[95]

2.1.2.2 Silver

Silver, much like copper is a well-known antimicrobial compounds used in dental amalgams, medical devices such as catheters and in water purification systems. This is all down to its low toxicity to human cells and it has no unfavourable effect on taste or colour.[96] Although risks of exposure to silver ions are low the prolonged exposure can be the cause of non-life threatening argyria and argyrosis characterised by an irreversible deposition of silver selenide and sulphide in the skin and the eyes.[97]

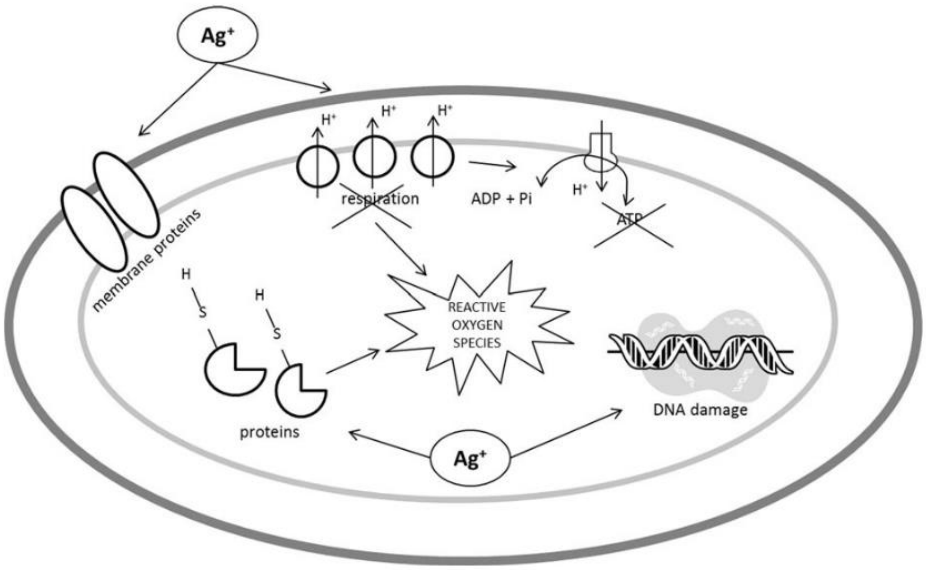

Figure 15. Antimicrobial effect of Ag+. Interactions with membrane protein and blocking respiration and electron transfer; inside cell, Ag+ ions interact with DNA, proteins and induce ROS production.[97]

Silver nanoparticles (AgNPs) with zero valent showed no antibacterial activities and only Ag^+ (a transition but forms ions with 1+ charge) showed antibacterial properties with smaller particles being more effective.[98–100] As in Figure 15 silver forms an S-Ag with sulfhydryl groups blocking electron transfer and preventing respiration.[101,102] This blockage of electron transfer causes de-energising the membrane resulting in cell death. Further damages to the DNA and RNA and proteins are caused by reactive oxygen species (ROS) much like copper.[103,104]

Silver containing glass composites has been picked as the next possible dental restoration material achieving antibacterial property by slow release of Ag+ ions.[105] Phosphate glass doped with silver showed significant increase in inhibition zones diameter with increasing Ag_2O content with phosphate released producing lower pH environment further enhancing its antibacterial property.[106]

2.1.2.3 Zinc

Zinc, like the silver and copper ions shows antimicrobial property by entering into the bacteria, disrupting its normal function[107] and is nontoxic to humans.[108] Zinc oxide's efficiency in bacterial eradication improved with decrease in ZnO nanoparticles with generation of ROS and disruption to proton motive force damaging lipid membranes, DNA and RNA.[109,110] Zinc oxide has been incorporated into polymers and used in food packaging material as it is listed to be safe by Food and Drugs Administration (FDA).[111] It has also been incorporated into borophosphate glass showing up to 99.99% decrease in

antimicrobial activity values showing its possible use as antimicrobial glass used in everyday since commercial borosilicate glasses include Pyrex® and Duran®.[112]

Glass being such a versatile material has the possibility to exhibit multiple properties. This thesis is very much interested in utilising this nature to find the right glass composition giving water softening properties by control release of phosphates and possible antimicrobial properties by incorporating well known antimicrobial metals as this glass is aimed at being used extensively at home in portable wet environments. It is also important to note that although metals explained above have excellent antimicrobial properties, at higher concentrations it is toxic, hence the need to control the metal ion concentration whenever it is used. However in this thesis the concentrations used are dramatically lower than the levels toxic to humans.[113,114]

Chapter 3

Dissolution Analysis of Phosphate Based Glass

3 Dissolution analysis of phosphate-based glass – P50Ca40Na10

3.1 Introduction

This chapter describes the synthesis and preparation of the glass and analysis of the dissolution properties of the phosphate glasses studied in this research. Development of phosphate glass of various compositions were carried out during this thesis. The $50P2O5 \cdot 40CaO \cdot 10Na_2O$ (mol%) or P50Ca40Na10 glass composition was most effective when tested with hard water. With this composition the humidifier was able to run over 22 months and able to continue to run compared to 1.5 months without it (Figure 2). The glass was produced in the UCL laboratories.

The purpose of this study was to understand the weight loss and ion release of the glass discs when they were under different immersion conditions. Static and immersed all the time (SI), static and dried when not in use (SD), dynamic and immersed all the time (DI) and dynamic and dried when not in use (DD). These immersion conditions were deliberately chosen to first, study the ions released and second, how these ions being released would be affected when introduced to different conditions which would be the case in common households, trying to replicate 'in service' conditions.

Filtered Tap Water (TW_F) was supplied from the laboratory supply: Eastman Dental Institute, UK.

Deionized water was obtained by filling reservoirs from tap pressure water (Eastman Dental Institute, London, UK) passing through an ion exchange resin tank first.

Environmental chamber (NuAire, TripleRed Ltd., Long Crendon, UK).

3.2 Experimental methodology

3.2.1 Glass sample synthesis

3.2.1.1 Phosphate glass composition calculation

Phosphate-based glass were prepared using the following chemicals: diphosphorous pentoxide (P_2O_5, 98%, VWR, Lutterworth, UK), sodium dihydrogen phosphate (NaH_2PO_4, 99%, VWR, Lutterworth, UK) and calcium carbonate ($CaCO_3$, 98.5%, VWR, Lutterworth, UK)

The amounts of each chemicals were calculated as follows:

When NaH_2PO_4 is heated it breaks down into:

$$2NaH_2PO_4 \rightarrow Na_2O + 2H_2O + P_2O_5$$

Molecular Mass	240	62	36	142
Molar Mass Fraction		0.258	0.150	0.592

The amount of NaH_2PO_4 was calculated as:

$$\frac{(Na_2O(mole\ fraction\ required)x\ 62)}{0.258} = NaH_2PO_4\ (g)required$$

The amount of P_2O_5 needs to be calculated but one of the broken-down components from NaH_2PO_4 is P_2O_5. With the amount of NaH_2PO_4 calculated, the amount of P_2O_5 obtained from the breakdown was calculated as:

$$NaH_2PO_4\ (g)added\ x\ 0.592 = P_2O_5\ (g)$$

All glasses prepared had 50 mol% of P_2O_5 and 10 mol% of Na_2O. Therefore, the total amount of P_2O_5 required was always 71.0 g. The P_2O_5 from the NaH_2PO_4 was always less than the required amount, hence the extra required was provided by adding additional pure P_2O_5.

When $CaCO_3$ is heated it breaks down into:

$$CaCO_3 \rightarrow CaO + CO_2$$

Molecular Mass	100	56	44
Molar Mass Fraction		0.56	0.44

Just like the previous calculation, amount of $CuSO_4$ required for each glass was calculated as:

$$\frac{(CaO(mole\ fraction\ required)x\ 56)}{0.56} = CaCO_3\ (g)required$$

3.2.1.2 Melting and annealing of glass samples

Various composition of phosphate-based glasses was synthesised. Each corresponding compound were weighed in Stomacher blender bags and were thoroughly mixed together for one minute due to highly hygroscopic nature of phosphorus pentoxide using a Stomacher 400 Circulator Lab Blender. The mixed powder was placed in a platinum crucible which was then inserted into a furnace set at 700 °C for the initial reaction for *ca.* 30 minutes then the

temperature was increased to 1100 °C furnace for *ca.* 1 hour until fully melted. The molten glass was poured into pre-heated cylindrical graphite mould with a 15 mm in diameter cavity to anneal at specific annealing temperature for 1 hour and switched off to allow it to slowly reach room temperature overnight. The glass rods (15 mm Ø) were cut into discs of 2 mm in thickness using a wafering saw. The discs received no further polishing or surface treatment and were used as-prepared in the subsequent procedures.

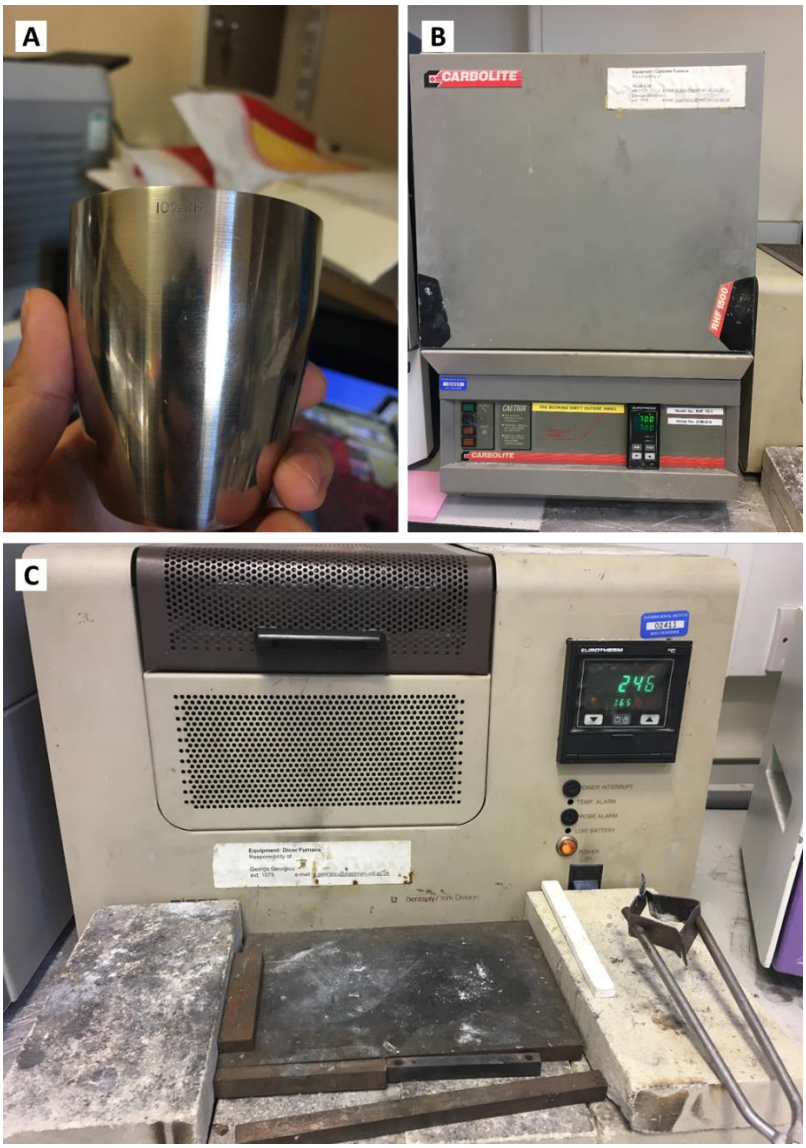

Figure 16. Equipment used to synthesise glass: A)platinum crucible, B)carbolite furnace to melt glass and C)dicor furnace for moulding and annealing glass.

Figure 17. Accutom-50 saw used with diamond blade to cut glass.

3.2.2 Immersion tests

Two conditions of water were tested: Tap Water (TW) and deionized water (dH_2O – obtained by means of an ion exchange resin column). Hard water samples were obtained directly from the tap-water supply and its conductivity was monitored on a regular basis. Values were found to vary between 684 and 729 μS/cm. For the case of tests running under deionized water the conductivity was found to vary between 0 and 12.

3.2.2.1 Static Immersion experiments

3.2.2.1.1 Static and immersed all the time (SI)

Glass discs (n = 3) were first weighed and the baseline weight (M_0) of each recorded. The exact dimensions of each sample were measured using a vernier calipers and the surface area was calculated. Samples were then placed in 20 mL of TW or dH_2O (n = 3) and incubated for 3 days at 30 °C in the environmental chamber. Following incubation samples were removed, blotted dry with tissue, and allowed to dry or 1h before the weight of each was again recorded (M_t). The immersion solutions were collected and stored under refrigeration (4 °C) until required for analysis of ionic composition. Each of the glass discs were then transferred to a fresh 20 mL TW or dH_2O volume for a further 2 or 3 days (3 days due to immersions over the weekend) and the above sampling processes repeated. In all, weight loss and ion release sampling procedures were repeated for the following total immersion times:

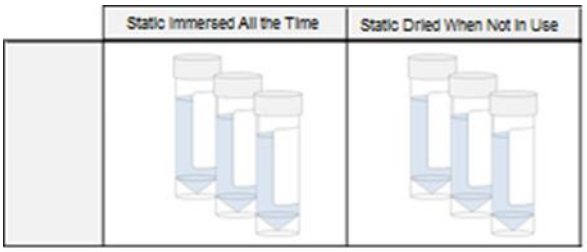

Figure 18. Figure of sample vials containing 20 mL of TW or dH_2O to pictorially show how they were stored during static immersion test.

Weight loss data was expressed as the change in weight per unit area (ΔM) using the equation: ΔM (mg.cm^{-2}) = M_0 (mg) - M_t (mg) ÷ A (cm^{-2}).

3.2.2.1.2 Static and dried when not in use

Much of the process was identical to SI. However, after collection of the effluent samples, the glass discs (n = 3) were left out 2 or 3 days before being again immersed in 20 mL of (fresh) TW or dH_2O. This is to try and simulate the discs being immersed and the not immersed as might occur in a domestic ultrasonic humidifier unit.

Figure 19. Representative scheme of the experimental procedure used for when the glass was dried when not in use. Numbers in circles depict the number of days after starting the testing; blue arrows represent the period of time during which the glasses were fully immersed in water; yellow arrows represent the period of time during which the glasses were dried and left outside the rigs. Collection of water samples were obtained after every cycle of drying/immersing and analysed for the anion release. Glass weight loss was also monitored.

3.2.2.2 Dynamic flow experiments

3.2.2.2.1 Dynamic and immersed all the time

A Dynamic Immersion Rig (DIR) was commissioned by Dyson Ltd. (Figure 20) which consisted of nine ≈ 60 mL reservoirs housed within an environmental chamber. Each reservoir was continually supplied with TW at a flow rate of 40 $mL.h^{-1}$ by means of pre-calibrated peristaltic pumps (Watson Marlow Pumps Ltd., Cornwall, UK). The DIR was then allowed to run for 24 hours at 30 °C prior to commencing the experiment. n = 3 glass discs of each composition were weighed, the exact dimensions measured using Vernier calipers and placed individually in separate reservoirs. The DIR was then allowed to run for 3 days at 30 °C before a further 15 mL of the effluent was collected from each reservoir. Following collection of the effluent, the supply of TW was stopped, and the glass disc removed from their respective reservoirs and allowed to dry thoroughly before the weight of each discs was again recorded.

The discs were then replaced and the flow of TW or dH_2O immediately continued. All effluent samples were stored at ≈ 4 °C until required for analysis of polyphosphate species present in solution. Weight loss and ion release sampling procedures were repeated for the following total immersion times:

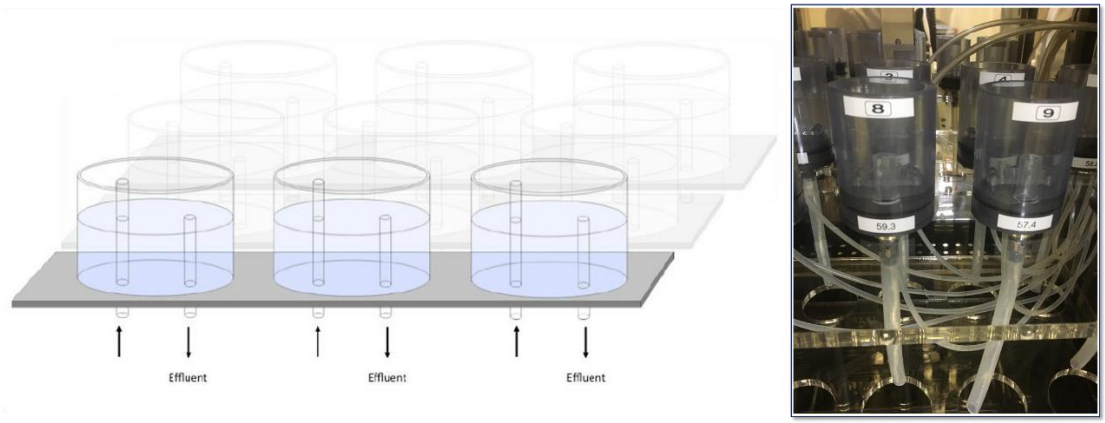

Figure 20. (Dynamic Immersion Rig): Directional arrows indicate the flow of TW (40 mL.h-1); glass discs were situated central to the base of each reservoir unit; ≈ 60 mL liquid volume kept constant by the overflow design.

Figure 21. NuAire environment chamber set at 30 °C for static and dynamic immersion tests.

3.2.2.2.2 Dynamic and dried when not in use

Much of the process was identical to DI. However, after collection of the first effluent samples, the glass discs (n = 3) were left out and placed back into the 60 mL reservoirs on day 7. Hence the samples were collected on alternating days of M_t = 3, 7, 12 and 17.

Much of the process was identical to SI. However, after collection of the effluent samples, the glass discs (n = 3) were left out 2 or 3 days before being again immersed in 20 mL of (fresh) TW or dH_2O.

3.2.3 Immersion experiments at varying pH

3.2.3.1 pH solution preparation for static immersion

Two pH values were initially set for this experiment: pH 5.82 and 8.26. At each point of immersion, a fresh solution of UPW was prepared for immersion. Diluted solutions of hydrochloric acid (HCl) and ammonium hydroxide (NH_4OH) were used to adjust the pH each time to achieve a pH value within ±0.1 of the pH of the first immersion. This experiment was carried out to study the glass discs under solutions of pH which would be expected at normal households.

3.2.3.2 pH static immersion experiments

Glass disks (n = 3) were first weighed and the baseline weight (M_0) of each recorded. The exact dimensions of each sample were measured using a Vernier calipers and surface area calculated. Samples were then placed in 20 mL of UPW set to a fixed pH (n = 3) and incubated for 3 days at 30 °C.

Following incubation, samples were removed, blotted dry with tissue, and allowed to dry for 1h before the weight of each again recorded (M_t). Each of the glass disks were then transferred to a fresh 20 mL of UPW of similar pH, for a further 2 days and the above sampling processes repeated. In all, weight loss and ion release sampling procedures were repeated for total immersion times: M_t = 3, 5, 7 and 10 days.

Weight loss data was expressed as the change in weight per unit area (ΔM) using the equation: ΔM (mg.cm^{-2}) = M_0 (mg) - M_t (mg) ÷ A (cm^{-2}).

3.2.4 Ion chromatography for phosphate analysis

The concentration of relevant ionic species was determined for polyphosphate $[PO_4]^{3-}$, $[P_2O_7]^{4-}$, $[P_3O_9]^{3-}$, and $[P_3O_{10}]^{5-}$. The release of phosphate species was analysed using an ICS-2500 ion exchange chromatography system equipped with a 50 µL sample injection loop calibrated at four concentrations (5, 10, 50 and 125 ppm). Standards were produced though serial dilution of a 1000 ppm stock solution detailed below in. Elution was performed between a KOH gradient of 25 mM to 40 mM over 32.5 minutes. Corrections were made to account for the expected purity of each phosphate salt used.

Figure 22. Ion chromatography equipment used A) cation and B) anions for phosphate analysis.

Table 1. (Phosphate Stock Solution): Corrections for the proportion of the molar mass contributed by the salt base were applied before calculating the mass required to produce the desired concentration of the anion. When necessary, corrections for mass were also applied to account for impurities in the chemicals as supplied (Purity < 99%).

Salt	Formula	Mass (g)	Anion Conc.	Purity	Supplier
Sodium Phosphate	Na_3PO_4	1.799	1000 ppm	= 96%	Sigma-Aldrich
Tetrasodium Pyrophosphate	$Na_4P_2O_7 \cdot 10H_2O$	2.563	1000 ppm	≥ 99%	Sigma-Aldrich
Trisodium Trimetaphophate	$Na_3P_3O_9$	1.359	1000 ppm	≥ 95%	Sigma-Aldrich
Pentasodium Tripolyphosphate	$Na_5P_3O_{10}$	1.711	1000 ppm	= 85%	Sigma-Aldrich

3.2.5 Statistical comparison

Statistical comparison carried out by analysis of triplet of each sample at each time point calculating the regarding standard deviation which was added to the results as error bars. Triplet of each sample was always used at all experimental and analysis step to achieve reliable and repeatable results. Each glass samples used in immersion tests were kept in the range of (2 ± 0.2) mm in thickness and (15 ± 1) mm in width and any outside of the range was discarded and not used.

3.3 Results and Discussion

3.3.1 Weight loss results

3.3.1.1 Weight loss in tap water

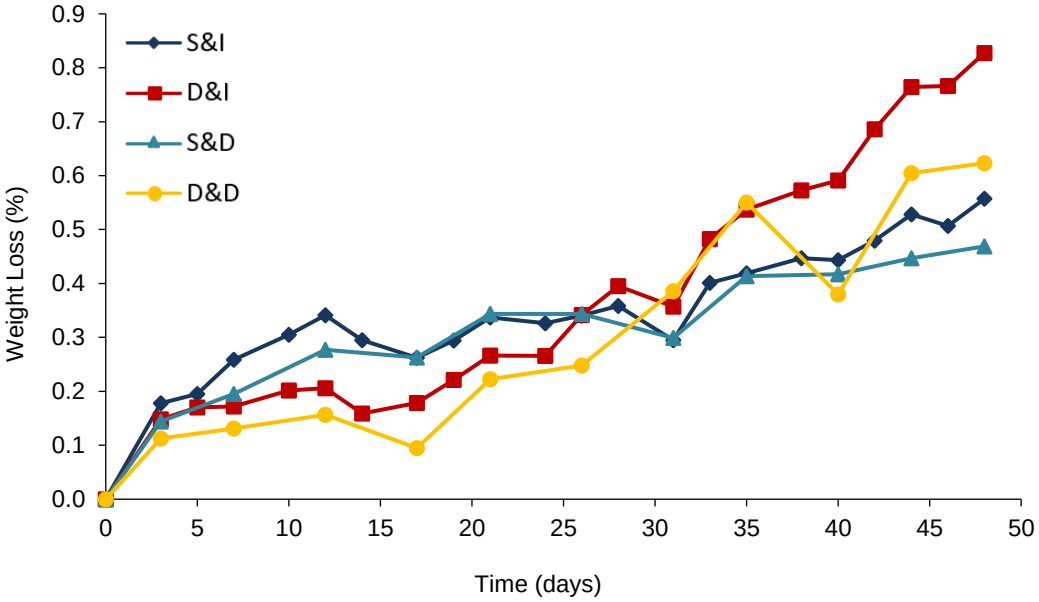

Figure 23. *Average p*ercentage weight loss over time in tap water at 30 °C. Error bars removed to see the fluctuations in results.

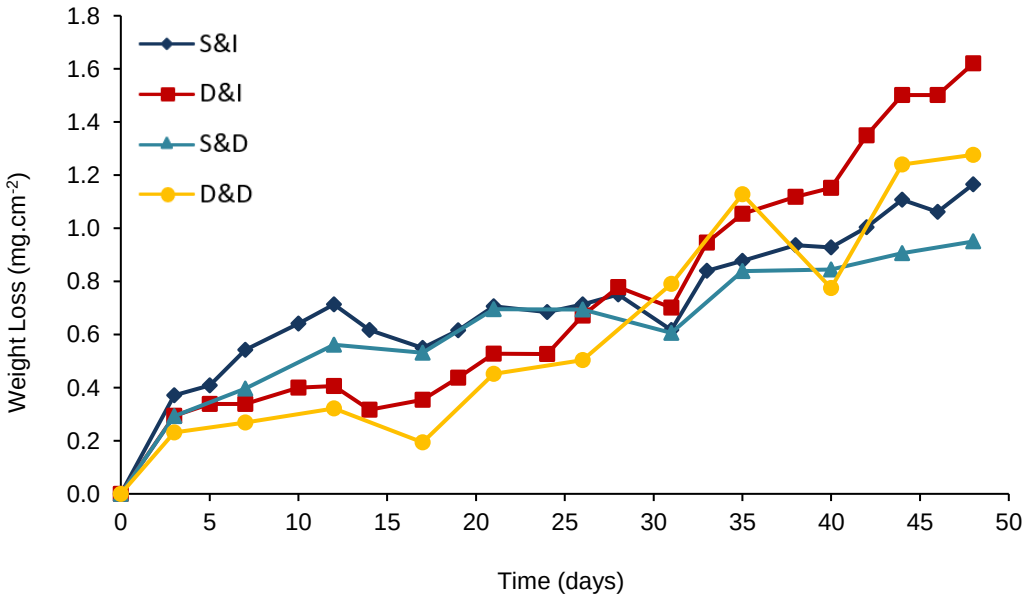

Figure 24. Average weight loss per unit is in tap water at 30 °C *Error bars removed to see the fluctuations in results.*

3.3.1.2 Weight loss in deionised water

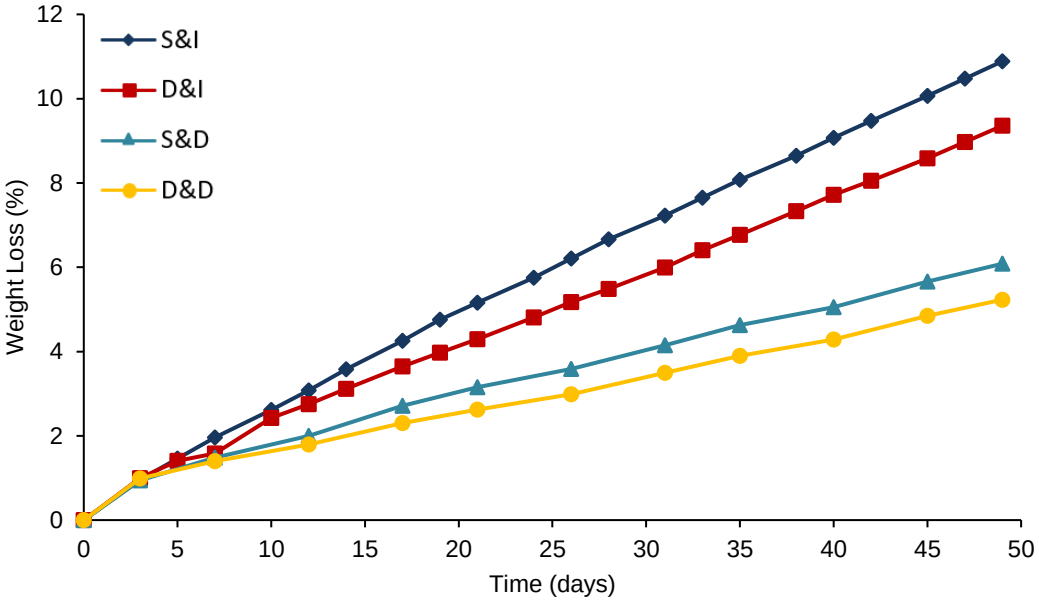

Figure 25. Average percentage weight loss over time in deionised water at 30 °C. *Error bars present, too small to be seen*.

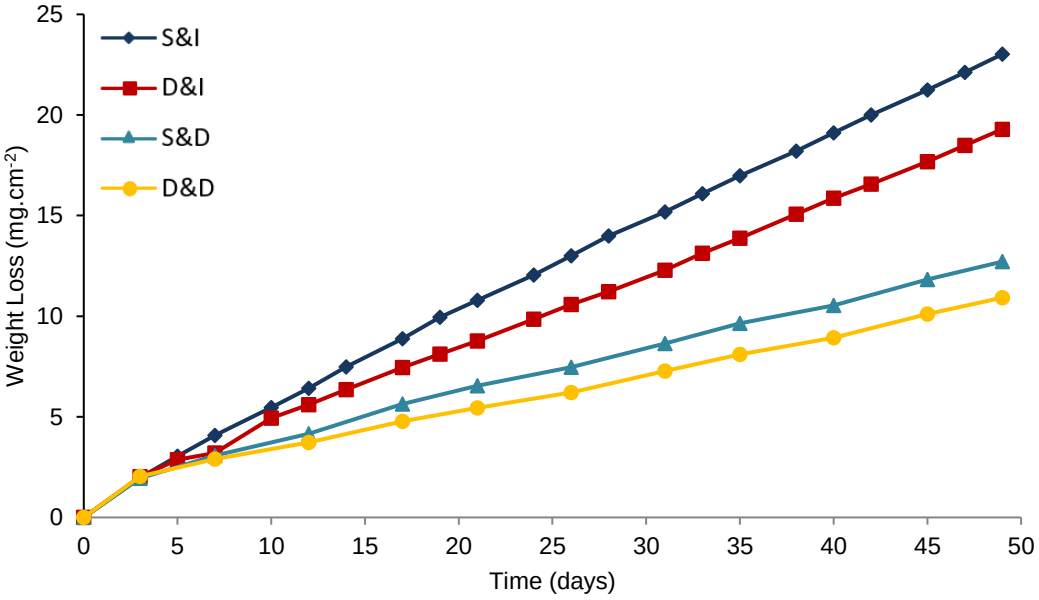

Figure 26. Average weight loss per unit area in tap water at 30 °C. *Error bars present, too small to be seen.*

Table 2. Table of average weight loss percentage in tap and deionised water immersion, alternate day data given.

Weight Loss (%) in Tap Water				
Time (days)	**SI**	**DI**	**SD**	**DD**
3	0.18	0.15	0.14	0.11
7	0.56	0.83	0.20	0.13
12	0.34	0.21	0.28	0.16
17	0.26	0.18	0.26	0.09
21	0.34	0.27	0.34	0.22
26	0.34	0.34	0.34	0.25
31	0.29	0.36	0.30	0.39
35	0.42	0.54	0.41	0.55
40	0.44	0.59	0.42	0.38
44	0.53	0.76	0.45	0.60
48	0.56	0.83	0.47	0.62
Weight Loss (%) in Deionised Water				
Time (days)	**SI**	**DI**	**SD**	**DD**
3	0.96	1.00	0.94	0.99
7	1.46	1.41	1.48	1.40
12	3.08	2.75	2.00	1.79
17	4.25	3.65	2.71	2.30
21	5.16	4.29	3.15	2.62
26	6.20	5.17	3.59	2.99
31	7.22	6.00	4.15	3.49
35	8.08	6.77	4.63	3.90
40	9.07	7.72	5.05	4.29
45	10.06	8.58	5.66	4.85
49	10.89	9.36	6.08	5.23

Table 3. Table of average weight loss per surface area in tap and deionised water immersion, alternate day data given.

Weight Loss ($mg.cm^{-2}$) in Tap Water				
Time (days)	**SI**	**DI**	**SD**	**DD**
3	0.37	0.29	0.29	0.23
7	0.54	0.34	0.40	0.27
12	0.71	0.41	0.56	0.32
17	0.55	0.35	0.53	0.19
21	0.71	0.53	0.69	0.45
26	0.71	0.67	0.69	0.50
31	0.62	0.70	0.61	0.79
35	0.88	1.05	0.84	1.13
40	0.93	1.15	0.84	0.78
44	1.11	1.50	0.91	1.24
48	1.17	1.62	0.95	1.28
Weight Loss ($mg.cm^{-2}$) in Deionised Water				
Time (days)	**SI**	**DI**	**SD**	**DD**
3	1.98	2.03	1.95	2.05
7	4.08	3.20	3.08	2.90
12	6.42	5.61	4.15	3.73
17	8.88	7.44	5.64	4.78
21	10.79	8.78	6.54	5.45
26	13.01	10.58	7.47	6.21
31	15.17	12.29	8.65	7.27
35	16.98	13.88	9.64	8.11
40	19.11	15.87	10.54	8.93
45	21.25	17.68	11.82	10.11
49	23.02	19.29	12.71	10.92

An increase in weight loss was observed for all immersion tests by the end of 48 or 49 days. The largest weight loss was observed for DI for tap water and in SI for deionised water. Immersions in deionised water was much larger than the ones in tap water, for SI in deionised water lost *ca.* 11% of its weight whilst 0.56% in tap water. The weight loss in tap water is erratic and shows increase

and decrease in weight loss during immersion period but this may be used to the low levels of values measured giving some variation in data. The error bars were removed in the tap water immersions in order to see the fluctuations also suggesting that the results within the tap water results do overlap which should be taken into consideration when interpreting the data. Whilst in deionised water (dH_2O) the weight loss gradually increases as the immersion time increases. The weight loss in tap water was greatest in DI followed by DD, SI and SD and the weight loss in dH_2O was greatest in SI followed by DI, SD and DD.

Ternary phosphate glass containing phosphates, calcium oxide and sodium oxide undergo dissolution process by loss of sodium ions first as they are less strongly attached to the phosphate glass network than calcium ions. The loss of positive ions is compensated by the positive H^+ or H_3O^+ from water/solution. Therefore dissolution rate or weight loss differences between different glass compositions are strongly determined by the added network modifying oxides which determines the number of cross-links in the glass "polymer".[31,115] Hence the above dissolution tests, using the same glass composition shows how the solution and its ion concentration and the immersion methods can affect the ion release its dissolution rates.

Weight loss is very much erratic in tap water immersions in Figure 23 and Figure 24 and overall weight loss is much lower than in deionised water for all cases. The overall lower weight loss is due to the ions already present in tap water causing lower concentration gradient between the glass discs and solution making a slower dissolution process. In tap water tests the immersion methods have greater impact on the weight loss by the end of day 50. Although

the difference between each weight loss can be seen as very small, dynamic methods caused more weight loss than static methods. The dissolution had increased due to the physical movement of the dynamic methods causing more ions to dissolve and to be absorbed into the glass.

Weight loss is much linear and greater in deionised water than in tap water, this is due to the absence of ions in deionised water which makes the ions in glass discs to diffuse much faster into the solution and H^+ and H_3O^+ diffuse much faster into the glass causing cleavage of phosphate network and causing faster dissolution overall. The immersed all the time discs also lost more weight than dried when not in use discs. This is due to simply the lack of contact time with the solution with the discs preventing continual dissolution. Static and immersed all the time immersion glass discs lost *ca.*3.73 $mg.cm^{-2}$ or 1.53% more weight than dynamic and immersed all the time discs by the end of 50 day immersions. This shows that the solutions that are static cause more weight loss than solutions that are continuously being flushed, a contrast to the tap water immersion. Although not by a significant amount it shows that the solution ion concentration has the majority affect in deionised immersion. Figure 25 and Figure 26 shows that as the immersion time increases each immersion tests also gets wider apart showing that with longer immersions the difference in weight loss will be greater.

3.3.2 Phosphate release measurements

3.3.2.1 Phosphate anion release measurements – Tap water

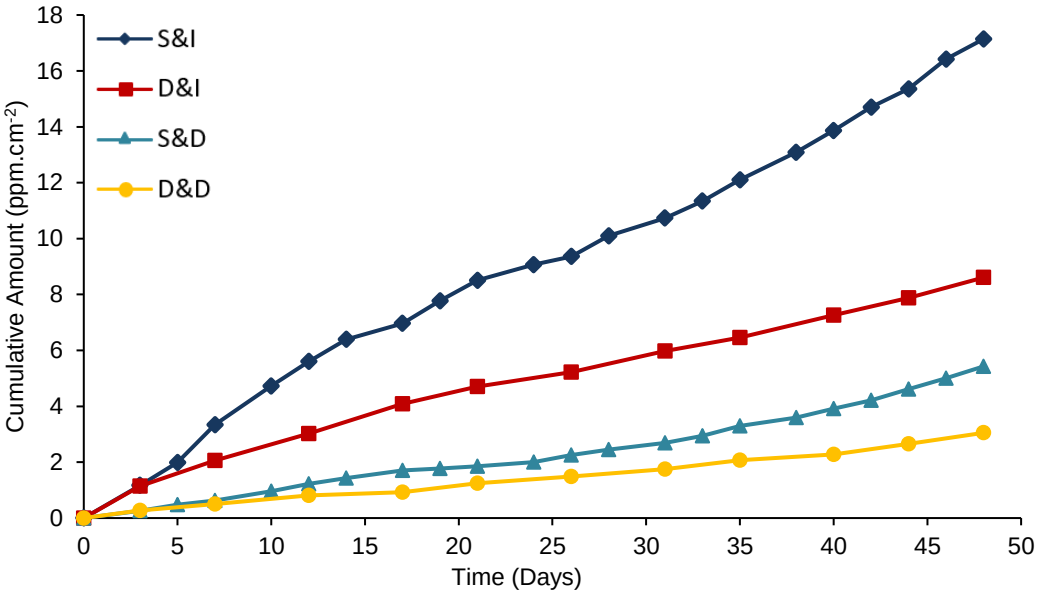

Figure 27. Average cumulative PO_4^{3-} release per surface area over time in tap water at 30 °C. *Error bars removed to see the fluctuations in results.*

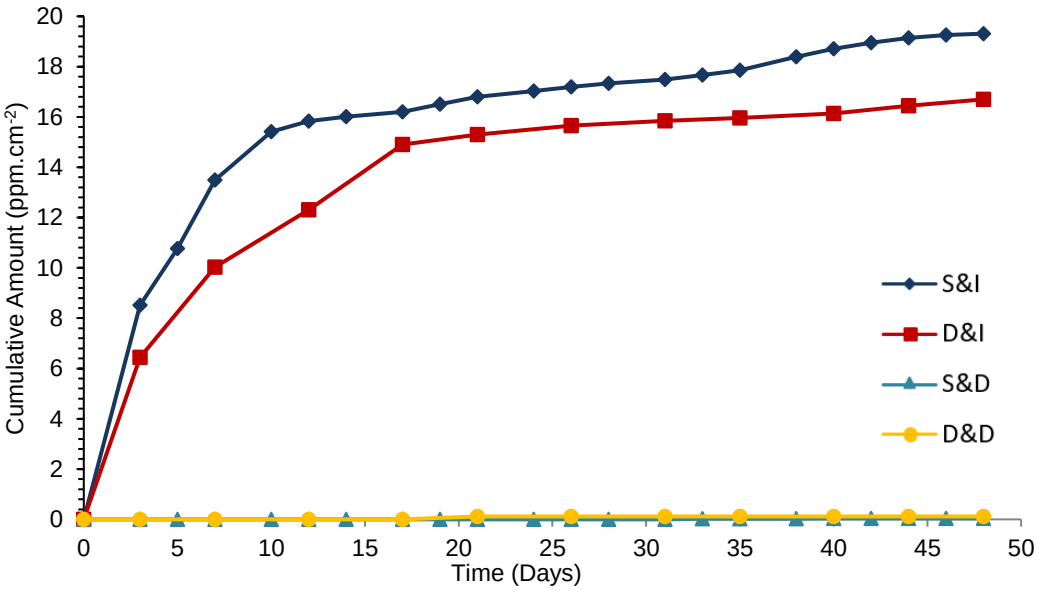

Figure 28. Average cumulative $P_3O_9^{3-}$ release per surface area over time in tap water at 30 °C. Error bars removed to see the fluctuations in results.

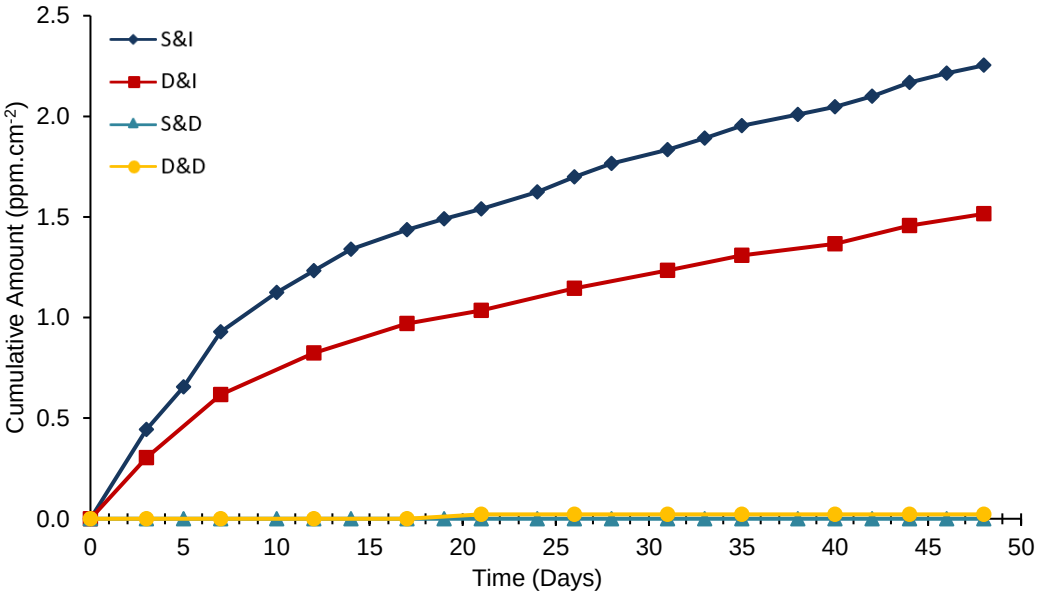

Figure 29. Average cumulative $P_2O_7^{4-}$ release per surface area over time in tap water at 30 °C. Error bars removed to see the fluctuations in results. Error bars removed to see the fluctuations in results.

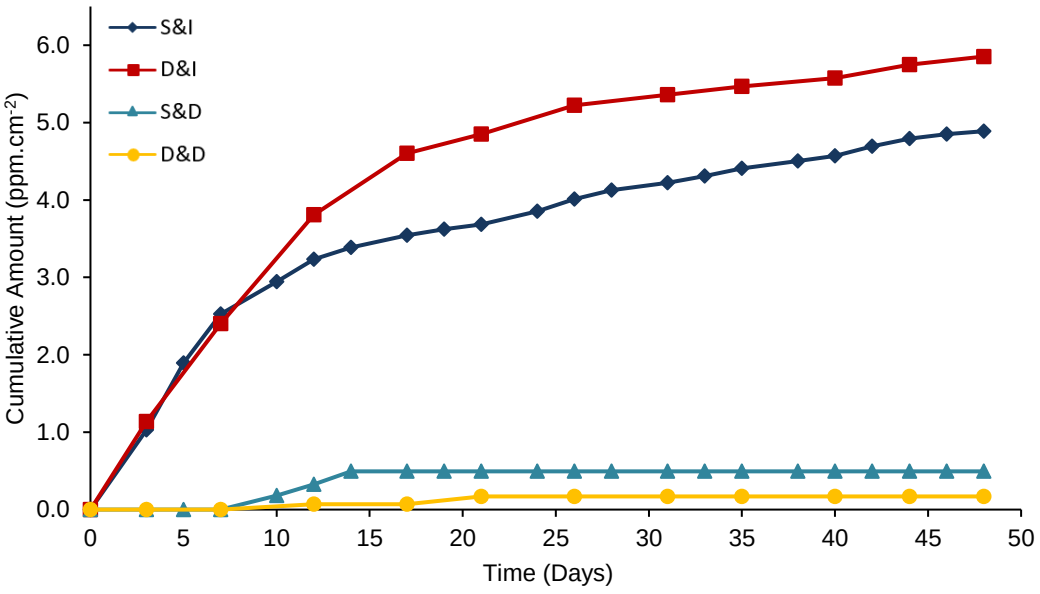

Figure 30. Average cumulative $P_3O_{10}^{5-}$ release per surface area over time in tap water at 30 °C. Error bars removed to see the fluctuations in results. Error bars removed to see the fluctuations in results.

Table 4. Table to show the cumulative phosphate ion release for tap water immersions on alternate days.

	Cumulative Amount in Tap Water				
	Time (days)	**PO_4^{3-}**	**$P_3O_9^{3-}$**	**$P_2O_7^{4-}$**	**$P_3O_{10}^{5-}$**
SI	3	1.17	8.52	0.44	1.03
	7	3.34	13.49	0.93	2.53
	17	6.96	16.20	1.44	3.54
	21	8.51	16.79	1.54	3.68
	31	10.73	17.49	1.83	4.22
	35	12.10	17.86	1.95	4.41
	44	15.36	19.14	2.17	4.79
	48	17.14	19.31	2.25	4.89
DI	3	0.26	0.00	0.00	0.00
	7	0.63	0.00	0.00	0.00
	17	1.86	0.00	0.00	0.49
	21	2.68	0.00	0.00	0.49
	31	3.30	0.02	0.00	0.49
	35	3.30	0.02	0.00	0.49
	44	4.62	0.04	0.00	0.49
	48	5.43	0.04	0.00	0.49
SD	3	1.15	6.44	0.30	1.14
	7	2.06	10.03	0.62	2.40
	17	4.09	14.90	0.97	4.60
	21	4.70	15.30	1.04	4.85
	31	5.97	15.85	1.23	5.36
	35	6.45	15.96	1.31	5.47
	44	7.88	16.44	1.46	5.75
	48	8.61	16.70	1.52	5.85
DD	3	0.27	0.00	0.00	0.00
	7	0.51	0.00	0.00	0.00
	17	0.92	0.00	0.00	0.07
	21	1.24	0.12	0.02	0.17
	31	1.75	0.12	0.02	0.17
	35	2.07	0.12	0.02	0.17
	44	2.65	0.12	0.02	0.17
	48	3.05	0.12	0.02	0.17

Table 5. Table to show the cumulative phosphate ion release for deionised water immersions on alternate days.

	Cumulative Amount in Deionised Water				
	Time (days)	**PO_4^{3-}**	**$P_3O_9^{3-}$**	**$P_2O_7^{4-}$**	**$P_3O_{10}^{5-}$**
SI	3	9.35	146	3.25	11.47
	7	12.93	203	5.19	18.33
	17	27.52	372	8.65	59.74
	21	38.48	510	9.37	85.36
	31	93.32	880	10.96	164
	35	105	1003	11.19	184
	45	137	1340	12.12	244
	49	150	1492	12.94	270
DI	3	2.32	0.76	0.02	0.55
	7	7.25	1.54	0.09	1.97
	17	10.30	2.70	0.17	3.03
	21	12.02	3.50	0.20	3.87
	31	14.22	5.44	0.51	5.75
	35	14.90	7.14	0.78	6.17
	45	16.16	10.17	1.11	6.93
	49	16.75	12.17	1.38	7.36
SD	3	8.96	137	3.11	11.96
	7	13.77	205	4.55	18.21
	17	21.46	311	6.56	27.97
	21	24.69	361	7.09	39.53
	31	57.38	553	8.15	78.05
	35	62.53	619	8.46	90.22
	45	74.33	794	10.81	125
	49	79.88	872	11.77	140
DD	3	1.06	0.18	0.00	0.17
	7	1.88	0.60	0.00	0.34
	17	7.86	9.18	0.20	3.71
	21	8.28	9.43	0.22	3.98
	31	9.37	10.11	0.75	4.68
	35	9.64	10.59	0.84	4.83
	45	10.14	11.62	1.03	5.16
	49	10.33	12.34	1.18	5.31

Figure 27 to Figure 30 depict the anion release observed for the four experimental conditions when using tap water as the immersion media. For the tested static conditions, it was observed a peak release at around day 3, which is in accordance with past results (collected for shorter periods of time). This initial high level is easily seen for all the anions except PO_4^{3-}. On the other hand, this boost was not easily detected when dynamic working conditions were used. Additionally, for all the four tested conditions, it was observed a fluctuation if the amounts over time with peak releases occurring occasionally.

It is considered that the initial hight levels is due to the typical glass dissolution stages observed for this type of glass in aqueous media. After a relatively fast initial dissolution rate there is a drop-in dissolution rate. It is considered that both stages are dominated by different mechanisms, with the first being controlled by water diffusion and ion-exchange at very short times (inter-diffusion and hydrolysis phenomena), and the second controlled by the progressive saturation of the solution, formation/precipitation of secondary products and various surface layers, water diffusion into the glass, etc. Therefore, this might explain the differences observed for the dissolution profiles obtained for static and dynamic conditions (with the last having water continuously flowing through the rig).

Larger amounts of polyphosphates have been released when working under static conditions, with $P_3O_9^{3-}$ being the most abundant anion for both immersing the glass all the time and drying it when not in use. In fact, the larger

amounts observed for static testing could be somehow anticipated, considering the saturation phenomena expected for this type of layout.

Under dynamic conditions, PO_4^{3-} was the only anion being continuously detected over time. This result was unexpected because higher order polyphosphates have been previously detected in similar conditions and reported elsewhere (please refer to past UCL reports). For the particular case of PO_4^{3-}, and considering all the tested conditions, the total amount released was always below 6.5 ppm for every 2-3 days of immersion (with the highest values observed for the static conditions). Although high order polyphosphates have not been detected when using dynamic conditions, some differences were observed for the static layout: (i) $P_2O_7^{4-}$ and $P_3O_9^{3-}$showed a peak release within the first days of testing (usually at around 3 days of immersion); (ii) $P_3O_{10}^{5-}$ showed a peak release at around day 3 when the glass was immersed all the time; (iii) $P_3O_{10}^{5-}$ showed a peak release at around day 12 when the glass was dried when not in use.

Overall, when using dynamic working conditions, it was observed a decrease in the total amount of species detected in the water collected. This is in accordance to what was expected considering that water was continually flowing through the rig. For this particular methodology, $P_3O_{10}^{5-}$ (which would be the most relevant anion[1]) has not been detected and conclusions became hard to be drawn. Nevertheless, and considering static working conditions, it seems that drying the glass when not in use does not negatively affect the tripolyphosphate release.

[1] From past experiments it was found that tripolyphosphate anion ($P_3O_{10}^{5-}$) was the polyphosphate able to achieve the best threshold inhibition.

3.3.2.1 Phosphate anion release measurements – Deionised Water

All graphs error bars present, too small to be seen.

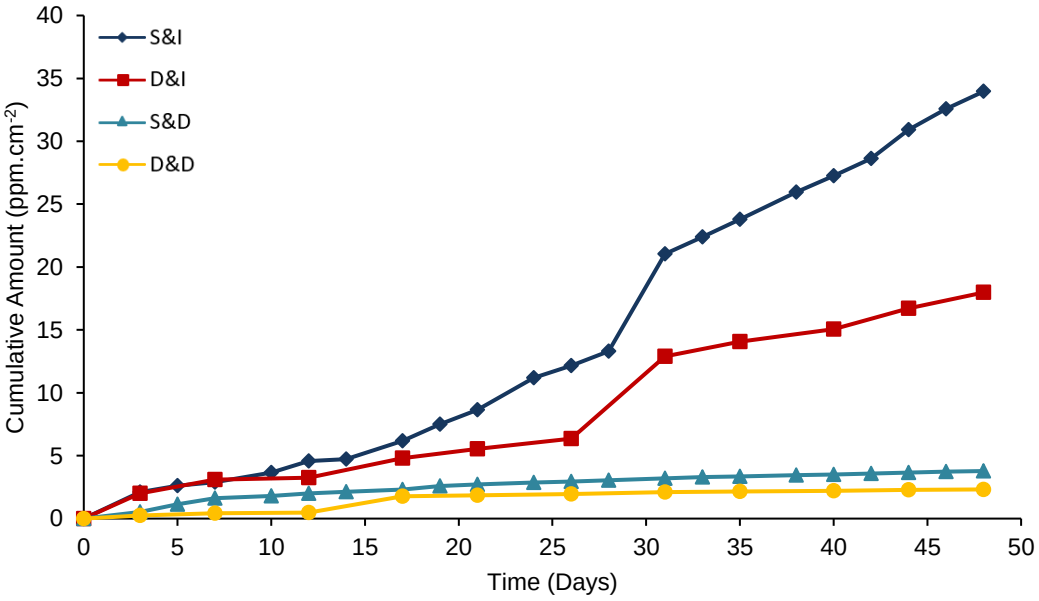

Figure 31. Average cumulative PO_4^{3-} release per surface area over time in deionised water at 30 °C.

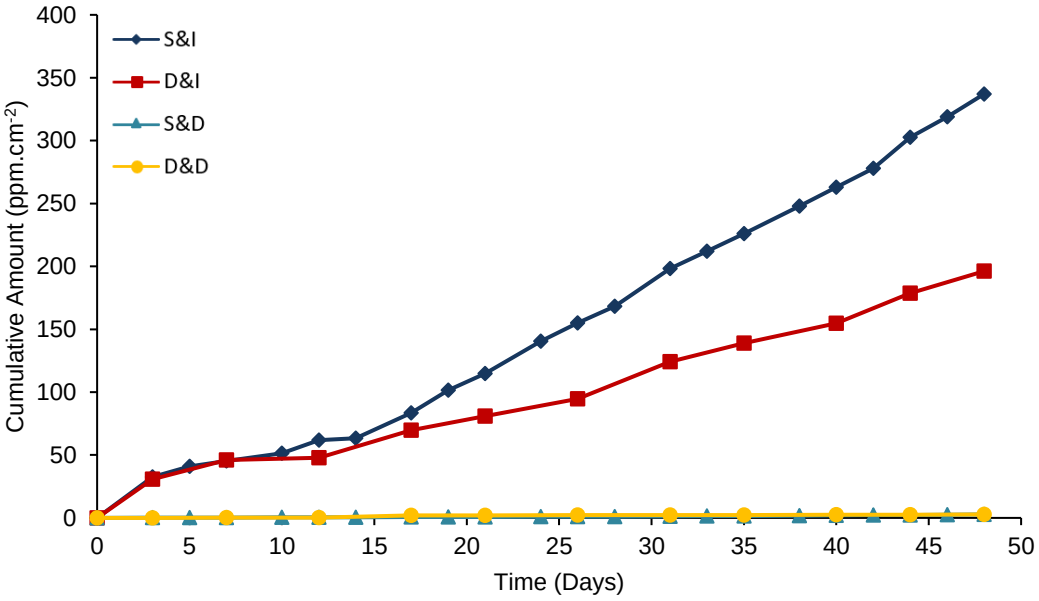

Figure 32. Average cumulative $P_3O_9^{3-}$ release per surface area over time in deionised water at 30 °C.

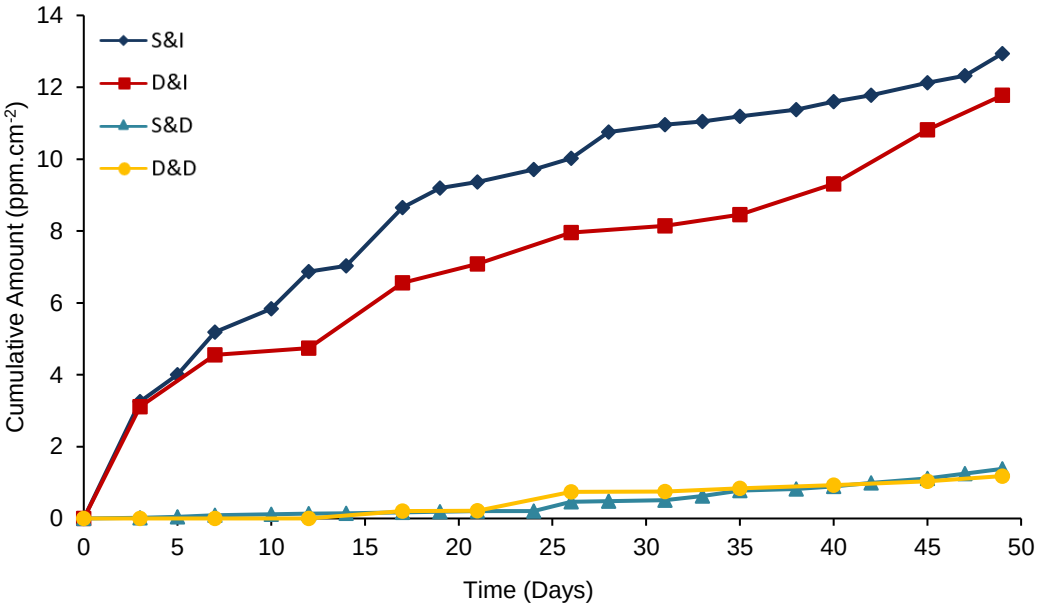

Figure 33. Average cumulative $P_2O_7^{4-}$ release per surface area over time in ionised water at 30 °C.

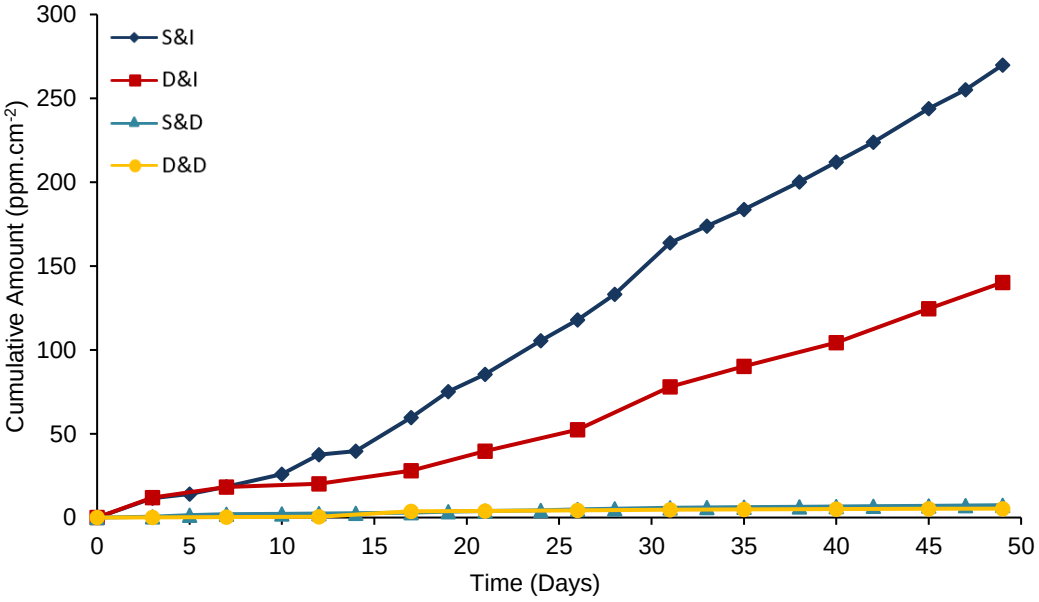

Figure 34. Average cumulative $P_3O_{10}^{5-}$ release per surface area over time in ionised water at 30 °C.

Figure 31 to Figure 34 depict the anion release (cumulative amounts per surface area) observed for the four experimental conditions when using deionised water as the immersion media. It is important to emphasise that, contrary to what was observed with (dynamic) tap water immersion, all four phosphate anions have been detected during this essay, independently on the experimental conditions used (static or dynamic).

Similar observations to those for tap water testing have been made for the static conditions: it was observed an initial peak release at the initial days of immersion (usually at around day 3). As before the initial boost in the degradation is due to the typical dissolution stage for this type of glass in aqueous media. However, unlike with the tap water degradation, a second peak was also noticed at around day 31 for which we don't have a direct explanation. It could be the case of high order polyphosphates degrading to PO_4^{3-} but all the solutions have been preserved at 4 °C to avoid that occurrence, this peak is also observed for $P_3O_9^{3-}$ and $P_3O_{10}^{5-}$, and there is no further evidence to support this hypothesis. Thus, we consider this behaviour to be related to the diffusion processes occurring in the glass surface and bulk structure which suffer changes over time. Noteworthy, the dissolution rate was maintained fairly high with irregular increase and decrease in dissolution rates (as observed for tap water testing). Higher dissolution rate was observed for degradation in deionised water due to the absence of ions in the water.

As before, larger amounts of polyphosphates have been released when working under static conditions, with $P_3O_9^{3-}$ being the most abundant anion for both immersing the glass all the time and drying it when not in use.

Under dynamic conditions, when immersing the glass all the time the typical initial peak previously observed is particularly noticeable for the case of PO_4^{3-} (which peaks its maximum at around 5 days of immersion). Noteworthy, PO_4^{3-} was the most abundant anion in the first 30 days of immersion after which $P_3O_9^{3-}$ becomes the most abundant one.

Under dynamic conditions, when drying the glass when not in use it is observed a peak release for all the anions but $P_2O_7^{4-}$ at around 17 days of immersion. For the latter this boost release was detected for 26 days of immersion instead. It was also interesting to see that during dried when not in used cyclic phosphates such as $P_3O_9^{3-}$ was observed the least and sing and short chain phosphate was released more. This suggests that repeated drying and reusing of the glass will not be as effective in releasing phosphates. Further dissolutions did show that eventual continual immersion showed comparable phosphate release but these continual intermittent drying is likely to effect phosphate release. This may be due to the surface of the glass being dried and forming spaces which when immersed back into water requiring time to form hydration layer. It may also be due to the depletion of ions near the surface making it more difficult for phosphates to diffuse out.

It was noticed that some samples frozen when in the fridge waiting for their analysis (depending on the rack where they were stored). This occurrence seems unlikely to explain this observation but apart from it no other change or occurrence was detected that could justify this behaviour for the glass. Any case, one has to bear in mind this has been a one-time testing and so it is plausible that slightly differences could occur if repeating the testing.

Nevertheless, the main conclusions shouldn’t be different to those herein drawn.

Overall, and considering the polyphosphates concentration individually and over time, it seems that drying the glass when not in use does not affect negatively the anions release (or the mostly important tripolyphosphate release).

3.3.3 Effect of pH on phosphate glass discs

3.3.3.1 pH Measurements

A prior note should be made before discussing the results obtained. Ultrapure water (UPW) has been used because we wanted to test the influence of the pH variation in the glass degradation. In general terms, UPW refers to water which has been purified to the highest standards by removing almost all contaminants such as organic and inorganic compounds, dissolved and particulate matter, volatile and non-volatile, reactive and inert, hydrophilic and hydrophobic, and dissolved gases. By using this type of water, we then may find correlations between the pH used and the glass properties observed. Because all the conductive components have been removed, UPW is very low-conductive. Plus, it is prone to temperature and contamination effects (such as absorption of CO_2 from the air and the formation of carbonic acid in the water, which would reduce the water pH). Overall, accurate pH measurements are very difficult to achieve under the circumstances here described. Achieving accurate and reliable readings using a traditional pH analyser is challenging and this fact should be taken into account when considering the variability of pH values measured during our experiments: pH 5.73-5.90 and 8.11-8.31.

3.3.3.2 Weight loss when immersed in different pH

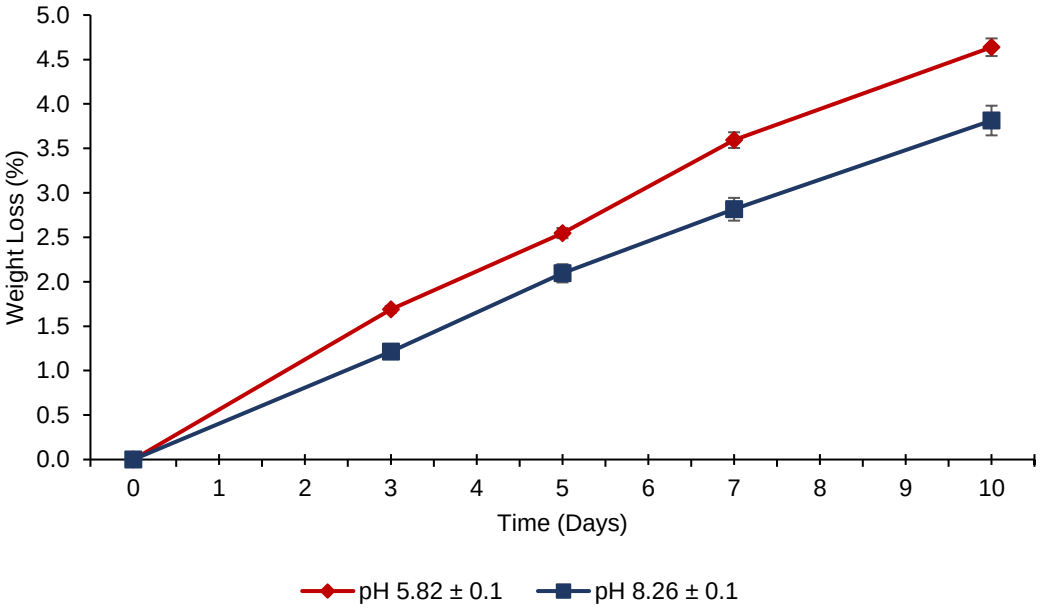

Figure 35. Average percentage weight loss during static immersion in pH 5.82 and 8.26 at 30 °C

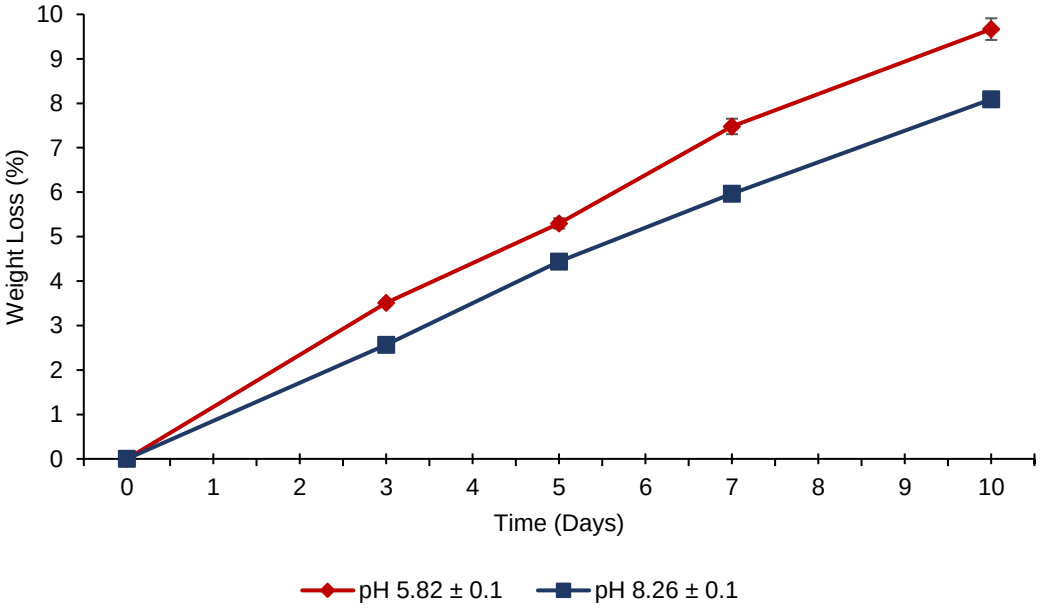

Figure 36. Average weight loss per unit during static immersion in pH 5.82 and 8.26 at 30 °C.

Table 6. Total weight loss (values in %) after 7 days and 10 days of testing with deionized water and ultrapure water.

		Static Immersion	
		7 days	**10 days**
Deionised water	---	1.96	2.61
Ultrapure water	pH 5.82	3.59	4.64
	pH 8.26	2.82	3.81

Weight loss is steadily increasing over time and is highly linear. Moreover, the total weight loss is greater when compared to that of tests run in deionised water and in tap water. As seen under tap water and deionised water immersion media. Greater weight loss for when deionised water was used. Hence, it is reasonable to consider that the present values (for UPW testing) would represent an accurate upper bound when calculating lifetime expectancy for the glass. Solely based on the conditions presented (excluding any influences from interfering agents, temperature variations, humidity, pressure, different types of water, etc.) it would be sensible to consider that the glass would last for at least 200 days (215 days if only considering weight loss at day 10).

Greater weight loss was observed with glass discs immersed at lower pH which would be expected since it is known that glass hydrolysis reactions are accelerated in acids which is also observed by Delahaye[116] *et al*. The dissolution rates in lower pH greatly depends on glass composition, as observed by Björkvik[117] *et al*. glass with higher silica content remaining unreacted lower pH promoted release of Na, Ca and P.

Using the hydration model to explain greater dissolution at lower pH due to protonated phosphate chains which disrupts the crosslinks between the chains allows water to penetrated into the glass much faster causing accelerated dissolution,[31] at lower pH, the concentration of H+ increases allowing faster hydration of glass causing increase in bond breakage. The increase in phosphate release in acidic solutions further lower the pH of the glass which is also seen by Lixin[118] *et al*. and Massera[119] *et al*. Noteworthy, after 10 days of testing the difference between the total weight loss observed for the two tested conditions is less than 1% ($\Delta = 4.64 - 3.81 = 0.83\%$) (see Table 6). Beating in mind such a small difference, and the fact that 3 replicates have been used for each experiment, it could be concluded that different pH, within the range investigated, does not have a significant effect on the glass disc weight loss. However, running a t-test (two-sample assuming unequal variances) it is concluded that the small difference obtained is statistically significant, and so the values are different. This conclusion is also true for the values found for 3, 5 and 7 days of testing. Thus, it is feasible to think it would be true for any values collected if continuing the testing for longer periods of time. This means the treatment applied (two different pH conditions) gives different degradation rates and so they should be considered independently.

3.3.3.3 Phosphate anion release measurements

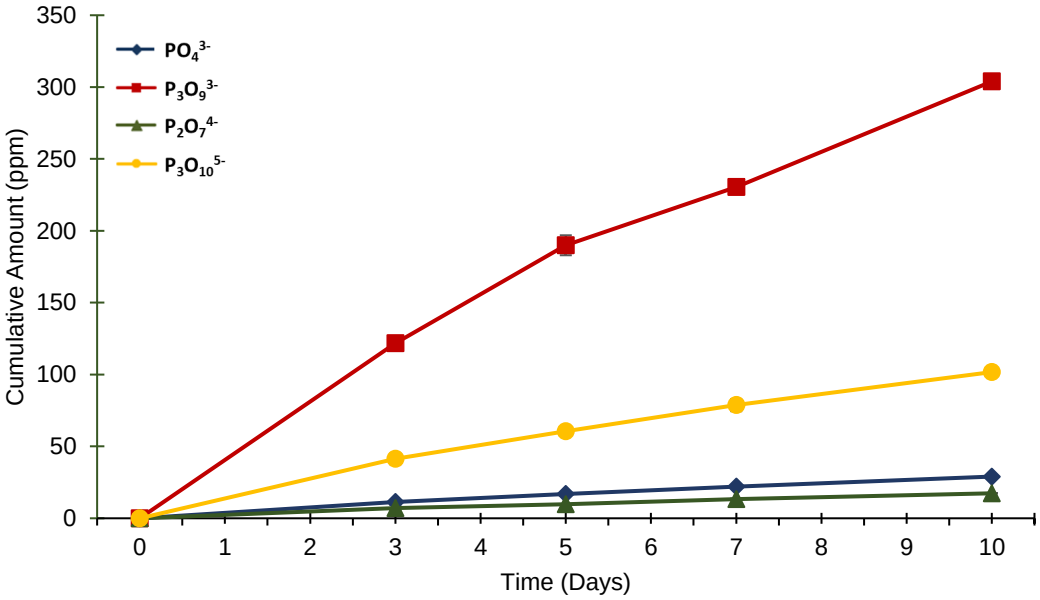

Figure 37. Average phosphate anions released during 7-day static immersion tests at pH 5.73-5.90

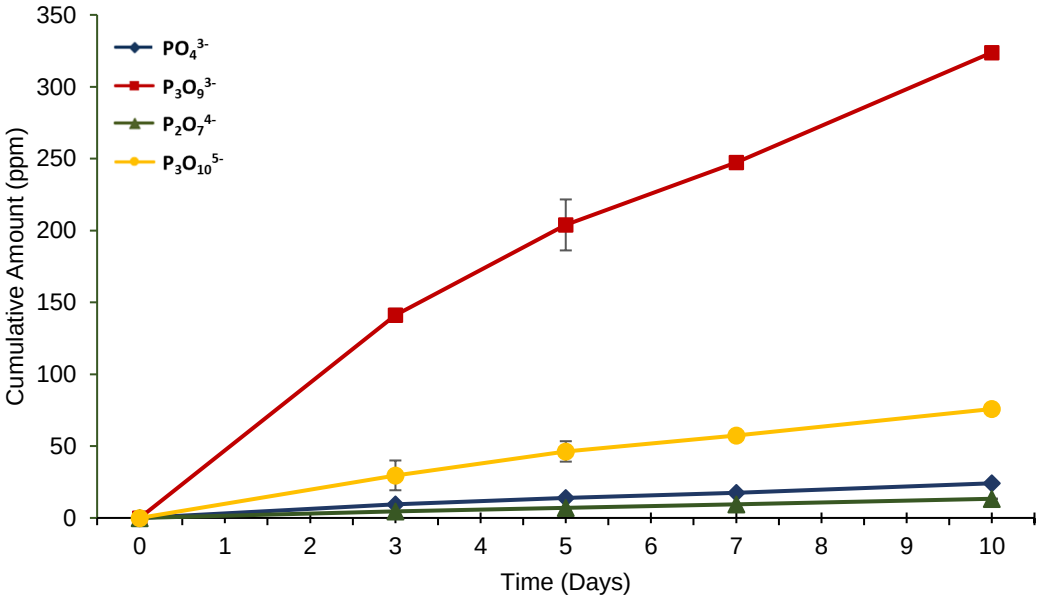

Figure 38. Average phosphate anions released during 7-day static immersion tests at pH 8.11-8.31

Table 7. Total phosphate release in ppm for the glass when studied under static immersion conditions, at 30 °C.

	Tap water		Deionised water		Ultrapure water	
					pH 5.73-5.90	pH 8.11-8.31
	10 days	49 days	10 days	49 days	10 days	10 days
PO_4^{3-}	21.2	76.8	16.3	150	29.0	24.1
$P_3O_9^{3-}$	69.1	86.6	229	1491	304	324
$P_2O_7^{4-}$	5.04	10.1	5.84	13.0	17.4	13.3
$P_3O_{10}^{5-}$	13.2	22.0	25.8	270	102	75.8

Anion Chromatography was carried out on the samples collected. In Figure 37 and Figure 38 it is clear that $P_3O_9^{3-}$ was released in greatest amounts followed by $P_3O_{10}^{5-}$, PO_4^{3-} and $P_2O_7^{4-}$. This anion release is a typical pattern also observed with previous immersion tests. It was interesting to observe that in this experiment with varied pH, we saw the greatest release in all phosphate ions in comparison to previous immersion tests. Also, with the exception for the $P_3O_9^{3-}$ anion, greater amounts were obtained when lower pH was used (pH 5.73-5.90). Again, these observations are in line with the fact that glass hydrolysis reactions are accelerated in acids and so higher concentrations (for the same period of time) should be observed. As previously seen, a peak release was found at around day 3, after which there is a drop in glass dissolution rate.

3.3.4 Final comments

With the above experimental and results when observing P50Ca40Na10 glass composition discs it has relatively constant dissolution property at weakly acidic and alkaline conditions which can show how it may behave in normal household (*ca.* pH 6.5-8.5), deionised (*ca.* pH 7) and bottled water (ca. pH 5-8). The above results confirmed our predictions about faster dissolution and greater ion release for lower pH, deionised, and static conditions. Overall, the dissolution mechanism was expected to be first, sodium ion loss followed up by protonated hydrogen absorption by the glass causing further cleavage of crosslinks and phosphate bonds with the preference of $P_3O_9^{3-}$ and PO_4^{3-} ions being released, this immersion study follows the trend of previous dissolution studies carried out by I.Ahmed[115] and H.Gao[30] . General phosphate ion release proportions were very similar across all experiments due to the phosphate presence is greatly determined by the glass composition and the network modifiers present. This shows that the P50Ca40Na10 glass composition this thesis suggests, is an excellent candidate for calcite inhibition is able to undergo controlled phosphate release for calcite inhibition in different conditions.

Chapter 4

Physical Analysis of Phosphate Based Glass

4 Physical analysis of ternary phosphate glass

4.1 Introduction

This chapter focuses on the physical analysis of the phosphate-based glass used in the previous chapter.

4.2 Experimental methodology

4.2.1 Durability test at varying humidity

Glass disks (n = 3) were first weighed and the baseline weight (M_0) of each recorded. Samples were then placed in an acrylic rack (Figure 39) in a humidity chamber set to a fixed humidity (n = 3). Saturated salt solutions were used to maintain a fixed relative humidity within each humidity chambers. Two relative humidity values were maintained,35 %RH and 75 %RH. Anhydrous calcium chloride was used to make the 35 %RH solution and sodium chloride was used to make the 75 %RH solution[120]. Each salt was added in excess to a beaker with 40 mL of ultra-pure water. The NuAire environment chamber was set at 30 °C where the glass samples were incubated for *ca.* 6 months. Following incubation samples were removed, before the weight of each was again recorded (M_t). Each of the bioglass disks were then transferred back into the same humidity chamber with the fixed humidity, until next measurement was taken.

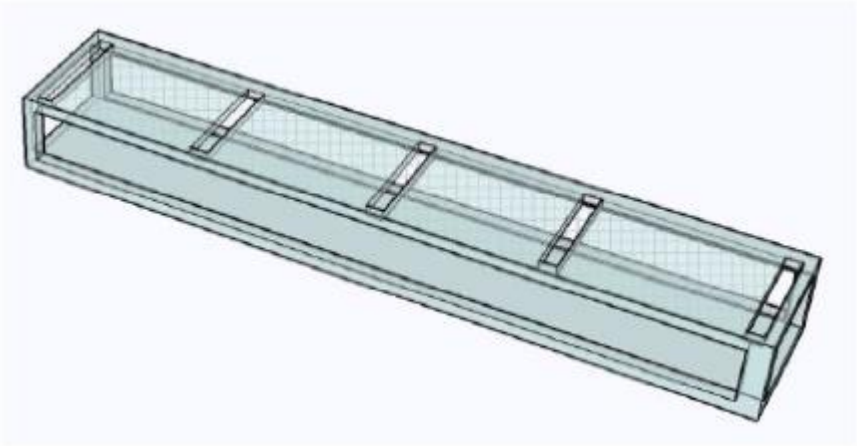

Figure 39. Acrylic Rack for Glass Discs

Figure 40. Air tight humidity chamber with saturated solution providing constant humidity and Tinytag device to record temperature and humidity.

4.2.2 Thermal analysis using differential thermal analysis (DTA) and differential scanning calorimetry

Glass pieces were ground for 20 min using a vibratory agate mill. Three main thermal parameters were measured: Tg the glass transition temperature, Tc the crystallisation temperature and Tm the melting temperature. The analysis was conducted on a Setaram differential thermal analyser (DTA), using an inert nitrogen atmosphere and a heating rate of 20 °C.min^{-1} up to a maximum temperature of 1000 °C. The data were baseline corrected by carrying out a blank run and subtracting this from the data obtained for the sample.

4.2.3 Water contact angle measurements

Water contact angle measurements were performed by using a CAM 200 optical contact angle meter instrument (KSV co, Finland). A special graduated needle (Hamilton co, Nevada, USA) was filled with distilled water to establish the hydrophobicity/hydrophilicity of the prepared and coated glass discs in the normal room temperature environment. Measurements were taken on triplicate samples of zinc glass discs (uncoated glass, PCL coated glass discs and CNT-PCL coated glass discs). The needle was placed in its clamp and was placed above the glass discs surface to ensure water droplet went onto the glass disk. The contact angle measurement was performed on the water droplet that dispersed on the glass discs surface by using the CAM200 shape analysis software and time lapse camera. This procedure was done by measuring the angle for 10 fast readings (40 ms intervals) and 10 slow readings (1 second interval).

4.2.4 Energy dispersive x-ray and scanning electron microscopy

Surface morphology and elemental analysis was done on a Philips XL30 ESEM with an Oxford Instruments EDS detector, and spectra were collected using Oxford Instruments INCA software. EDX was done with working at 20 kV with a working distance of 10 mm, and imaging was carried out at 5 kV and working distance was 10mm.

4.2.5 Biaxial flexural strength testing

Specimens underwent a biaxial flexural strength test (ISO 6872 standard) using a Zwick HC10 servohydraulic Testing frame (Zwick Ltd.). Each glass discs was placed centrally on three metal balls (with the diameter of 3 mm, positioned 120^{o} apart on a support circle with the diameter of 11mm). One side of the glass disc was loaded with a flat punch (diameter of 1.5 mm and length 1mm) at a cross head speed of 1 mm/min until failure occurred. The load to failure (N) was recorded for all twenty samples and the biaxial flexural strength (MPa) was calculated using the following equations (1)-(3).

$$S = -0.2387 \frac{P(X-Y)}{d^2} \quad (1)$$

Where *S* is the maximum tensile strength in Pascals, *P* the total load causing fracture in Newtons and *d* is the specimen thickness at fracture origin in millimetres. [1] X and Y were determined as:

$$X = (1 + v)\ ln(\frac{r_2}{r_3})^2 + [\frac{(1+v)}{2}](\frac{r_2}{r_3})^2 \quad (2)$$

$$Y = (1 + v)\left[1 + ln\left(\frac{r_2}{r_3}\right)^2\right] + (1 + v)(\frac{r_1}{r_3})^2 \quad (3)$$

Where *v* is the Poisson's ratio. The Poisson's ratio = 0.25 was used; r_1 was the radius of the support circle in millimetres; r_2 is the radius of the loaded area in millimetres; r_3 the radius of the specimen in millimetres; d is the specimen thickness at fracture origin in millimetres.

4.3 Results and discussion

4.3.1 Effect of humidity on phosphate-based glass

4.3.1.1 Visual inspection of glass discs during humidity tests

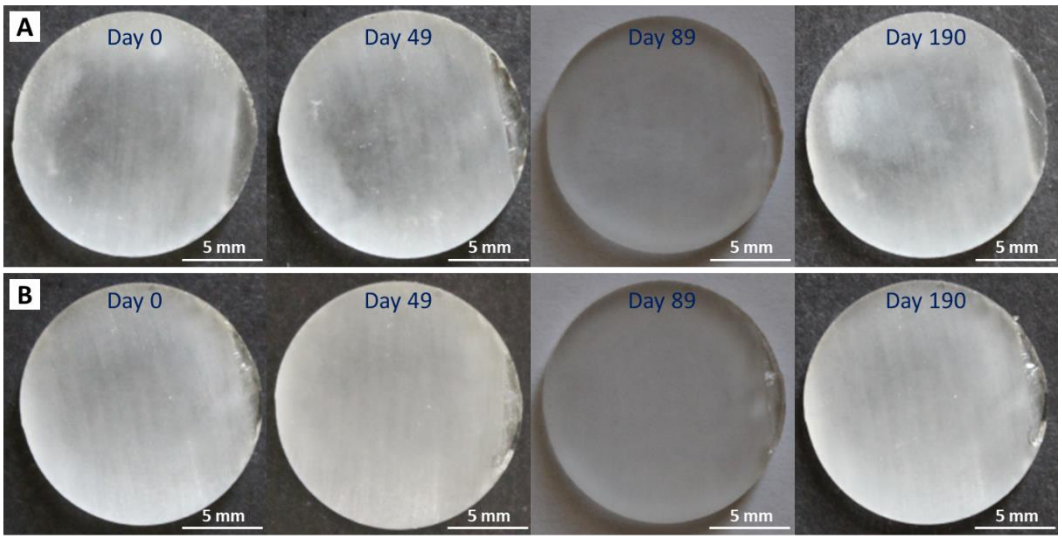

Figure 41. Images of glass discs after denoted days of exposure to A. 35 %RH and B. 75 %RH at 20 °C

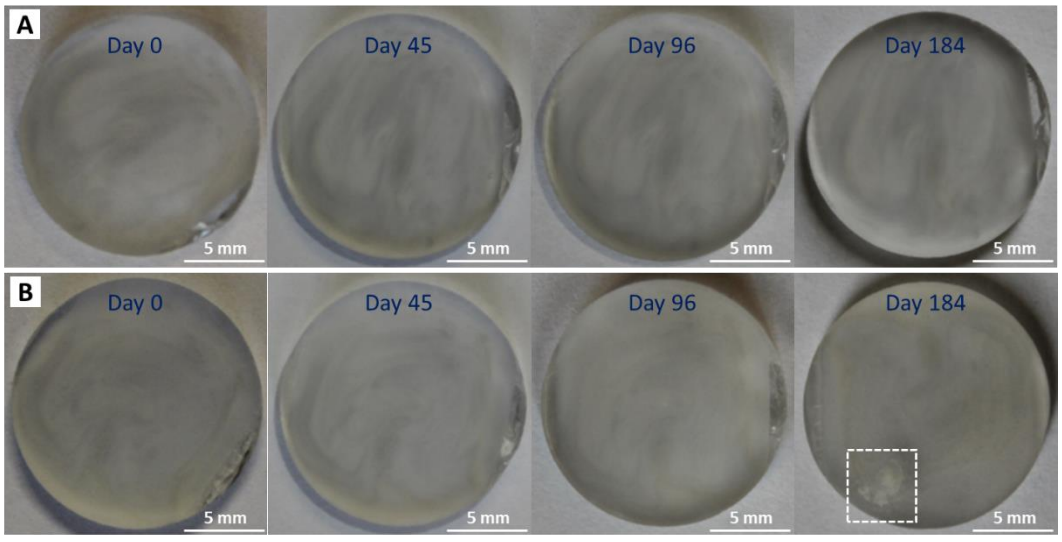

Figure 42. Images of glass discs after denoted days of exposure to A. 35 %RH and B. 75 %RH at 30 °C

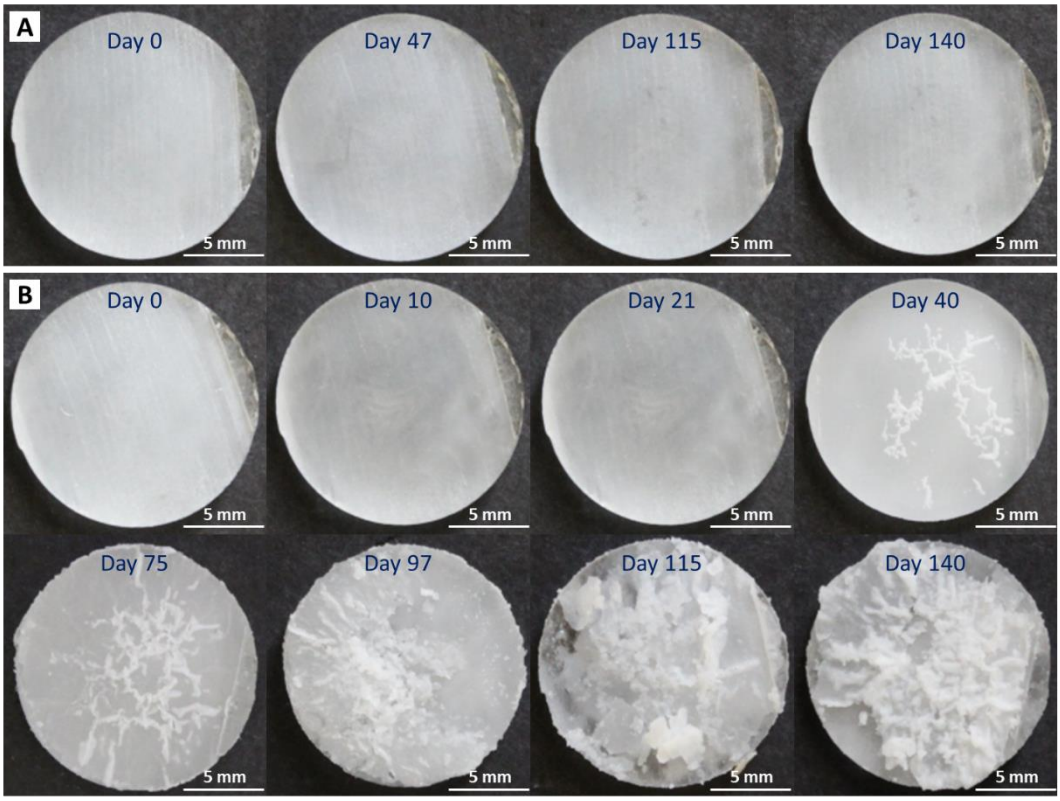

Figure 43. Images of glass discs after denoted days of exposure to A. 35 %RH and B. 75 %RH at 40 °C

Figure 41 to Figure 43 shows the glass discs exposed to 35 and 75 %RH humidity at 20, 30 and 40 °C. There is no visible difference in glass discs at 35 %RH across all temperature and time of exposures. After 184 days of exposure in 75%RH at 30 °C white precipitate is visible, this precipitate is shown much earlier in glass discs exposed to 75%RH at 40 °C. The precipitate was first observed on day 40 in discs exposed to 78%RH at 40 °C and grew in size to cover the whole surface of the glass discs by day 75. The precipitate also grew in volume to extrude from the surface to eventually parts of it falling off the surface on day 115 and above. Precipitates were white, flaky and sticky in consistency. The precipitate formed may be due to the absorption of moisture in the air at higher temperature allowing formation of deposits on the surface.

4.3.1.2 Weight loss data

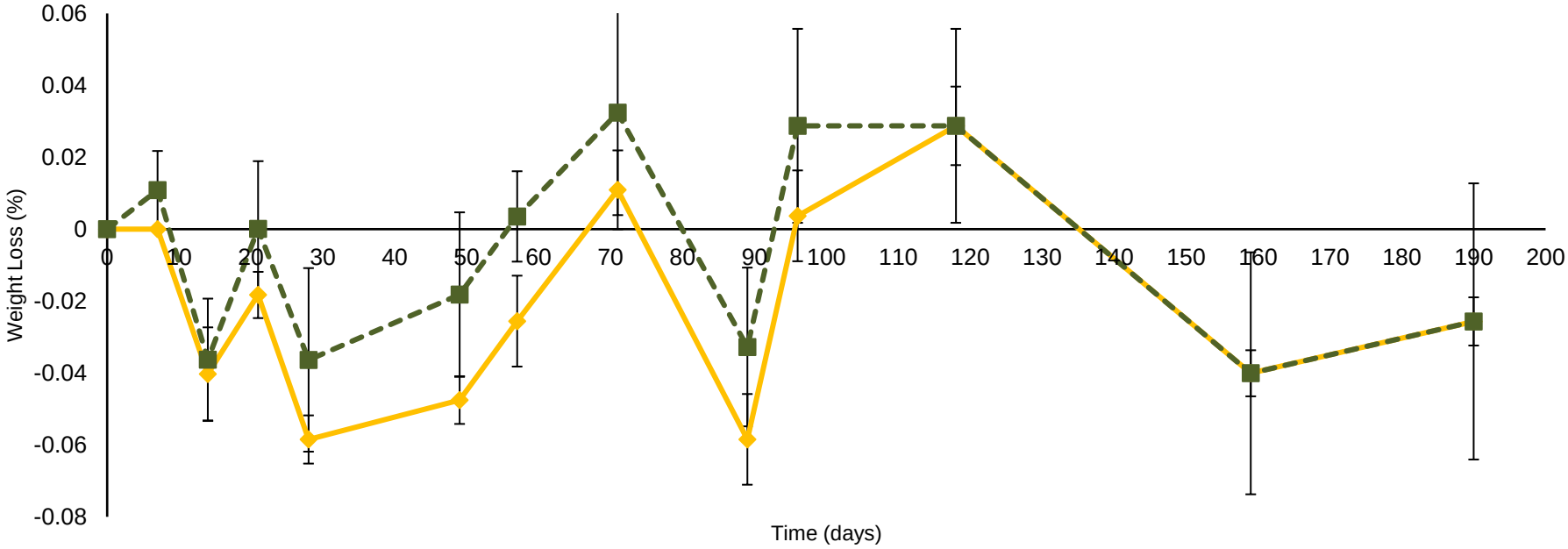

Figure 44. Average percentage weight loss over 190-day period in 35 and 75 %RH at 20 °C

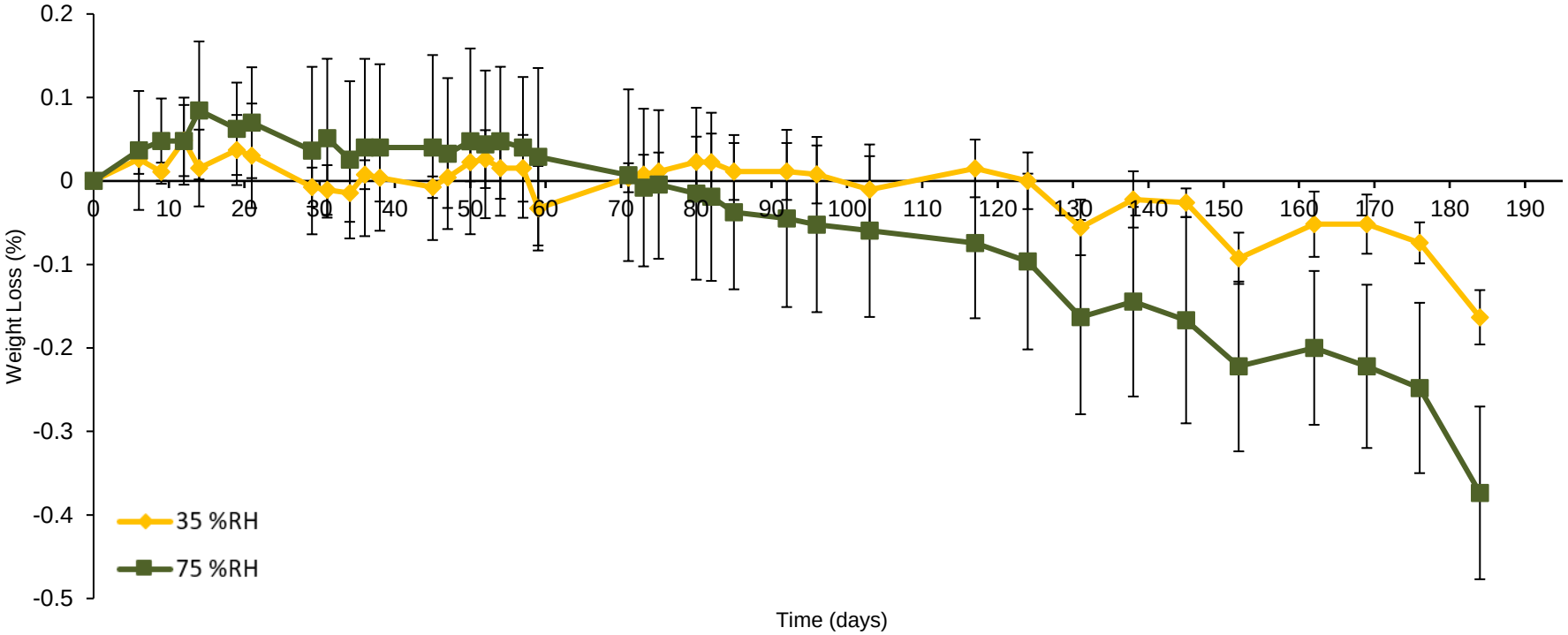

Figure 45. Average percentage weight loss over 190-day period in 35 and 75 %RH at 30 °C

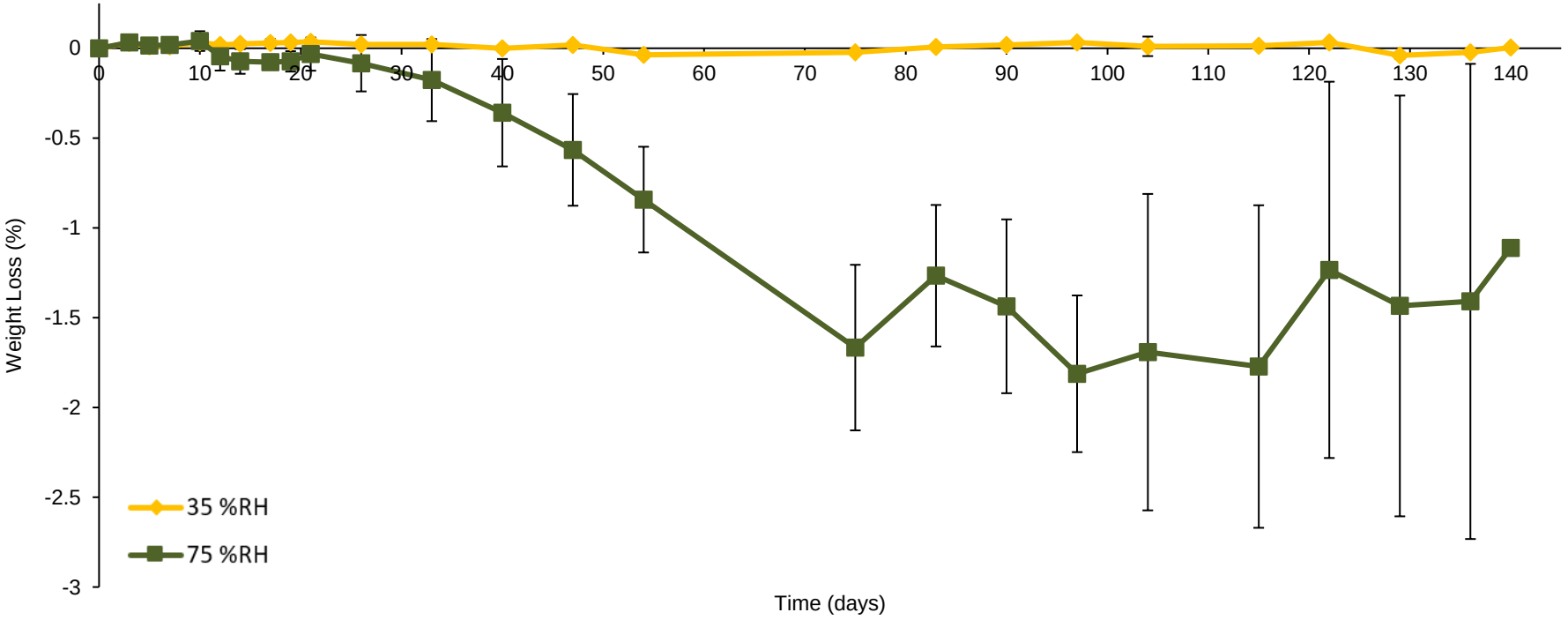

Figure 46. Average percentage weight loss over 190-day period in 35 and 75 %RH at 40 °C

Figure 44 to Figure 46 shows the weight loss of P50Ca50Na10 glass discs exposed to different humidity conditions at 20, 30 and 40 °C. For glass discs in 20 and 30 °C it was found that both humidity levels had very little or negligible effect on mass for the first 3 months, and even after the full 6 months of testing, there was less than 0.4% increase in mass. Glass discs exposed to extreme high temperature of 40 °C showed negligible change at 35%RH, however at 75%RH the weight data fluctuated with an increase of up to 1.8%. The increase in weight is likely to be due to the precipitate formation seen in Figure 43. This shows that the suggested glass discs are durable in structure even in extreme high humidity and temperatures.

4.3.2 Static immersion of glass discs after prolonged exposure to extreme humidity.

The following static immersion tests were carried out to phosphate-based glass discs that was exposed to up to 190 days in 35 %RH and 75 %RH respectively at 20, 30 and 40 °C. The static immersion tests followed the previously carried out static and immersed all the time methodology in 5.1.2.2 for period of 10 days.

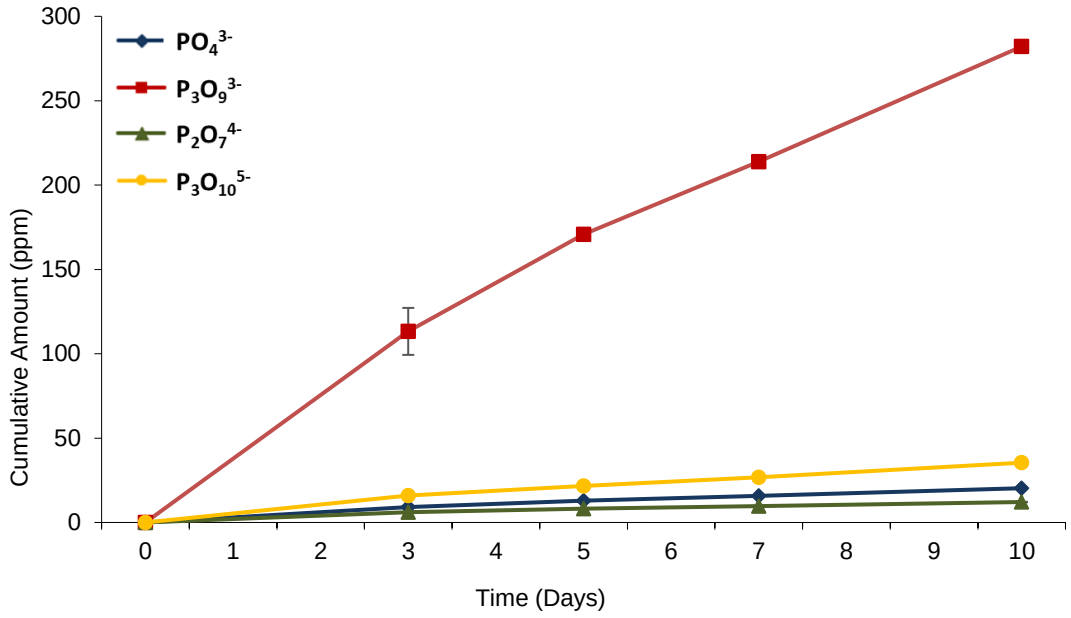

Figure 47. Cumulative phosphates released for phosphate glass exposed to 35 %RH at 20 °C for 190 days, immersed in deionised water for 10-day period.

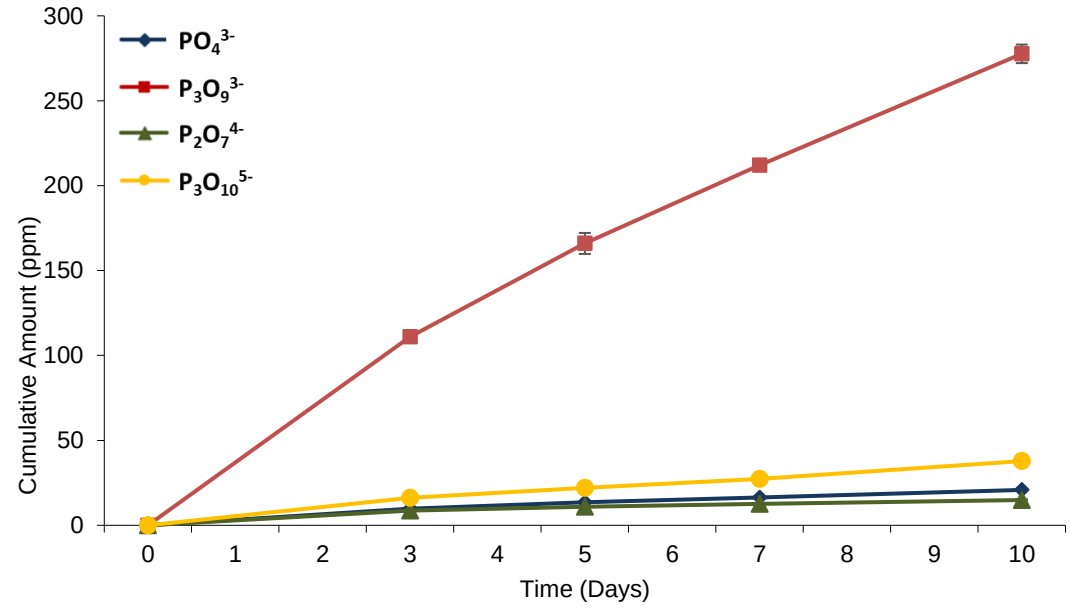

Figure 48. Cumulative phosphates released for phosphate glass exposed to 75 %RH at 20 °C for 190 days, immersed in deionised water for 10-day period.

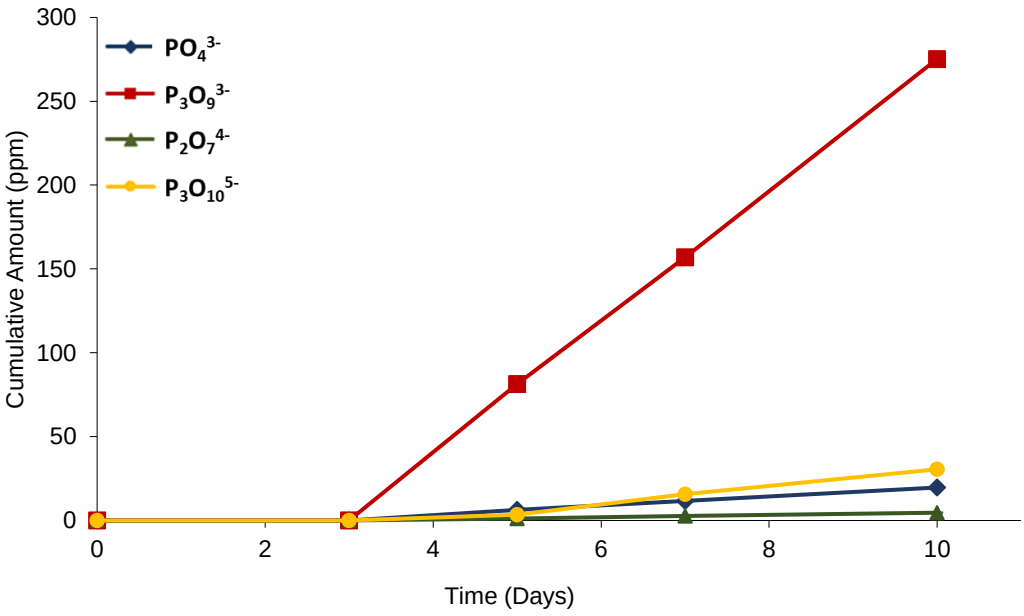

Figure 49. Cumulative phosphates released for phosphate glass exposed to 35 %RH at 30 °C for 184 days, immersed in deionised water for 10-day period.

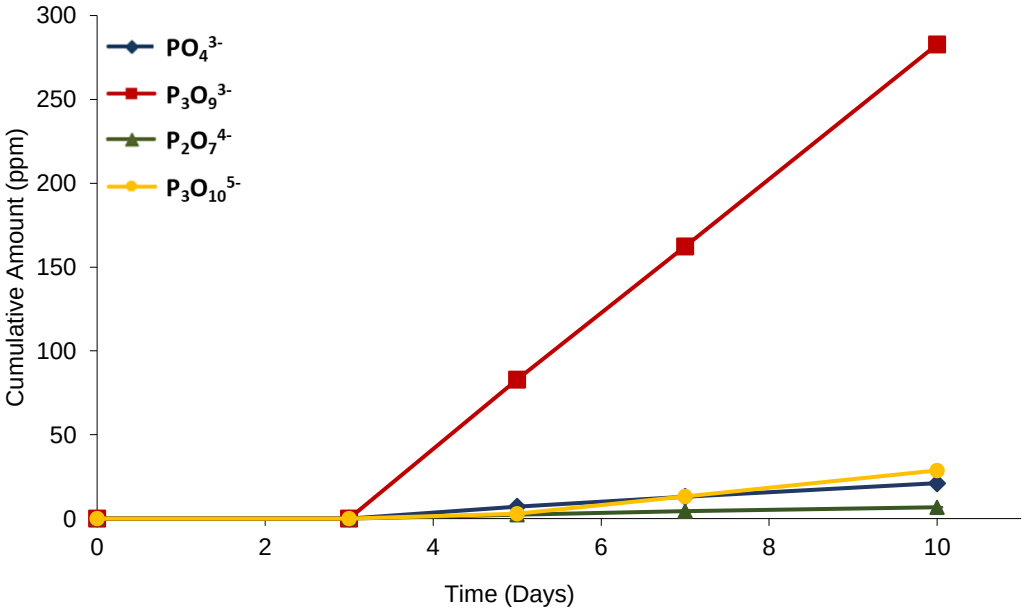

Figure 50. Cumulative phosphates released for phosphate glass exposed to 75 %RH at 30 °C for 184 days, immersed in deionised water for 10-day period.

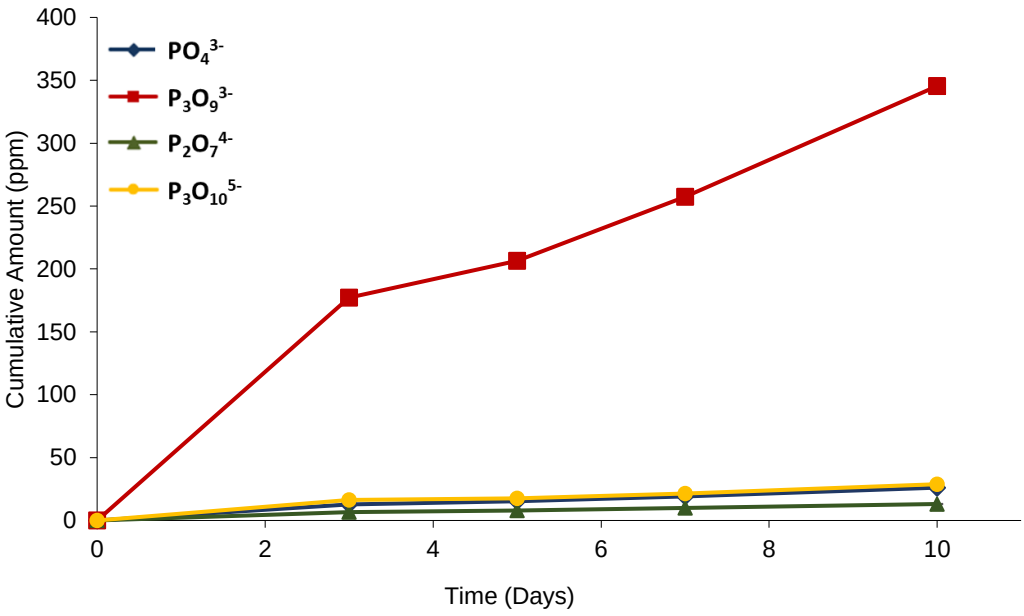

Figure 51. Cumulative phosphates released for phosphate glass exposed to 35 %RH at 40 °C for 140 days, immersed in deionised water for 10-day period.

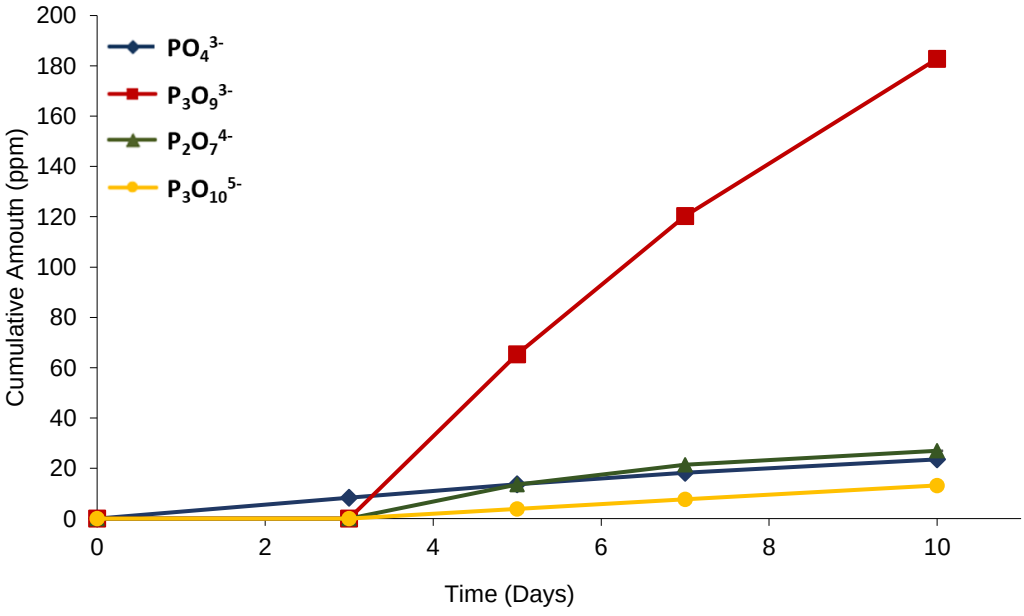

Figure 52. Cumulative phosphates released for phosphate glass exposed to 75 %RH at 40 °C for 140 days, immersed in deionised water for 10-day period.

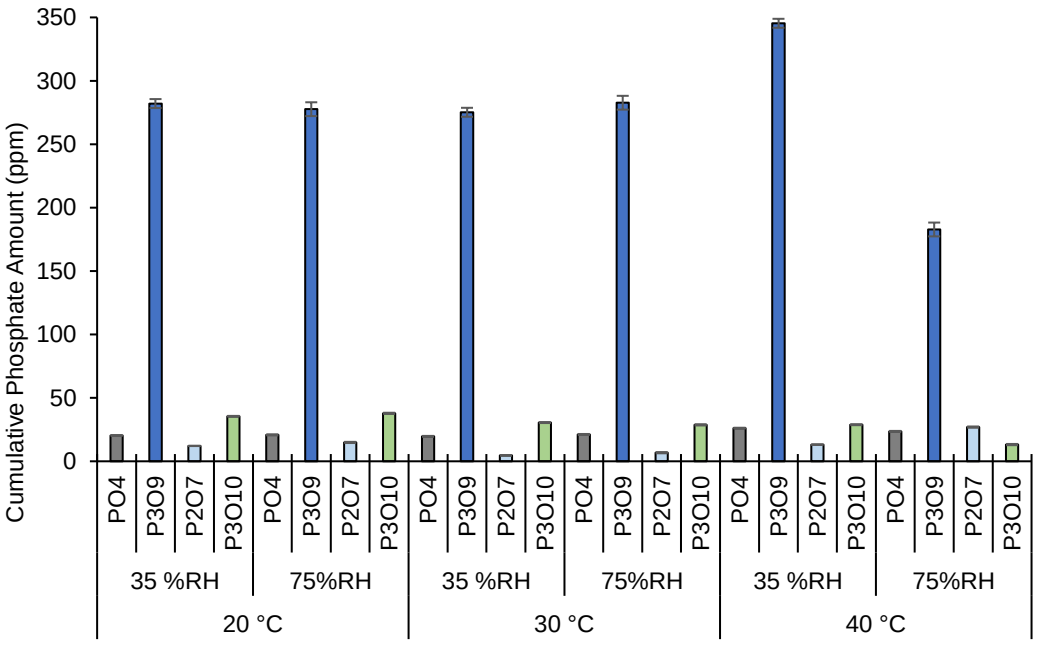

Figure 53. Cumulative amount of phosphate ions released after 10 day static immersion in deionised water.

Figure 47 to Figure 52 shows average cumulative phosphate ion release for glass discs exposed to different humidity and temperatures. As seen in Figure 53 in all cases $P_3O_9^{3-}$ was released the most over 10 day static immersion period. Glass discs in 20 and 30 °C environments showed very similar total phosphate release meaning that the glass discs were not affected by the environment. The glass discs exposed to 30 °C showed no release of ions on day 3 and showed release from day 5 which was also observed for discs in 75% RH at 40 °C which may be due to longer time required for the water to form a hydration layer on glass for dissolution due to surface being dried out or in the case at 40 °C, the formation of the precipitate on glass surface may have effected the dissolution. Discs exposed to 20 °C showed no difference in immersion with previous immersion tests Glass discs at 40 °C and 75%RH showed a 47% decrease in $P_3O_9^{3-}$, 54% decrease in $P_3O_{10}^{5-}$, 10% decrease in

PO_4^{3-} and an increase of 106% in $P_2O_7^{4-}$ when compared to the discs at 40 °C and 35%RH. This means that lower proportion of phosphate were present in the tripolyphosphate ($P_3O_{10}^{5-}$) form which is also required for an effective scale prevention.

Weathering tests for phosphate glass has not been studied extensively and above results gives an insight to their durability at extreme conditions. From the humidity test it can be concluded that the glass is very durable across extreme humidity and temperatures showing very little or no physical change but prolonged exposure to very hot and humid conditions can reduce the dissolution and phosphate release property of the glass.

Table 8. Table showing the total cumulative ppm of phosphate ions released after 10 day immersion.

	20 °C		**30 °C**		**40 °C**	
	35 %RH	**75%RH**	**35 %RH**	**75%RH**	**35 %RH**	**75%RH**
PO4	20.31	20.82	19.66	21.13	26.10	23.54
P3O9	282.09	277.63	275.20	282.74	345.38	182.79
P2O7	12.12	14.87	4.64	6.77	13.10	26.97
P3O10	35.44	37.80	30.53	28.72	28.84	13.19

4.3.3 Differential thermal analysis (DTA)

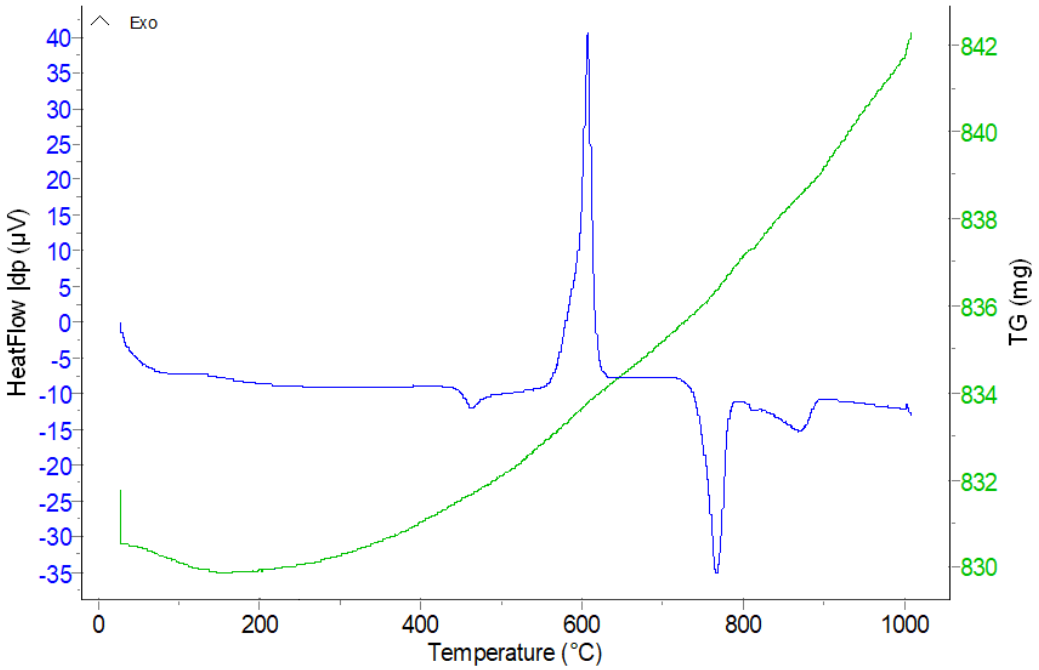

Figure 54. A plot given as result after running differential thermal analysis on P50Ca40Na10

Differential thermal analysis of the P50Ca40Na10 glass discs were carried out by heating glass sample from 300 °C up to 1600 °C at a heating rate of 20 °C/min, to give glass transition temperature (Tg) of 454.81 °C, glass crystallisation temperature (Tc) of 606.81 °C and glass melting temperature of 765.86 °C. It was found that as the CaO increased and Na_2O decreased the Tg and Tc increased which was also seen in research by Samickannian[121] *et al*. and Lee[122] *et al*. this is due to CaO existing as Ca^{2+} forming cross-links between chains. During the process of selection of glass composition, as CaO increased whilst decreasing Na_2O the dissolution rate dramatically changed from few hours (P50Ca10Na40) to more than several months (P50Ca40Na10)

which is also in line with the research by Parsons[123] *et al*. where they observed in decrease from 0.3 to 9E-06 $g.cm^{-2}.g^{-1}$ in degradation rate from 0 CaO to 40 CaO. It was also difficult for them to determine sodium glass degradation due to the speed of the degradation.

4.3.4 Water contact angle

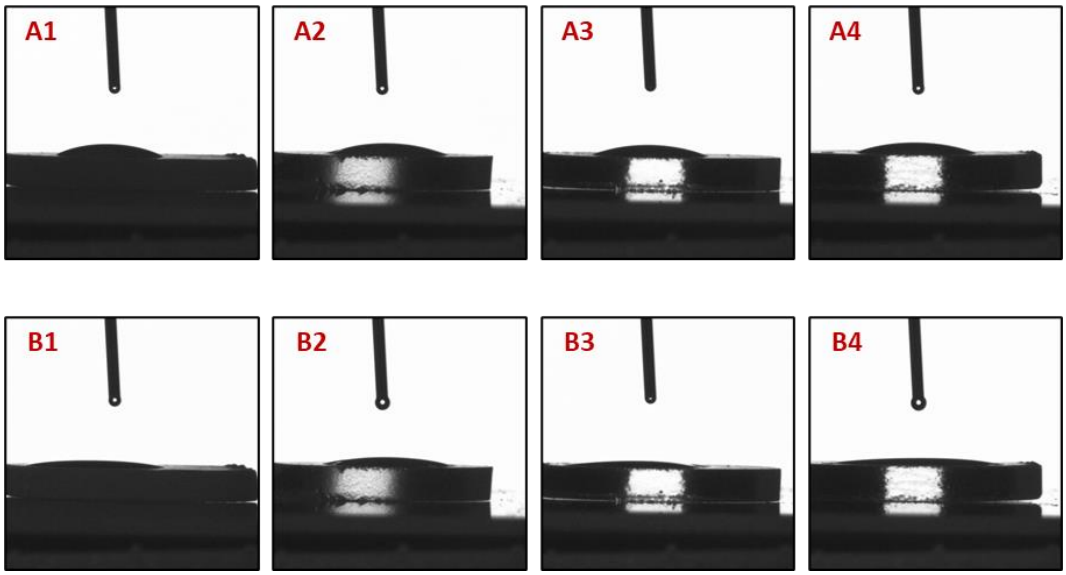

Figure 55. Figures of water contact angle, **A:** when water is first dropped and **B:** up to 3 seconds after A. The numbers after the A or B correlates to glass composition of P50Ca10Na40, P50Ca20Na20, P50Ca30Na20 and P50Ca40Na10 in this order.

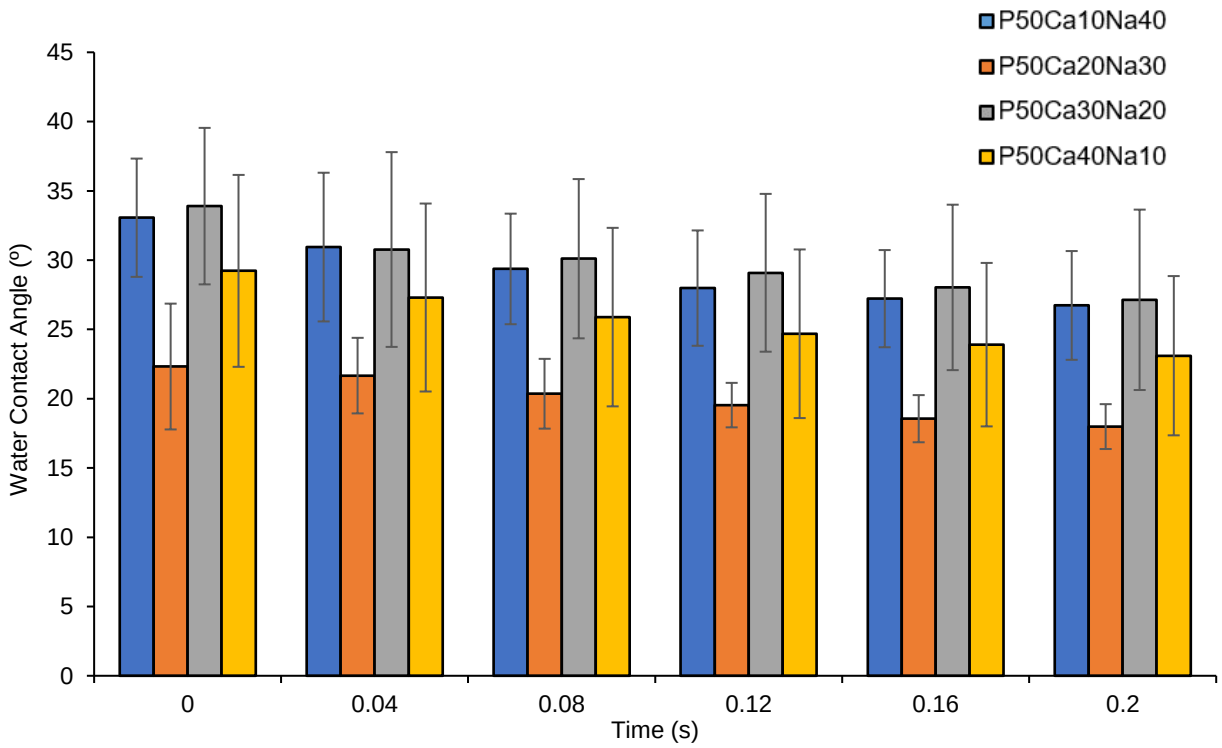

Figure 56. Figures of water contact angle value for phosphate glass.

Figure 55 and Figure 56 shows the water contact angle measurements carried out onto the glass disc surface. From Figure 56 all phosphate ternary glass compositions show water contact angle of less than 35° meaning a hydrophilic surface.[124] The hydrophilic surface of the disc is expected as glass dissolves in water and the presence of ions, formation of hydration layer suggesting a hydrophilic surface. Although there are some differences in the contact angle measurements between different compositions since the values lies within the error bars it is difficult to conclude weather increase or decrease in certain ion results in increase or decrease in hydrophilicity.

4.3.5 Biaxial flexural strength testing

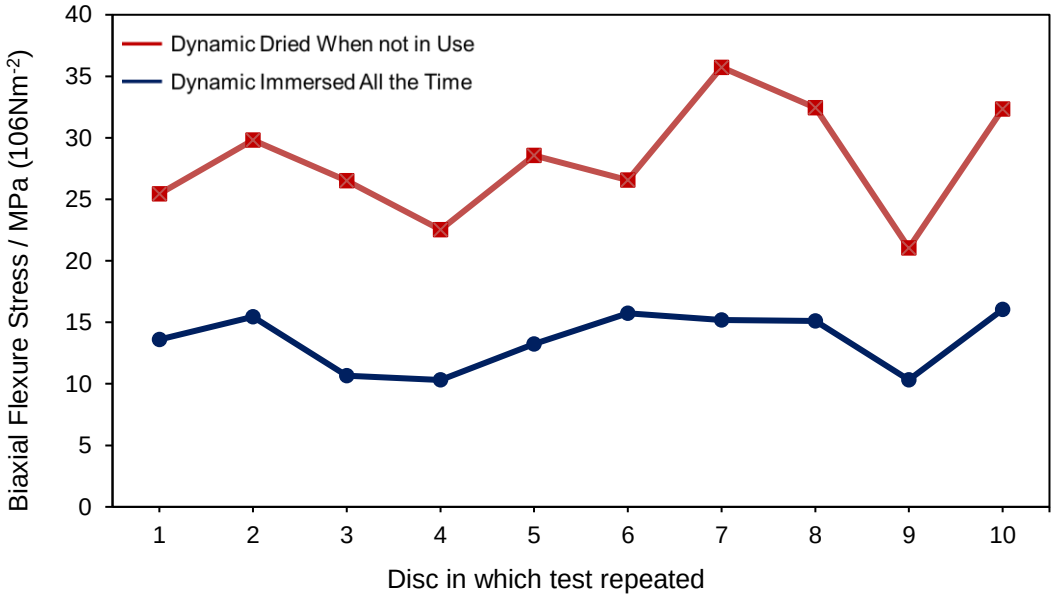

Figure 57. Biaxial flexure stress of C40 glass after 10 day immersion in dynamic conditions of immersed all the time and dried when not in use.

Figure 57 shows the biaxial flexure stress related to each glass discs at two different immersion conditions. Overall, the glass discs dried when not in used show larger biaxial flexure stress in all cases. At highest, the force required to break was twice as high meaning that the absence of water seems to have made the glass discs more durable and resistant to force. This may have been due to glass discs drying out on surface, making it more difficult to break by forming a hardened surface. However, when comparing the average biaxial flexure stress, it was less than 1 MPa (10^6.Nm^{-2}) which shows that there is not a major difference in strength. The average biaxial flexure stress was 13.7 MPa for immersed all the time and 14.5 MPa for dried when not in use.

4.3.6 Energy dispersive x-ray (EDX) and scanning electron microscopy (SEM)

4.3.6.1.1 SEM

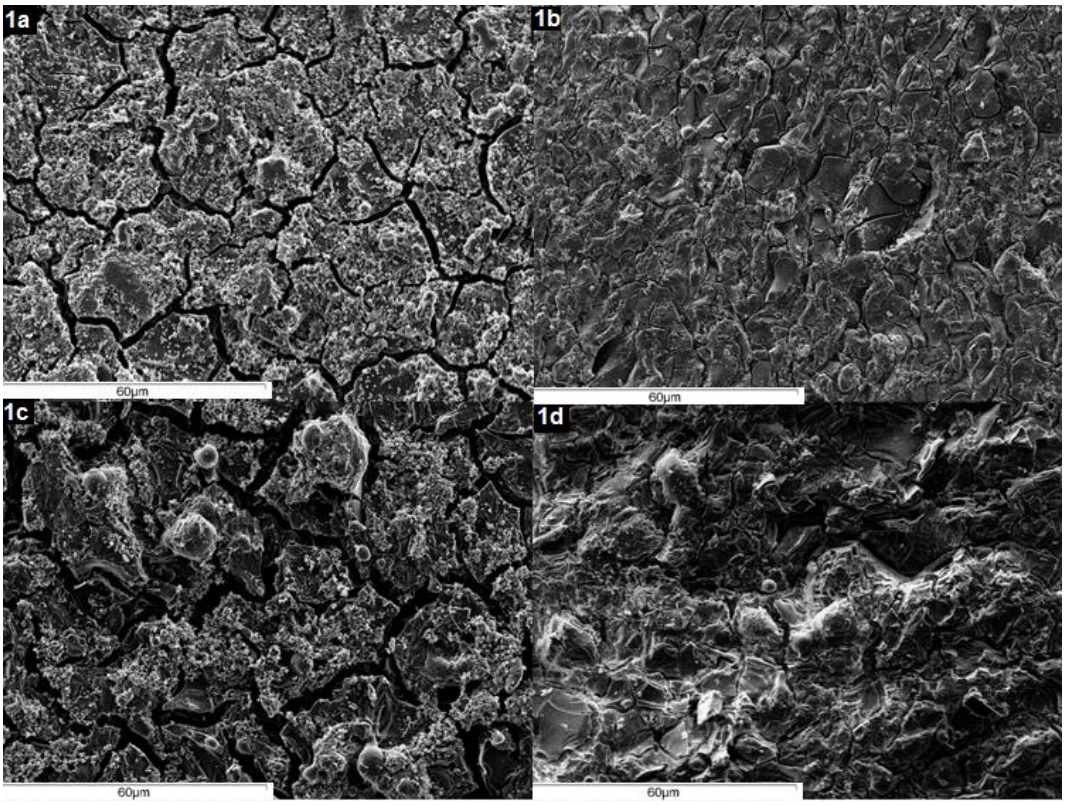

Figure 58. SEM Morphology of the Glass Discs Immersed in Tap Water, at x 1000 Magnification and at 30 °C: 1a) Static Immersed All the Time, 1b) Static Dried When Not in Use, 1c) Dynamic Immersed All the Time, 1d) Dynamic Dried When Not in Use.

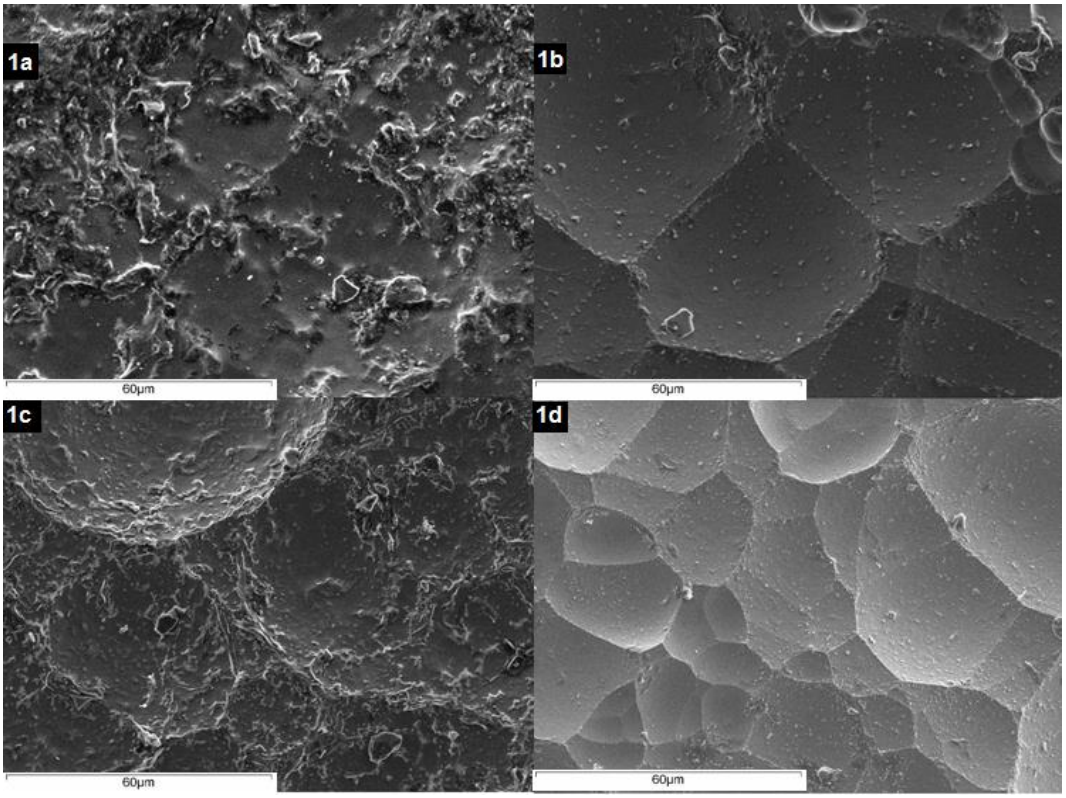

Figure 59. SEM Morphology of the Glass Discs Immersed in Deionised Water, at x 1000 Magnification and at 30 °C: 1a) Static Immersed All the Time, 1b) Static Dried When Not in Use, 1c) Dynamic Immersed All the Time, 1d) Dynamic Dried When Not in Use.

Figure 58 and Figure 59 shows SEM images of P50Ca40Na10 glass disc surfaces after immersion tests at chapter 3.2.2. There is a noticeable difference in the surface of the glass discs immersed in tap and deionised water. The glass discs immersed in deionised water shows much more clear smooth areas which resembles “scoops’ resulting from large uniform dissolution from the surface which is also seen in dissolution by Barba[125] *et al*. and Ma[126] *et al*. Discs immersed in all the time in deionised water shows some

rough surfaces on the boundaries of the “scoops” which may be dues to partial non-uniform dissolution of the surface.

Looking at discs in tap water in Figure 58, there is a clear difference to deionised water. It resembles cracks with wider cracks in discs which were immersed all the time. This may be due to non-uniform dissolution due to ions already being present in tap water affecting how the ions from the glass diffuse into the water and vice-versa. The wider cracks in immersed all the time is likely to be due to longer immersion period than in dried when not in use which also relates to the weight loss shown Figure 23 where immersed all the time glass discs lost 48% more weight in static and 32% more in dynamic conditions. Wider cracks are wider in dynamic conditions which may be due to more agitation in the solution.

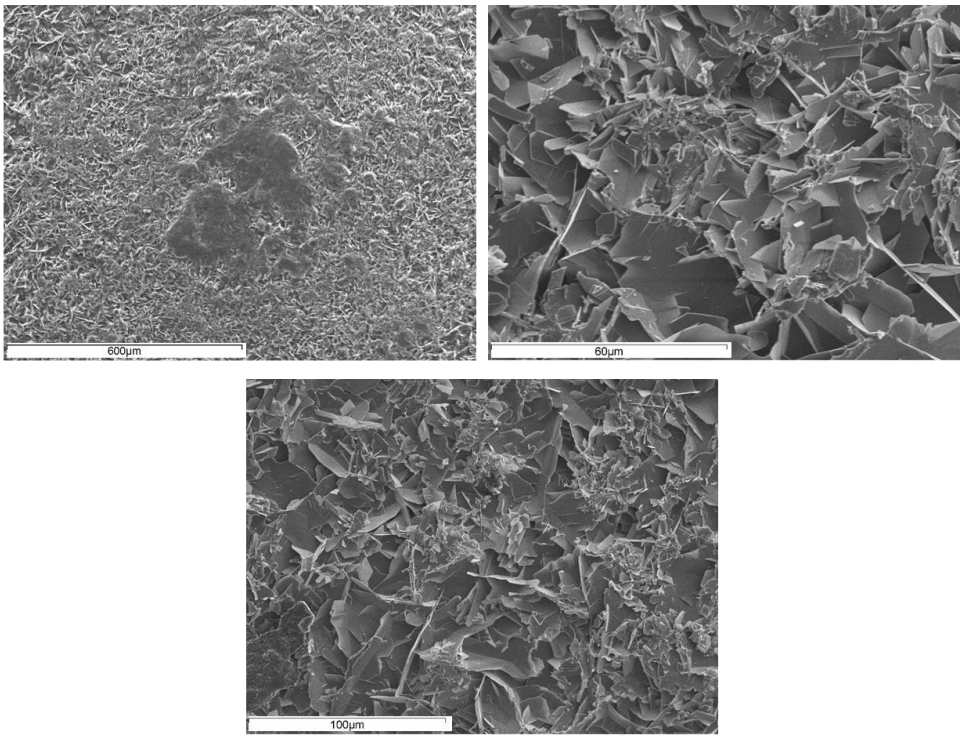

Figure 60. SEM images of the precipitate formed on the surface of the glass discs exposed to 75 %RH humidity at 40 °C.

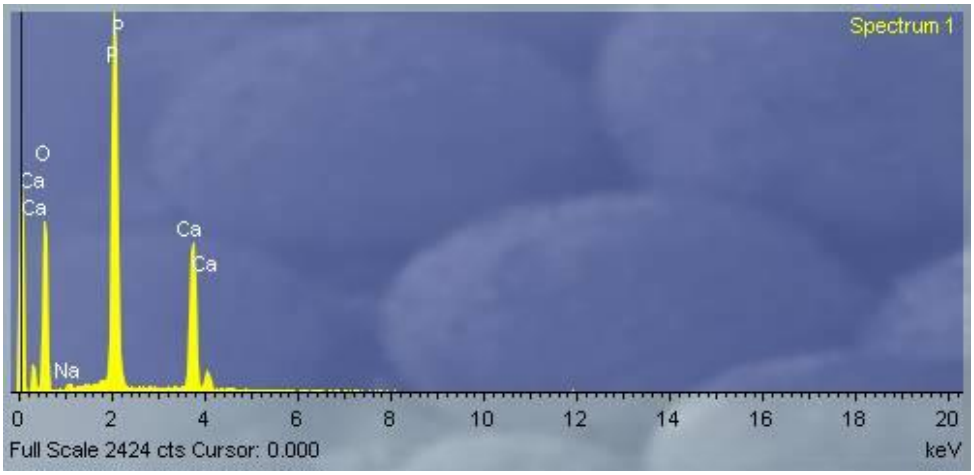

Figure 61. Elemental analysis of the precipitate formed on the surface of the glass discs exposed to 75 %RH humidity at 40 °C.

Figure 60 and Figure 61 shows analysis of the precipitate on glass discs exposed to 75%RH at 40 °C. Figure 60 shows how the precipitate appears to be very flaky and sharp in structure and appears to have form like layers suggesting that it can grow in size over time. Elemental analysis shows that the precipitate consists of phosphorous, calcium, sodium and oxygen; present in the ratio as the glass composition suggesting that the precipitate is formed from the glass itself. The possible mechanism is that the moisture in the air at high temperature allows it to enter the glass causing dissolution and bond breakage. However, since there is no solution for it to be removed, it allows the ions in the glass to form crystals precipitates on the surface, sticky and flaky in nature.

Chapter 5

Copper Doped Quaternary Phosphate Based Glass

5 Copper doped quaternary phosphate glass

This chapter extends on the previous experimental and analysis of ternary phosphate glass systems P_2O_5-CaO-Na_2O by doping copper oxide to form quaternary phosphate glass of P_2O_5-CaO-Na_2O-CuO. The purpose of this study is to understand how the addition of a network modifying copper oxide will affect the intrinsic glass properties as well as its dissolution properties.

In addition to the analysis, copper is widely known to have antimicrobial properties. In 2008 copper was announced as the first solid antimicrobial material by the U.S. Environmental Protection Agency.[127] It has undergone extensive research to use it for everyday use, now even more so with the COVID 19 pandemic reminding us of the importance of prevention of spreading and effective killing. Copper was chosen out of well known antimicrobial metals (i.e. silver, cobalt and nickel) [128] due to its cost, ease of access and its excellent antibacterial properties. Copper has the ability to kill more than 99.9% of disease causing bacteria such as *Pseudomonas aeruginosa, Staphylococcus aureus, Enterobacter aerogenes, Escherichia coli* and so on, within 2 hours of being in contact.[129] Several properties increases the effectiveness of copper's antimicrobial properties such as: high copper content, high temperature and high relative humidity. Copper use a mechanism called *contact killing* to kill bacteria which includes: copper dissolving into cells and causing damage, cell membrane rupture, generation of reactive oxygen species and degradation of genomic and plasmid DNA.[84] Therefore an antimicrobial property is an attractive addition to the scale

preventing P50Ca40Na10 glass to be used in domestic wet environments such as humidifiers.

5.1 Experimental methodology

5.1.1 Copper phosphate glass Synthesised

5.1.1.1 Chemicals

Copper doped phosphate-based were prepared using the following chemicals: diphosphorous pentoxide (P_2O_5, 98%, VWR, Lutterworth, UK), sodium dihydrogen phosphate (NaH_2PO_4, 99%, VWR, Lutterworth, UK), calcium carbonate ($CaCO_3$, 98.5%, VWR, Lutterworth, UK), strontium carbonate ($SrCO_3$, 98.5%, BDH Laboratory Supplies, Poole, UK) and copper (II) sulphate ($CuSO_4$, 99%, VWR, Lutterworth, UK)

5.1.1.2 Glass sample synthesis precursor chemical calculations

Amount of each reagent required using Copper Phosphate Glass as an example – $P50Ca_xNa10Cu_x$

Copper containing phosphate based glass were prepared by using the chemicals sodium dihydrogen phosphate (NaH_2PO_4), calcium carbonate ($CaCO_3$), phosphorous pentoxide (P_2O_5) and copper sulphate ($CuSO_4$).

The amounts of each chemicals were calculated as follows:

When NaH_2PO_4 is heated it breaks down into:

$$2NaH_2PO_4 \rightarrow Na_2O + 2H_2O + P_2O_5$$

Molecular Mass	240	62	36	142
Molar Mass Fraction		0.258	0.150	0.592

The amount of NaH_2PO_4 was calculated as:

$$\frac{(Na_2O(mole\ fraction\ required)x\ 62)}{0.258} = NaH_2PO_4\ (g)required$$

The amount of P_2O_5 needs to be calculated but one of the broken-down components from NaH_2PO_4 is P_2O_5. With the amount of NaH_2PO_4 calculated, the amount of P_2O_5 obtained from the breakdown was calculated as:

$$NaH_2PO_4\ (g)added\ x\ 0.592 = P_2O_5\ (g)$$

All glasses prepared had 50 mol% of P_2O_5 and 10 mol% of Na_2O. Therefore, the total amount of P_2O_5 required was always 70.9715 g. The P_2O_5 from the NaH_2PO_4 was always less than the required amount, hence the extra required was provided by pure P_2O_5.

When $CaCO_3$ is heated it breaks down into:

$$CaCO_3 \rightarrow CaO + CO_2$$

Molecular Mass	100	56	44
Molar Mass Fraction		0.56	0.44

Just like the previous calculation, amount of $CuSO_4$ required for each glass was calculated as:

$$\frac{(CaO(mole\ fraction\ required)x\ 56)}{0.56} = CaCO_3\ (g)required$$

When $CuSO_4$ is heated it breaks down into:

$$CuSO_4 \rightarrow CuO + SO_3$$

Molecular Mass	160	80	80
Molar Mass Fraction		0.5	0.5

In the above equation we are assuming that the copper was present as copper(ll) oxide only, as it will take the most stable, highest oxidation state when reacted.

Therefore, the amount of $CuSO_4$ was calculated as:

$$\frac{(CuO(mole\ fraction\ required)x\ 80)}{0.5} = CuSO_4\ (g)required$$

In total of 4 compositions of copper-phosphate glass were synthesised. Each corresponding compound were weighed in Stomacher blender bags and were thoroughly mixed together for one minute due to highly hygroscopic nature of phosphorus pentoxide using a Stomacher 400 Circulator Lab Blender. The mixed powder was placed in a platinum crucible which was then inserted into

a furnace set at 700 °C for the initial reaction for *ca.* 30 minutes then the temperature was increased to 1100 °C furnace for *ca.* 1 hour until fully melted. The molten glass was poured into pre-heated cylindrical graphite mould with a 15 mm in diameter cavity to anneal at specific annealing temperature for 1 hour and switched off to allow it to slowly reach room temperature overnight. The glass rods (15 mm Ø) were cut into discs of 2 mm in thickness using a wafering saw. The discs received no further polishing or surface treatment and were used as-prepared in the subsequent procedures.

Table 9. List of glass composition prepared

Glass Code	mol% of oxides in glass			
	P_2O_5	CaO	Na_2O	CuO
PCN	50	40	10	0
Cu 1	50	39	10	1
Cu 5	50	35	10	5
Cu 10	50	30	10	10
Cu 20	50	20	10	20

5.1.2 Immersion tests

5.1.2.1 Water samples

Two conditions of water were tested: Tap Water (TW) and deionized water (dH_2O – obtained by means of an ion exchange resin usage). Hard water samples were obtained directly from the tap-water supply and its conductivity

was monitored in a regular basis. Values were found to vary between 684 and 729 μS/cm. For the case of tests running under deionized water the conductivity was found to vary between 0 and 12.

5.1.2.2 Static and immersed for fixed time

Glass discs (n = 3) were first weighed and the baseline weight (M_0) of each recorded. The exact dimensions of each sample were measured using a Vernier calipers and the surface area was calculated. Samples were then placed in 20 mL of TW or dH_2O (n = 3) and incubated for fixed 1, 3 and 7 days at 30 °C in the environmental chamber. Following incubation samples were removed, blotted dry with tissue, and allowed to dry for 1h before the weight of each was again recorded (M_t). The immersion solutions were collected and stored under refrigeration (4 °C) until required for analysis of ionic composition. In all, weight loss and ion release sampling procedures were repeated for the following total immersion times:

5.1.2.3 Static and immersed all the time (SI)

Glass discs (n = 3) were first weighed and the baseline weight (M_0) of each recorded. The exact dimensions of each sample were measured using a Vernier calipers and the surface area was calculated. Samples were then placed in 20 mL of TW or dH_2O (n = 3) and incubated for 3 days at 30 °C in the environmental chamber. Following incubation samples were removed, blotted dry with tissue, and allowed to dry for 1h before the weight of each was

again recorded (M_t). The immersion solutions were collected and stored under refrigeration (4 °C) until required for analysis of ionic composition. Each of the bioglass discs were then transferred to a fresh 20 mL TW volume for a further 2 or 3 days (3 days due to immersions over the weekend) and the above sampling processes repeated. In all, weight loss and ion release sampling procedures were repeated for the following total immersion times:

5.1.3 Phosphate glass fibre synthesis

The fibers were produced continuously using a melt-spinning, fiber drawing method (Fiber-rig as previously detailed in (I. Ahmed, Collins, Lewis, Olsen, & Knowles, 2004)). For both glass compositions, the pulling were at 800 rpm, which is leading averagely 20 µm fiber sizes.

Glass fibres were obtained using a fibre drawing method, from a newly acquired Fibre-rig (BiomaterialsDepartment, UCL). The fibre-rig consists of a toploading furnace (Lenton Furnaces) with a Pt/10% Rhcrucible (Johnson Matthey, UK) consisting of a bushingwith an approximate 1 mm hole, and a tip approxi-mately 15 mm long. Glass was placed into the crucibleand left for an hour to melt and to homogenise. The temperature of the furnace was then dropped to achieve a viscosity suitable for fibrisation of the glass.

5.1.4 Ion Chromatography for Phosphate Analysis

The concentration of relevant ionic species was determined for polyphosphate $[PO_4]^{3-}$, $[P_2O_7]^{4-}$, $[P_3O_9]^{3-}$, and $[P_3O_{10}]^{5-}$. The release of phosphate species was analysed using an ICS-2500 ion exchange chromatography system equipped with a 50 µL sample injection loop calibrated across 4 levels (5, 10, 50 and 125 ppm). Standards were produced though serial dilution of a 1000 ppm stock solution detailed below in. Elution was performed between a KOH gradient of 25 mM to 40 mM over 32.5 minutes. Corrections were made to account for the expected purity of each phosphate salt used.

5.1.5 Inductively coupled plasma – optical emission spectroscopy

Varian 720-ES, machine was used in measuring the ion concentration of the effluent samples of P50Ca39Na10Cu1 and P50Ca20Na10Cu20 after static immersions in deionised water. Two sets of identical calibration standard as seen in

Table **10** was prepared from ICP multielement standard V solution (Merck). This was done by diluting the ICP multielement standard solution with 5 % Nitic acid solution. The standard was run every 10 samples to make sure that the measurements were being done correctly.

Table 10. (Ion Standard Solution): Dilutions of standard solutions prepared for ICP-OES

Calibration Samples	Calcium (ppm)	Copper (ppm)	Sodium (ppm)	Phosphorous (ppm)

1	0	0	0	0
2	0.25	0.05	0.50	0.25
3	0.50	0.10	1	0.50
4	2.50	0.50	5	2.50
5	5	1	10	5
6	10	2	20	10

5.1.6 Water contact angle measurements

Water contact angle measurements were performed by using a CAM 200 optical contact angle meter instrument (KSV co, Finland). A special graduated needle (Hamilton co, Nevada, USA) was filled with distilled water to establish the hydrophobicity/hydrophilicity of the prepared and coated glass discs in the normal room temperature environment. Measurements were taken on triplicate samples of zinc glass discs (uncoated glass, PCL coated glass discs and CNT-PCL coated glass discs). The needle was placed in its clamp and was placed above the glass discs surface to ensure water droplet went onto the glass disk. The contact angle measurement was performed on the water droplet that dispersed on the glass discs surface by using the CAM200 shape analysis software and time lapse camera. This procedure was done by measuring the angle for 10 fast readings (40 ms intervals) and 10 slow readings (1 second interval).

5.1.7 Differential scanning calorimetry (DSC)

Discovery DSC 25 manufactured by TA Instruments were used to measure the modulated heat flow under continuous heating rates of 10 K/min up to 550

ºC. The glass transition temperature (T_g) was calculated from the obtained plot. DSC used helium gas at 50 ml/min with a nitrogen base purge of 300 ml/min.

5.1.8 ^{31}P Magic Angle Spinning Solid-State Nuclear Magnetic Resonance (MAS NMR)

^{31}P MAS NMR data was quired at ambient temperature (*ca.* 25 °C) using a Bruker AVANCE III-500 spectrometer operating at a ^{31}P Larmor frequency of 202.46 MHz. All measurements were facilitated using a Bruker 4 mm dual channel HX probe MAS frequencies of 12 kHz for this thesis. These ^{31}P MAS NMR data were acquired using single pulse (direct detection) methods and the pulse calibration and chemical shift referencing was performed using solid the secondary reference ammonium dihydrogen phosphate ($NH_4H_2PO_4$, δ 0.9 ppm) with respect to the IUPAC primary reference of 85% H_3PO_4 (δ 0.0 ppm). An π/2 excitation pulse of 3 μm and a recycle delay of 60 s were used in all experiments; this relaxation delay was checked again longer recycle delays to ensure full spin-lattice (T_1) relaxation. Between 20 and 88 transients were acquired for each measurements, and all spectra were simulated using the Dmfit software package. [130]

5.1.9 X-ray photoelectron spectroscopy and DEPTH profile

X-ray photoelectron spectroscopy (XPS) was performed using a Thermo Scientific K-alpha photoelectron spectrometer using monochromatic Al-K_α radiation. Survey scans were collected in the range 0-1100 eV (binding energy) at a pass energy of 160 eV. Higher resolution scans were recorded for the main core lines at a pass energy of 20 eV. Valence band spectra were also recorded. Peak positions were calibrated to adventitious carbon (284.5 eV) and analysed using CasaXPS software.

5.1.10 Antimicrobial properties of copper doped phosphate glass

As seen in Figure 62 glass fibres pulled were cut into 3 cm in length and of *ca*. 0.02 g in weight underwent sterilisation in UV and were placed into 99.99% ethanol and UV sterilised sealed glass containers until used for the antimicrobial tests.

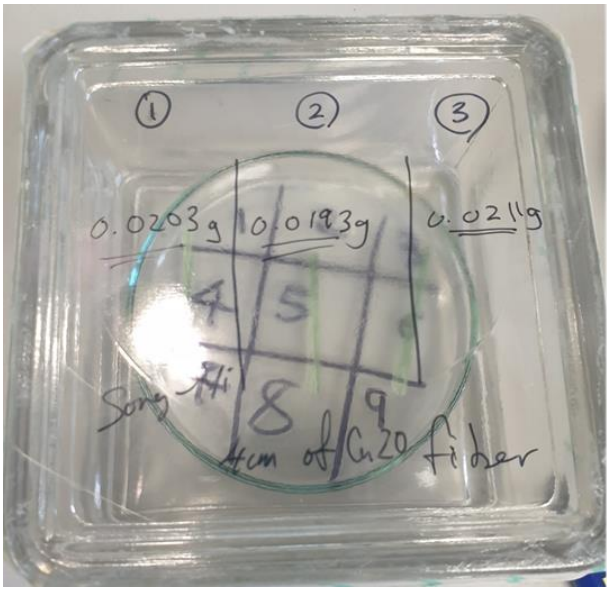

Figure 62. Sterilising copper glass fibres in UV light for 5 minutes and kept in sterilised containers before antimicrobial tests.

5.1.10.1 Preparing 20% agar plates

Pseudomonas aeruginosa, a gram-negative bacterium is a common bacteria found in water, soil and plants. It was chosen for the above reasons to test the antimicrobial properties of copper doped glass.

In a 1000 ml ISO bottle 500 ml of ultra-pure water was mixed with 5 ml of glycerol (99.5% Sigma Aldrich), 24.2 g of pseudomonas agar base (Oxoid) and 1.8 g of MacConkey agar number 3 (Oxoid). The mixture was placed in an autoclave. When removed from the autoclave the 10 ml of agar solution was evenly placed into 100 x 50 mm agar plates and was allowed to set (Figure 63)

Figure 63. Preparation of 20% agar plates in a 100 x 50 mm petri dish.

5.1.10.2 Growing pseudomonas aeruginosa

Figure 64 shows the colonies grown and the following agar plate of pseudomonas of one colony. Colonies of pseudomonas aeruginosa were grown by roughly swiping the picked up pseudomonas onto an agar plate, place upside down overnight in a 37 °C incubator. Then one colony was picked up with a sterile cotton bud and was spread across the agar plate to produce a pseudomonas agar plate for antimicrobial test.

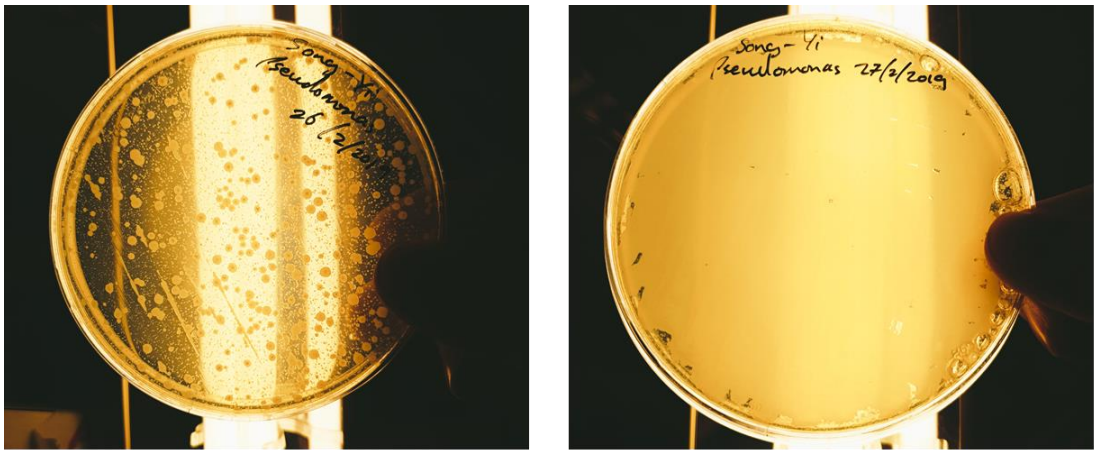

Growing colonies of pseudomonas aeruginosa

Growing one colony of pseudomonas aeruginosa for antimicrobial testing

Figure 64. Growing colonies of pseudomonas aeruginosa and producing petri dish full of one colony bacteria for antimicrobial testing.

5.2 Results and discussion

5.2.1 Physical appearance of copper glass discs after static immersion

The glass was prepared by reducing the amount of calcium oxide and replacing it with copper oxide. This was as the copper(II) oxides were assumed to be present in the final glass. Figure 65 shows as the amount copper oxide increases the glass discs go darker in colour of green. There is no visible difference in the glass discs after each immersions and maintained their structure integrity.

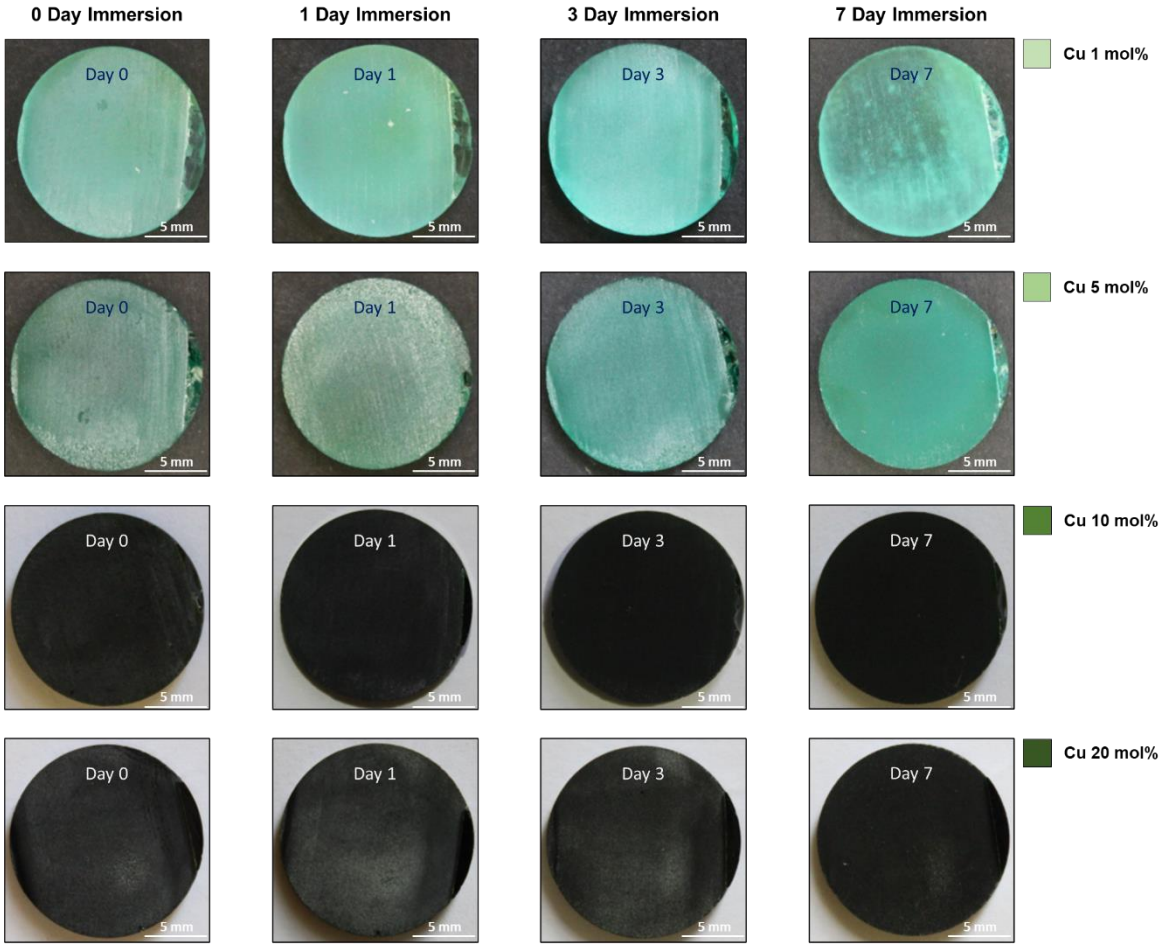

Figure 65. Copper doped phosphate glass at separate 0, 1, 3 and 7 day immersions. Showing four compositions with increasing copper oxide amount of 1, 5, 10 and 20 mol%.

Table 11. Glass code for the copper doped ternary phosphate glass

Glass Composition	Glass
P50Ca40Na10	PCN
P50Ca39Na10Cu1	Cu10
P50Ca35Na10Cu5	Cu5
P50Ca30Na10Cu10	Cu10
P50Ca20Na20Cu20	Cu20

5.2.2 Phosphate release from immersion test of copper doped phosphate glass

5.2.2.1 Fixed day static immersions – deionised water

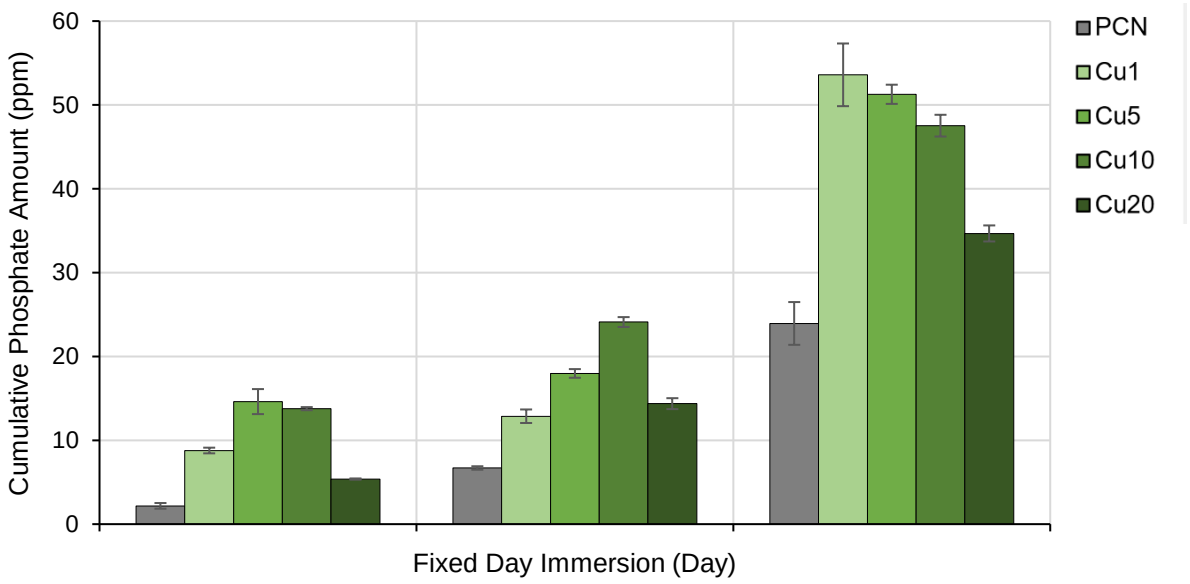

Figure 66 (PO_4^{3-}). Amount of phosphate ion released for each fixed day immersion for each glass disc compositions.

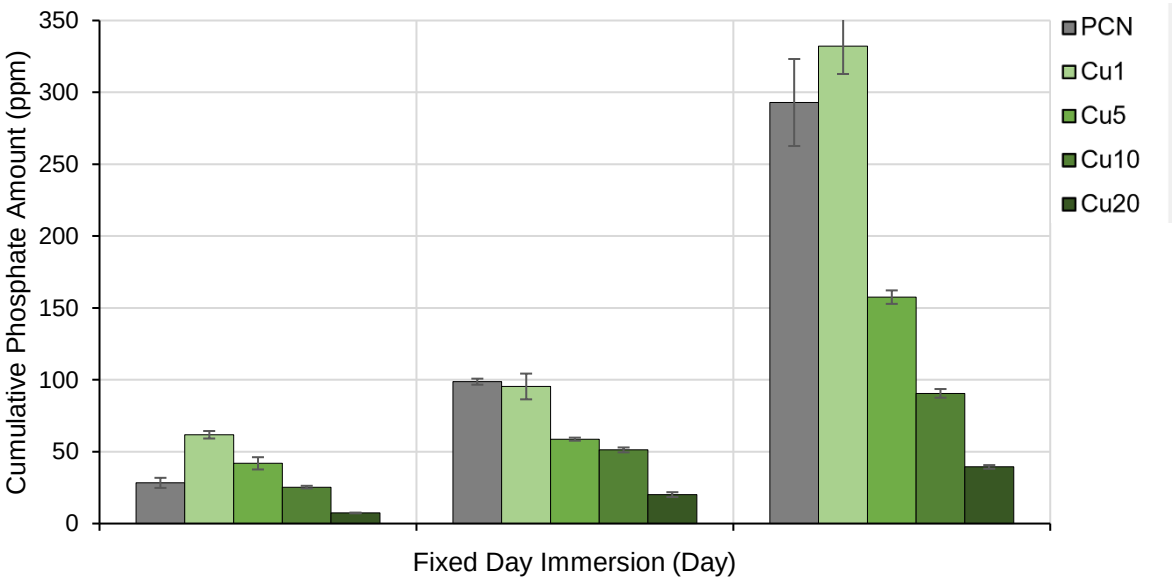

Figure 67 ($P_3O_9^{3-}$). Amount of phosphate ion released for each fixed day immersion for each glass disc compositions.

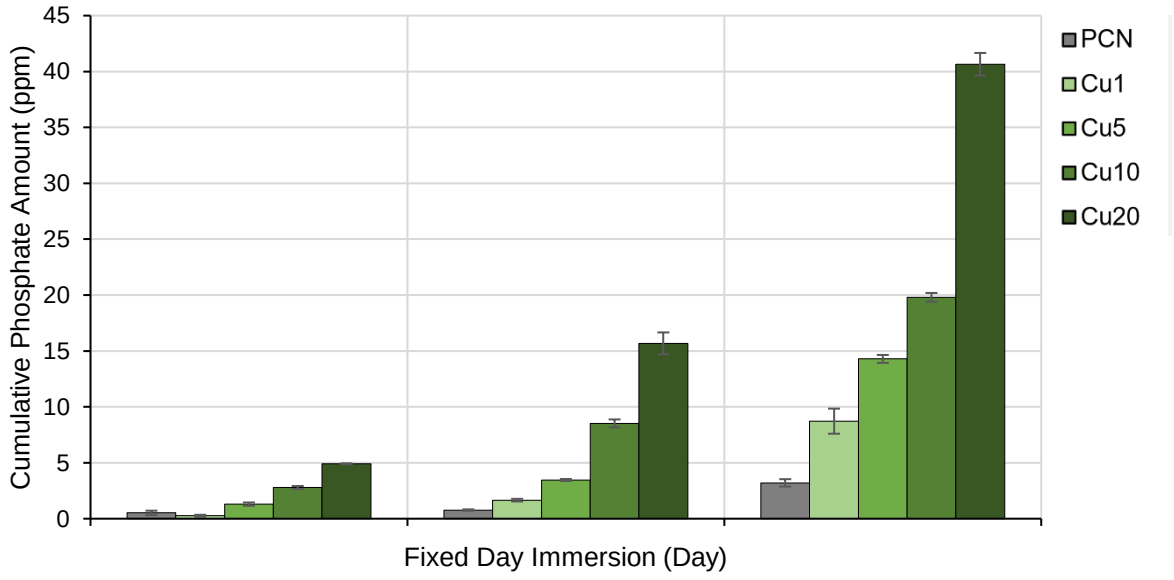

Figure 68 ($P_2O_7^{4-}$). Amount of phosphate ion released for each fixed day immersion for each glass disc compositions.

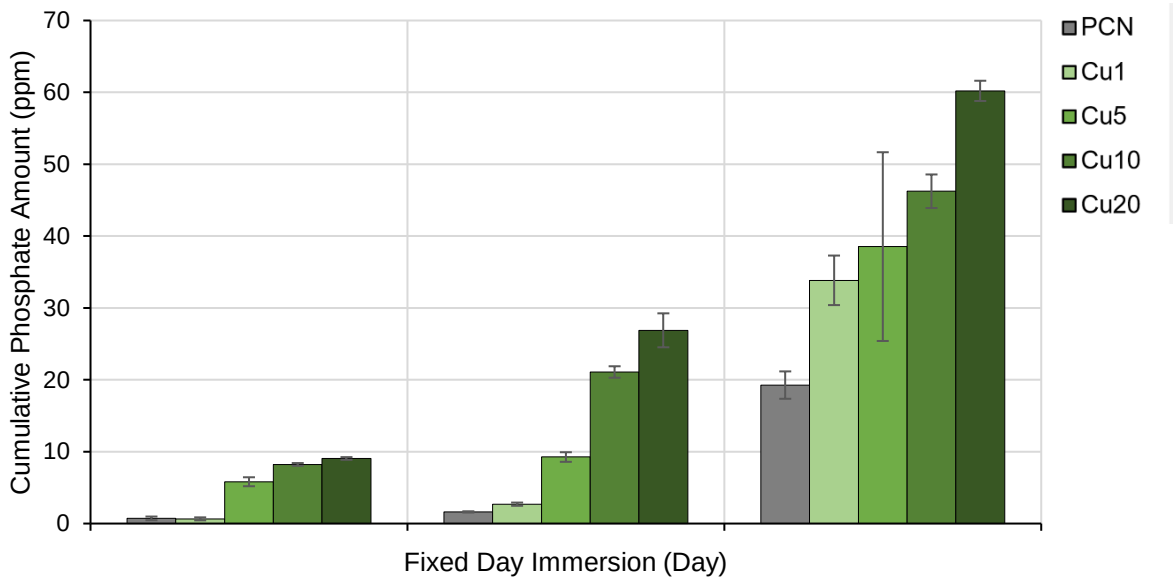

Figure 69 ($P_3O_{10}^{5-}$). Amount of phosphate ion released for each fixed day immersion for each glass disc compositions.

Table 12. Table to show the phosphate releases for each immersion.

	PO_4^{3-} (ppm)			$P_3O_9^{3-}$ (ppm)		
	1 Day	**3 Days**	**7 Days**	**1 Day**	**3 Days**	**7 Days**
PCN	2.2	6.7	23.9	28.3	98.7	292.9
Cu1	8.8	12.9	53.6	61.8	95.4	332.1
Cu5	14.6	18.0	51.3	41.9	58.7	157.5
Cu10	13.8	24.1	47.5	25.4	51.3	90.6
Cu20	5.4	14.4	34.7	7.4	20.1	39.4

	$P_2O_7^{4-}$ (ppm)			$P_3O_{10}^{5-}$ (ppm)		
	1 Day	**3 Days**	**7 Days**	**1 Day**	**3 Days**	**7 Days**
PCN	0.5	0.8	3.2	0.7	1.6	19.3
Cu1	0.3	1.7	8.7	0.7	2.7	33.8
Cu5	1.3	3.5	14.3	5.8	9.3	38.5
Cu10	2.8	8.5	19.8	8.2	21.1	46.2
Cu20	4.9	15.7	40.7	9.1	26.9	60.2

Table 13. Table to show total phosphate release after 7 day continual immersion

	PO_4^{3-}	$P_3O_9^{3-}$	$P_2O_7^{4-}$	$P_3O_{10}^{5-}$	Total
PCN	23.9	292.9	3.2	19.3	339.3
Cu1	53.6	332.1	8.7	33.8	428.2
Cu5	51.3	157.5	14.3	38.5	261.6
Cu10	47.5	90.6	19.8	46.2	204.1
Cu20	34.7	39.4	40.7	60.2	175

Figure 66 to Figure 69 shows each phosphate releases in static immersion in deionised water for fixed day period of 1, 3 and 7. We can observe that the addition of copper shows a completely different phosphate release pattern.

In the undoped PCN glass the order of most abundant phosphate release is $P_3O_9^{3-}$ followed by PO_4^{3-}, $P_3O_{10}^{5-}$ and $P_2O_7^{4-}$. Which is identical to the previous immersions carried out in chapter 3 and 4. Whilst with Cu20 glass, order of most abundant phosphate release in 7 day immersion is $P_3O_{10}^{5-}$ followed by $P_2O_7^{4-}$, $P_3O_9^{3-}$ and PO_4^{3-}.

With PO_4^{3-}, orthophosphate (Figure 66) the addition of copper increased its release in all immersions compared to PCN. $P_3O_9^{3-}$, cyclic trimetaphosphate (Figure 67) showed slight increase with Cu1 but as the proportion of copper dopants increased there was a clear decrease in $P_3O_9^{3-}$ release as much as 87% decrease in 7 day immersion. In $P_2O_7^{4-}$, pyrophosphate (Figure 68) the addition of copper showed a steady increase in its release to as much as 1172% increase with 7 day immersion when comparing PCN with Cu20. With $P_3O_{10}^{5}$-, tripolyphosphate (Figure 69) as copper dopant concentration increased,

$P_3O_{10}^{5-}$ increased. As much as 212% in with Cu20 in 7 day immersion. This change in the phosphates released shows a change in glass structure.

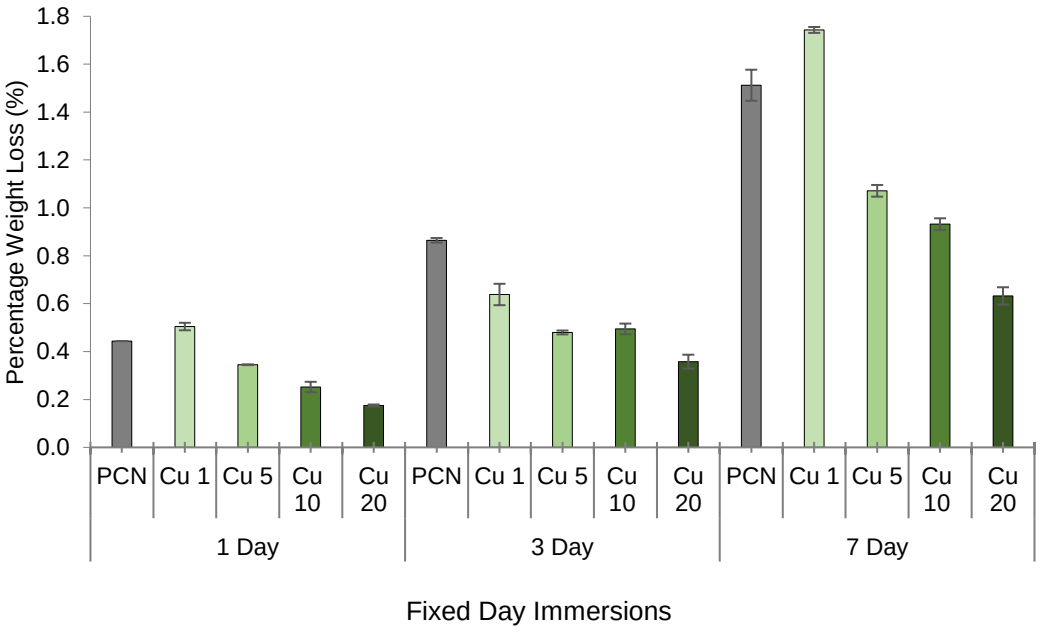

Figure 70. Percentage weight loss of glass discs after fixed day immersions in deionised water.

As expected, longer immersions resulted in increase in weight loss percentage. The percentage weight lost also correlated with the total amount of phosphate ions released. As the copper content increased the degradation rate decreased which was also observed by Neel[131] *et al*. The decrease in degradation may be due to the change in the glass structure which can be also seen by the difference in the phosphates released. Cu^{2+} has an ionic radius of *ca*. 87 pm and Ca^{2+} of *ca*. 114 pm. The size of the atom and the strength of the bonding is expected to change. It has been reported that near 20 mol% the tetrahedral local boning arrangements change which may be why we observe this change with 20 mol% of CuO.[17] The addition of copper brough

more even ion release across the phosphates when compared to PCN where most of the phosphates released were $P_3O_9^{3-}$. The increased release of $P_3O_{10}^{5-}$ is ideal as tripolyphosphate is the phosphate which is most effective against scale formations.

5.2.2.2 Phosphate release measurements

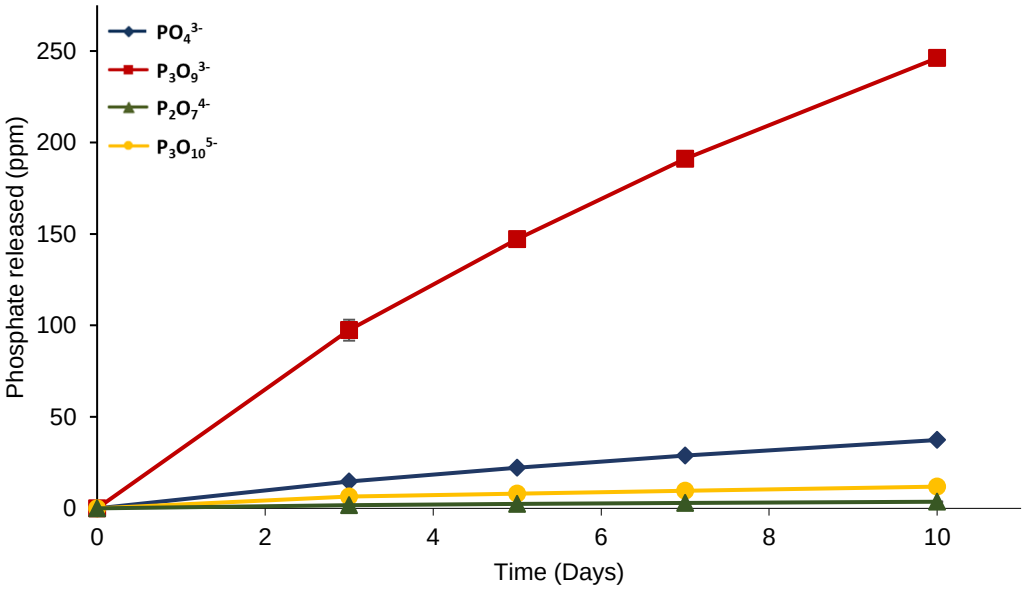

Figure 71. Cumulative phosphate anions released of Cu 1 glass discs during 10-day static immersion tests at 30 °C in deionised water.

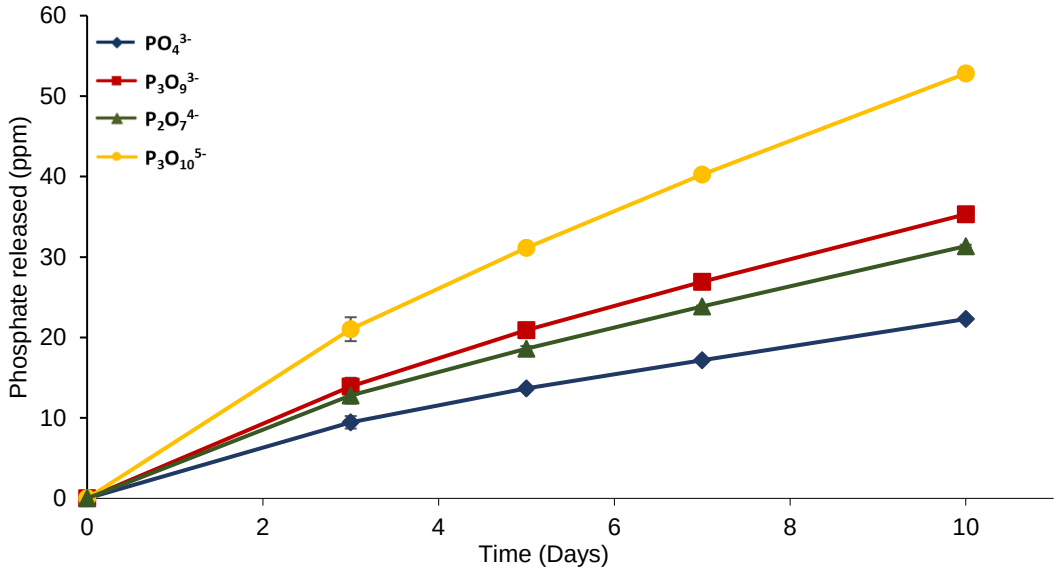

Figure 72. Cumulative phosphate anions released of Cu 20 glass discs during 10-day static immersion tests at 30 °C in deionised water.

Figure 71 and Figure 72 shows the cumulative phosphate release of Cu1 and Cu20 discs in deionised water over 10 day immersion. The experiment was repeated following the fixed day immersion to observe the ion release during continual immersion. Cu1 showed very similar trends to the phosphate release of static immersion of PCN discs (results in Table 7) in deionised water, in acidic and alkali solutions and with discs exposed to extreme humidity. However, much like the results from the fix day immersions, Cu20 shows completely different ion release property. Showing more balance release of all phosphate ions with $P_3O_{10}^{5-}$ again being the most released. This suggests that the structure of the glass in Cu20 has less cyclic structure of $P_3O_9^{3-}$ and is likely to be less porous than PCN with stronger crosslinks and bonding resulting in slower degradation.

5.2.3 Cumulative cation releases of Cu1 and Cu20 glass.

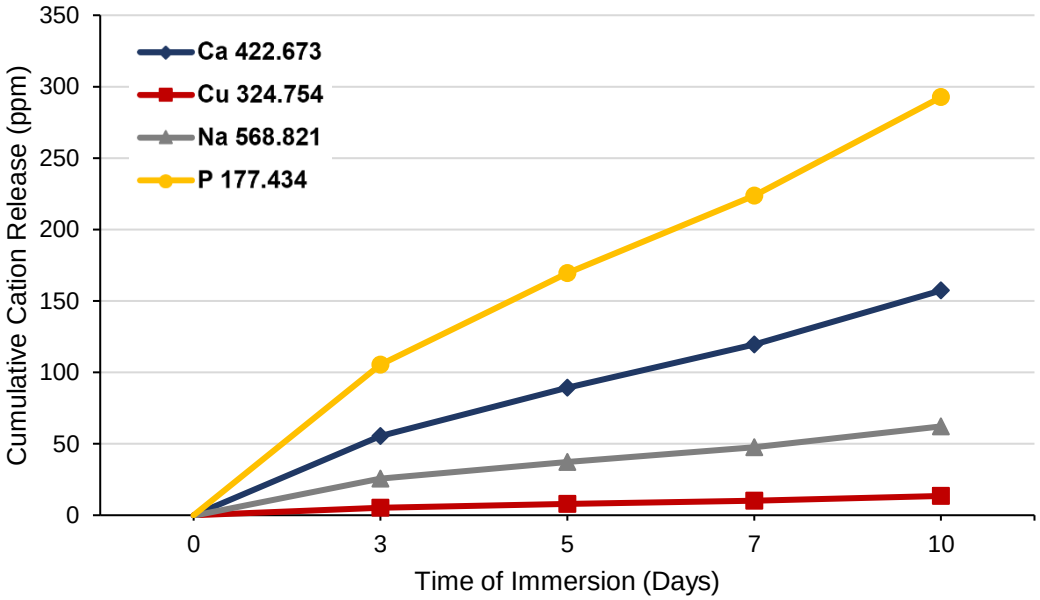

Figure 73. Cumulative elements released of Cu1 glass discs for 10 day static immersion tests at 30 °C in deionised water.

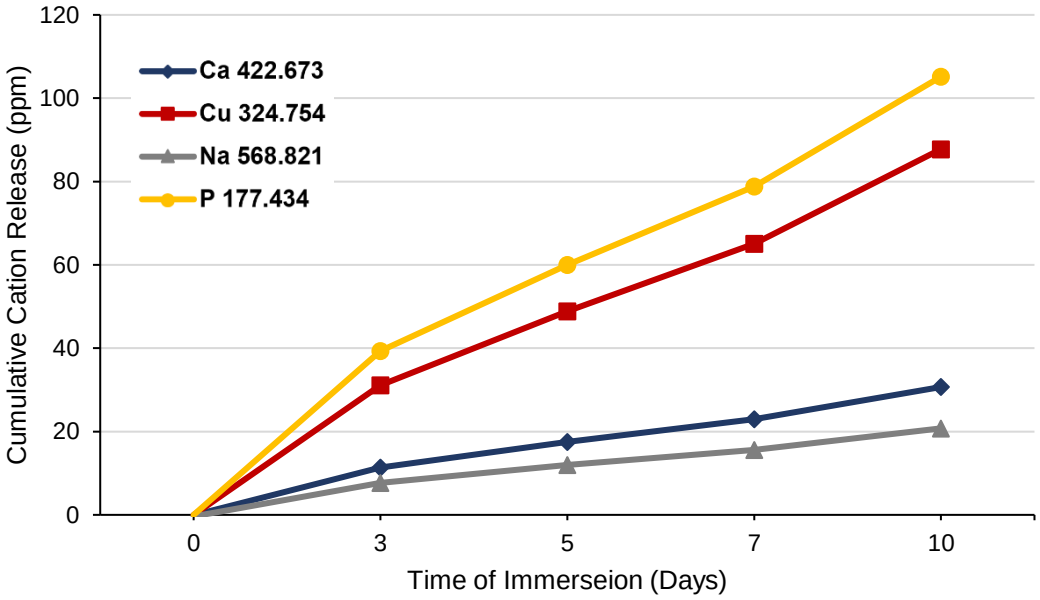

Figure 74. Cumulative elements released of Cu20 glass discs for 10 day static immersion tests at 30 °C in deionised water.

The figures above show the cumulative amounts of elements released measured using ICP-OES, by glass discs immersed in deionised water over 10 day static immersions. Cu20 showed decrease in overall release of elements of phosphorous, sodium and calcium. Calcium was expected as Ca^{2+} was replaced with Cu^{2+} in the synthesis, the decrease in sodium and phosphorous with the decrease in phosphates in previous results suggest an increase in cross-links the glass structure. Amount of copper released increased by more than 500% by the end of day 10 in Cu20 than Cu1 which is mainly due to increase in copper content. Increase in cross-links can also be due to Cu^{2+} having ionic radii of *ca*. 87 pm which is much smaller than Na^{+} of 102 pm and Ca^{2+} of 114 pm smaller, more positive ion.

5.2.4 Water contact angle

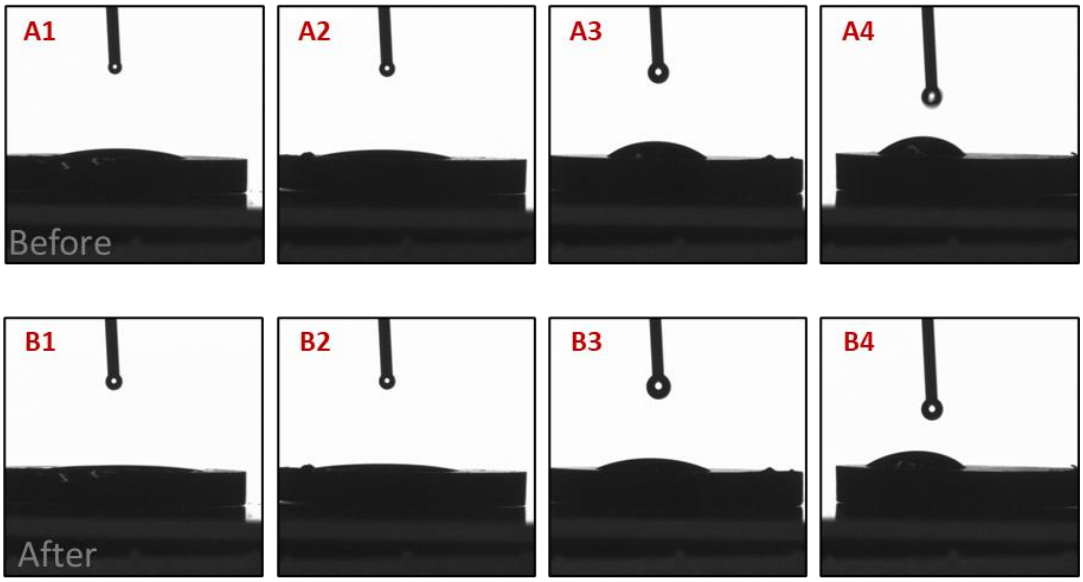

Figure 75. Figures of water contact angle, **A:** when water is first dropped and **B:** up to 0.3 seconds after A. The numbers after the A or B correlates to glass composition of P50Ca39Na40Cu1, P50Ca35Na10Cu5, P50Ca20Na10Cu10 and P50Ca20Na10Cu20 in this order.

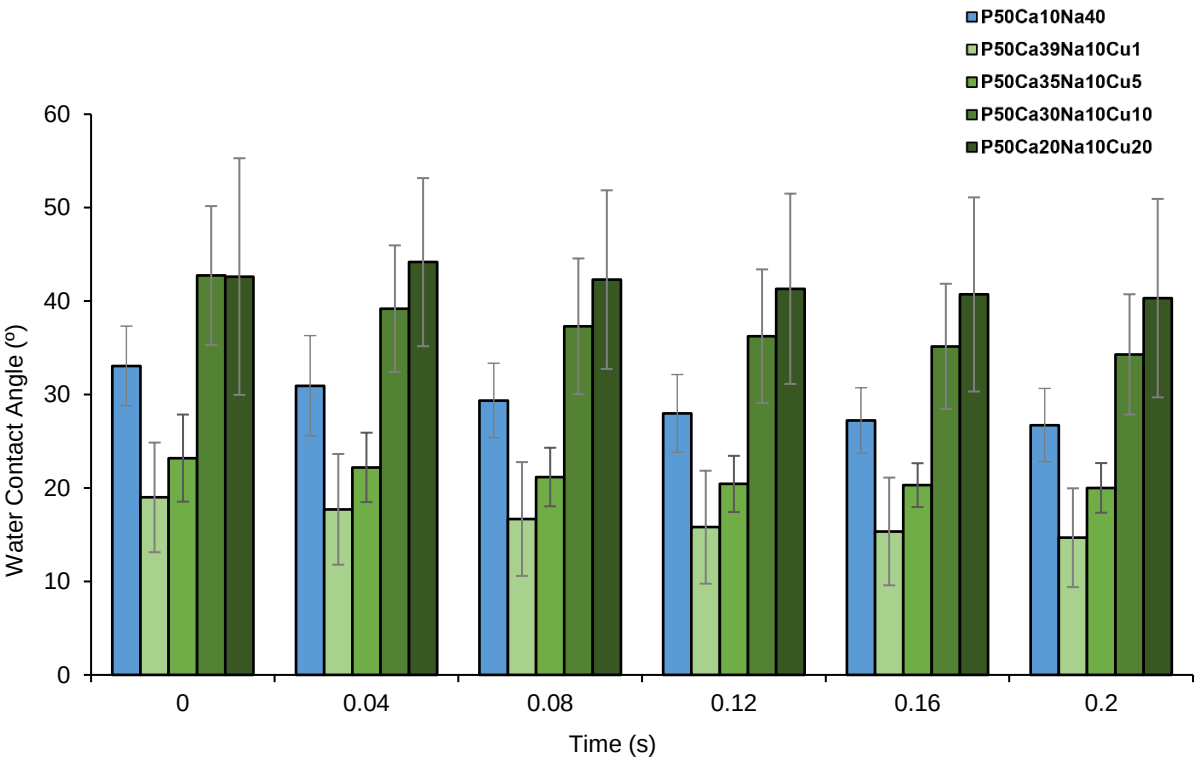

Figure 76. Figures of water contact angle value for PCN and copper doped glass discs.

Figure 75 Figure 76 shows the water contact angle measurement results, by looking at the images alone we can tell the difference in surface hydrophilicity of the glass discs. From Figure 76 we can see that although there is a decrease in water contact angle from PCN with Cu 1 and Cu5 there is an increase in water contact angle from Cu1 with more copper content leading to increase in water contact angle. When compared to the water contact angle (Figure 55) of the PCN glass discs with increasing copper content there seems to be a pattern. However, all values are below 90° suggesting a hydrophilic surface in all and the values lie in each other's error range. Further research in the future investigating how different network modifying oxides affect surface hydrophilicity and has correlation to its degradation rates.

5.2.5 Differential scanning calorimetry

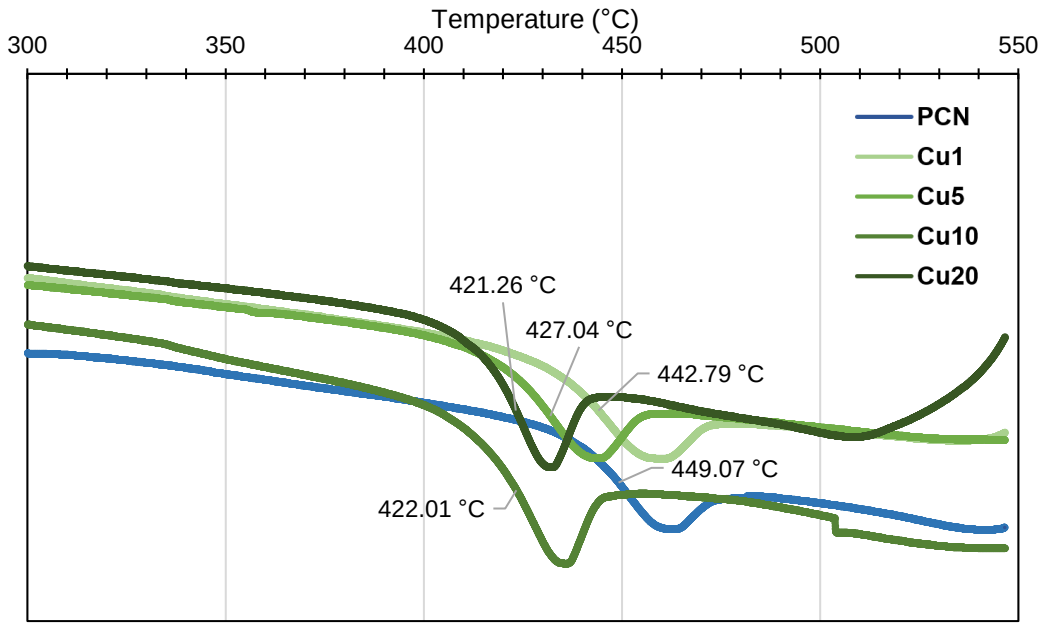

Figure 77. Figures of DSC plot of PCN and copper doped compositions with their glass transition temperatures.

Table 14. Table showing the glass transition (T_g) temperatures

Glass	T_g (°C)
PCN	449.07
Cu1	442.79
Cu5	427.04
Cu10	422.01
Cu20	421.26

Figure 77 and Table 14 shows the glass transition temperature results from DSC measurements of the glass. As the CuO content increases the glass transition temperature decreases which is different to results from Neel *et al*. (2005)[131] where they observed an increase in Tg with increasing CuO. The difference is due to this thesis substituting CaO instead of Na_2O.

5.2.6 ^{31}P Magic Angle Spinning Solid-State Nuclear Magnetic Resonance (MAS NMR)

5.2.6.1 11.7 T ^{31}P NMR Data (V_r = 20 kHz)

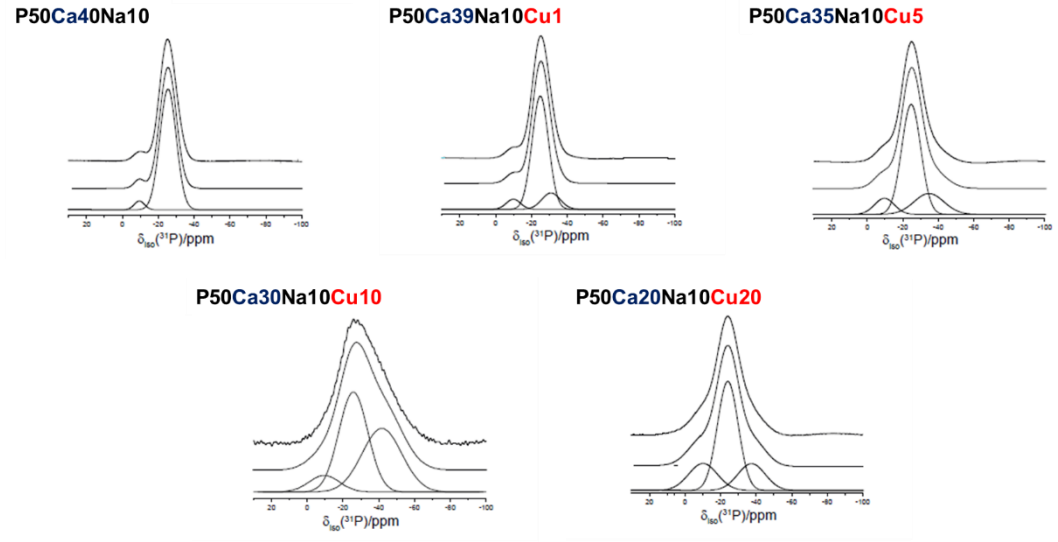

Figure 78. ^{31}P MAS NMR Data

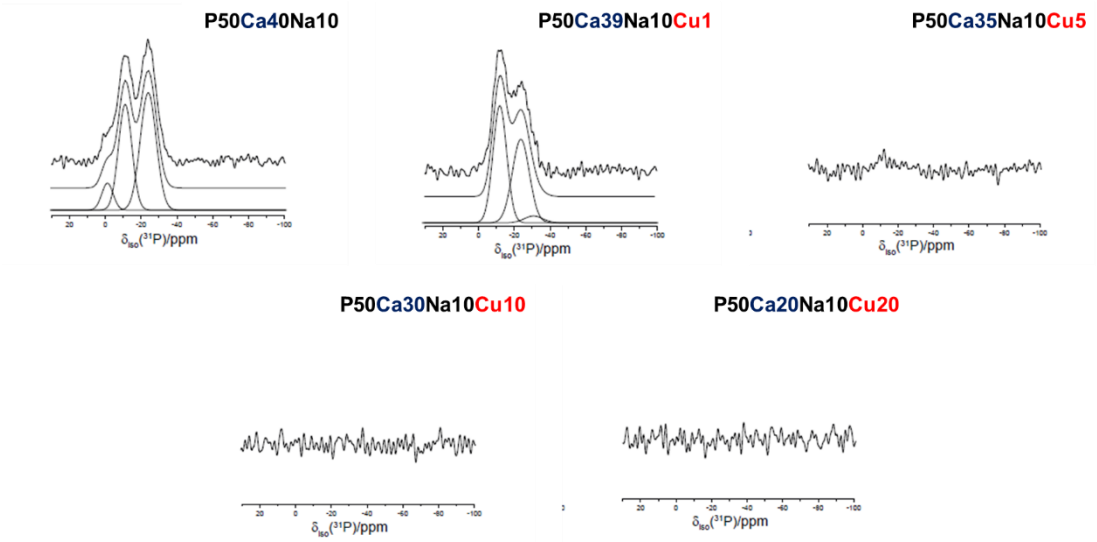

Figure 79. ^{31}P CPMAS NMR Data

Table 15. The percentage of each of the fitted components in the ^{31}P MAS NMR data ($v_r = 20\ kHz$)

Sample	δ_{iso} [ppm]	*I* [%]	δ_{iso} [ppm]	*I* [%]	δ_{iso} [ppm]	*I* [%]
P50Ca40Na10	-9.46	4.3	-25.5	95.7		
P50Ca39Na10Cu1	-9.90	6.3	-24.9	80.7	-30.9	13.0
P50Ca35Na10Cu5	-9.67	10.4	-24.7	69.0	-34.7	20.6
P50Ca30Na10Cu10	-10.1	20.5	-24.1	60.0	-37.4	19.5
P50Ca20Na10Cu20	-9.46	8.59	-25.8	48.7	-41.7	42.7

31P MAS NMR has been used to characterise the phosphate glass structure as copper is increased. As seen in Table 15, the chemical shifts of *ca.* -9.5 ppm are responsible for the Q^1 pyrophosphate ($P_2O_7^{4-}$) species and shifts of *ca.* -25 ppm are responsible for the Q^2 (-P-O-P-) species. With PCN glass the majority of the glass, 95.7% is Q^2 with 4.3% of Q^1. This is as observed with other metaphosphate glasses[132–134] showing that the glass is formed with chains of infinite length.[135] The chemical shift at -30.9 ppm observed with Cu 1 mol% is not present in the glass with no copper, suggesting that incorporation of copper leads to the presence of this peak. This chemical shift at -30.9 ppm seems to get greater in intensity and shifts to the right as the copper content increases and does so at the expense of the Q^2 peaks. This may be the species/bonding relating to the decrease in degradation rate. The Q^1 peaks also seems to increase in intensity until 10 mol% of copper which is observed with other copper glasses[136] and is described to be the depolymerisation of phosphate chains as CuO increases. The Q^2 peaks in the copper glass shows the covalent P-O-Cu links which shortens the phosphate chains in the process.[137]

In Figure 79 Presence of peaks with CPMAS (cross polymerise MAS) shows the presence of hydrogen and in this case mostly likely to be hydroxyl groups. We can also observe that as the copper content increases the peaks are no longer visible. This may be due to copper possible displacing the hydrogen of the hydroxyl group. Which means that the incorporating copper affects the end species.

5.2.6.2 2.35 T ^{31}P NMR Data (V_r = 60 kHz)

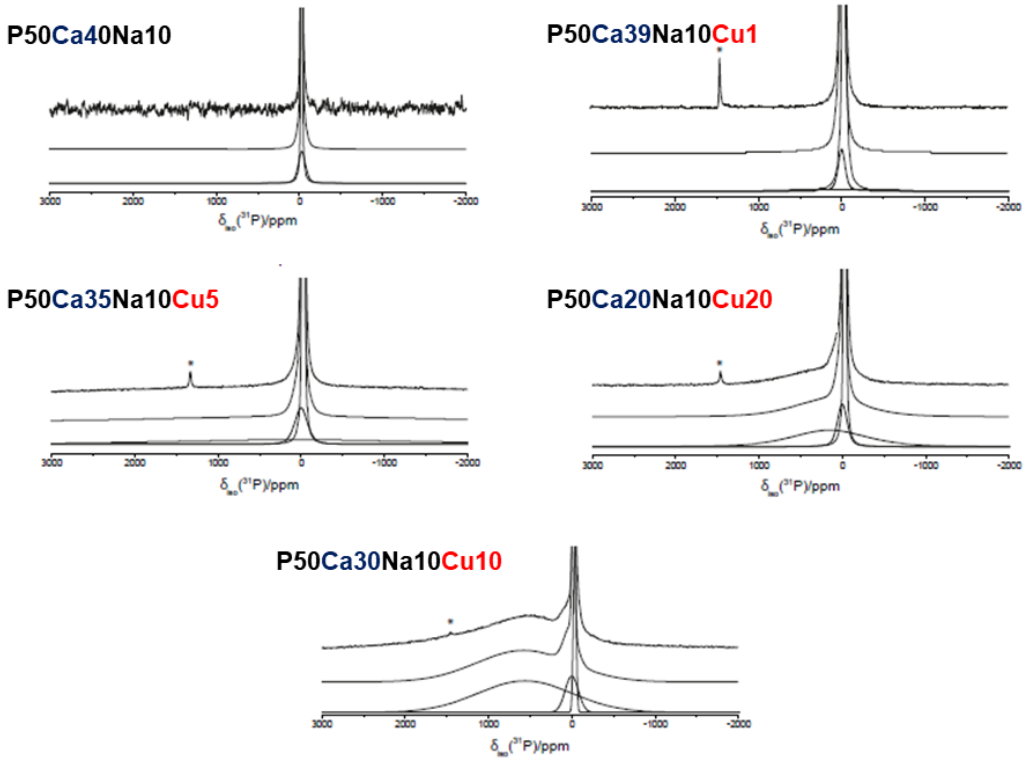

Figure 80. 2.35 T ^{31}P NMR Data (V_r = 60 kHz) at relaxation delay = 0.1 s

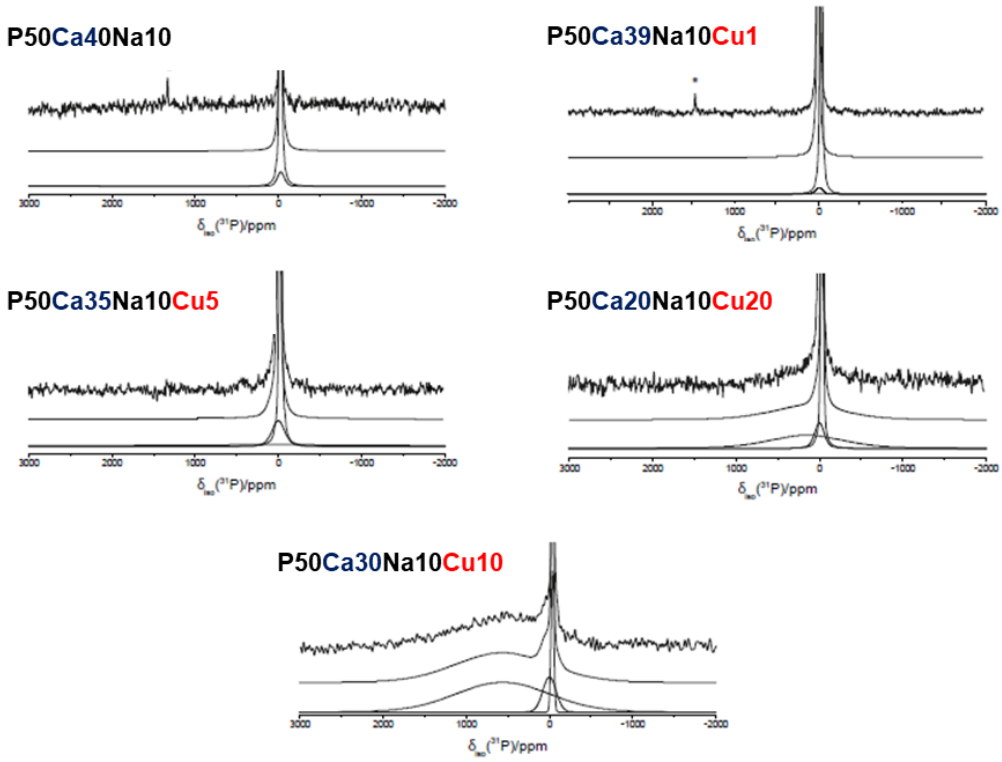

Figure 81. 2.35 T ^{31}P NMR Data (V_r = 60 kHz) at relaxation delay = 35 s

Table 16. The percentage of each of the fitted components in the ^{31}P MAS NMR data $(v_r = 60\ kHz)$

Sample	0.1 s relaxation delay						35 s relaxation delay					
	δ_{iso} [ppm]	I [%]	δ_{iso} [ppm]	I [%]	δ_{iso} [ppm]	I [%]	δ_{iso} [ppm]	I [%]	δ_{iso} [ppm]	I [%]	δ_{iso} [ppm]	I [%]
PCN			-30.6	18.8	-28.1	81.2			-30.6	4.1	-28.1	95.9
Cu1	42.6	2.7	0.4	4.9	-28.2	92.4	42.6	4.8	0.4	2.1	-28.2	93.1
Cu5	78.4	28.3	0.4	12.3	-27.7	59.4	78.4	14.5	0.4	10.9	-27.7	74.5
Cu10	155	34.8	0.5	11.9	-30.4	53.3	155	37.9	0.5	9.8	-30.4	52.3
Cu20	562	75.5	0.2	12.2	-35.3	12.3	562	76.1	0.2	12.7	-35.3	11.2

Figure 80, Figure 81and Table 16 is 31P NMR carried out at much lower field. The 600 ppm broad peak at Cu20 is shifts towards 0 ppm as Cu decreases. This suggests the presence of other species as more copper is added containing phosphorous. The broadening of the peak is a common phenomenon with copper containing glass.

5.2.7 X-ray photoelectron spectroscopy and DEPTH profile

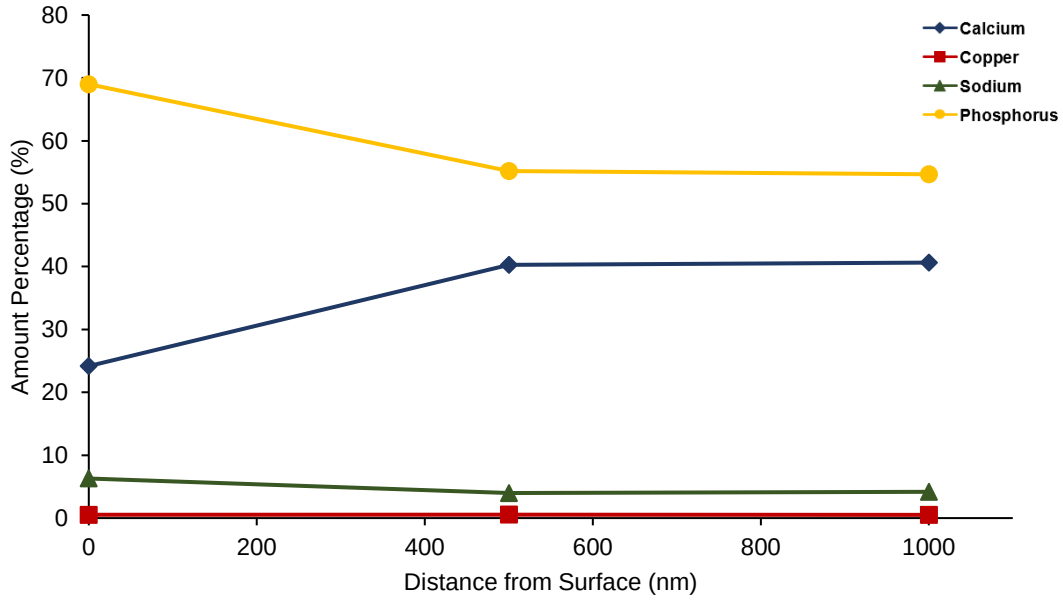

Figure 82. Average elemental percentage of elements at difference distance from the surface of Cu1 glass discs before immersion tests.

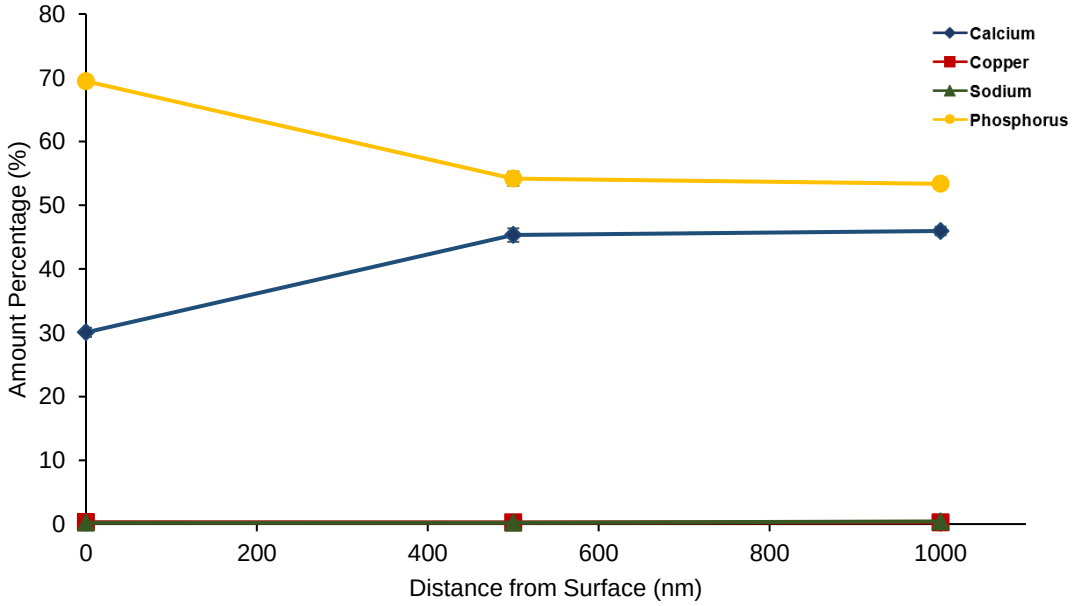

Figure 83. Average elemental percentage of elements at difference distance from the surface of Cu1 glass discs after 7 day static immersion in deionised water.

Figure 82 and Figure 83 shows the elemental composition of Cu1 glass before and after immersion tests. Before immersion the elemental composition from 500 nm resembles the composition of the glass, the surface composition may be different due to glass been cut with diamond saw in presence of water. After 7 day immersion there is an increase in calcium and depletion of copper and sodium till 1000 nm with phosphorous remaining same as before immersion. This is possibly due to the sodium ion diffusing out of the glass first due to the hydration mechanism of glass dissolution, but generally the composition remained constant before and after immersion.

Figure 84 and Figure 85 shows the elemental composition of Cu20 glass before and after immersion tests. Again, the difference between the surface and 500 nm is expected due to the glass being cut in a wet environment in before test glass. The bulk composition from *ca*. 500 nm again represents the increase in copper and decrease in calcium. After immersion, copper content is much greater than the calcium at the surface and 1000 nm into the bulk. Whilst the mol% of CaO is present equally as CuO. This may be due to Cu^{2+} being small and easier to diffuse to the surface and is able to form stronger attraction with negative ions than Ca^{2+} and Na^{+}. This is an interesting result as the dissolution rate and the phosphate release decreases, the release of antimicrobial copper increases. Making an ideal candidate for an antimicrobial glass composition.

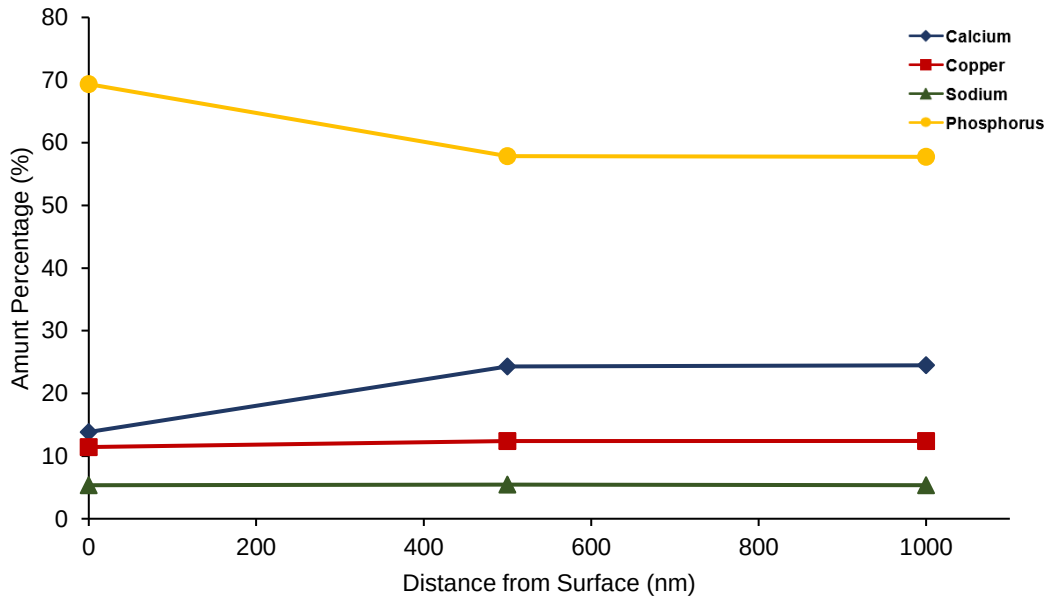

Figure 84. Average elemental percentage of elements at difference distance from the surface of Cu20 glass discs before immersion tests.

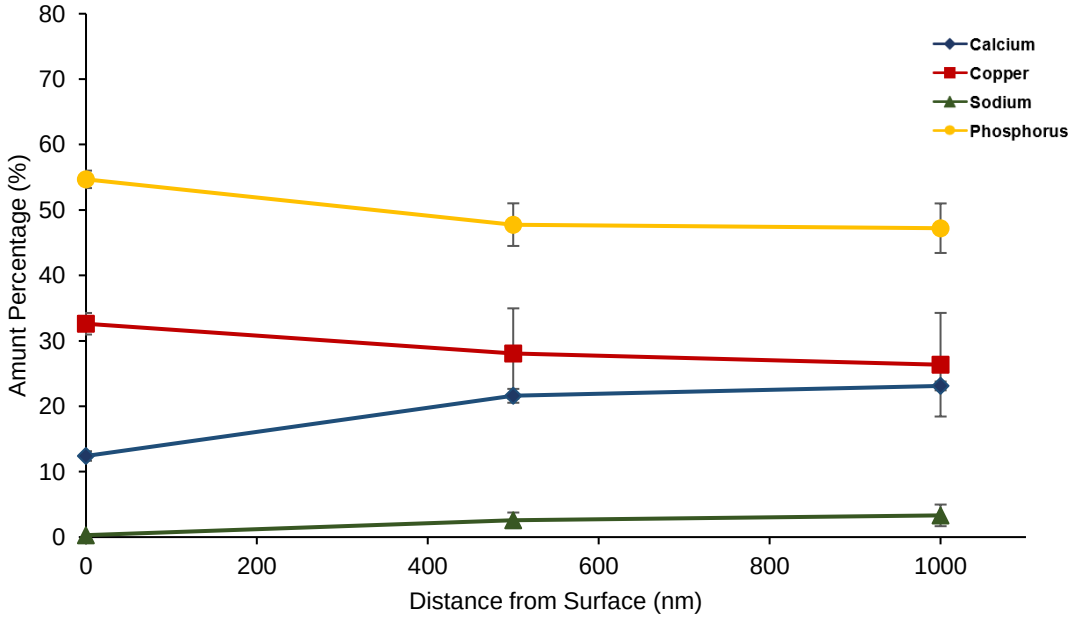

Figure 85. Average elemental percentage of elements at difference distance from the surface of Cu20 glass discs after 7 day static immersion in deionised water.

5.2.8 Antimicrobial properties of copper doped phosphate glass

Figure 86. Agar plate with Cu20 glass fibre placed on top before incubation.

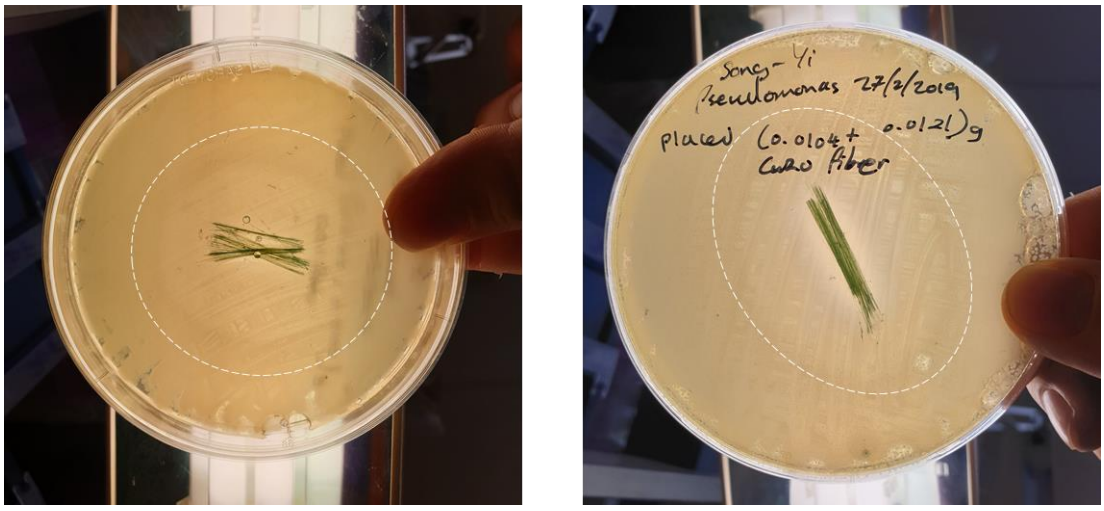

Figure 87. Agar plate after 1 day incubation with Cu20 glass fibre showing zones where bacteria has been killed.

Antimicrobial tests were carried out to observe the bacterial killing effect of copper containing glass. Glass was pulled out into fibres and noticeable results came from fibres, since antimicrobial testing with glass discs were impractical and not possible. An agar plate covered with pseudomonas aeruginosa was prepared and sterilised Cu20 glass fibres was placed on top and were incubated overnight. From Figure 87 we can clearly see zones where pseudomonas aeruginosa was killed, showing that even with 1 day incubation the Cu20 glass fibre is capable of killing bacteria. Copper ions released from the glass fibres are likely to be greater than the glass discs due to their high surface are to volume ratio. The Cu^{2+} ions will undergo contact killing, where the pseudomonas aeruginosa losing the structural integrity of the cell membrane and damages to the genetic material.[138,139] Further research into copper doped phosphate glass as fibres would be suggested as glass fibres are often used in filters and having anti scaling and antimicrobial property it would be an ideal candidate.

Due to the limited time and current global situation the microbial test could not progress further.

6 Final discussion and Future Work

The researched conducted in this thesis aimed to use ternary phosphate based glass and copper doped quaternary phosphate glass for anti scaling applications. Experimental works were performed on glass discs, understanding their intrinsic nature and controlled ion release properties of the $50P_2O_5 \cdot 10Na_2O \cdot 40CaO$ (mol%) or *PCN from hereon* and reaching $50P_2O_5 \cdot 10Na_2O \cdot 20CaO \cdot 20CuO$ composition of glass for possible antimicrobial applications.

Degradation experiments were carried out to determine the controlled ion release efficiency and degradation rates under static, dynamic, continual and intimate immersions. We observed that lower sodium oxide (Na_2O) content allowed for more slower degradation as Na^+ being the first ion to leach into the water allowing faster hydration layer formation on glass surface. Increasing calcium oxide (CaO) mol% also reduced the degradation rate due to the presence of higher positive 2+ ions in the glass network forming stronger interactions. These adjustments of oxides allowed controlled release of ions, especially polyphosphates necessary for scale inhibition making the more tuneable.

Degradation was much faster in deionised water as high as *ca*. 1800% faster in static and immersed all the time. This was expected when comparing to tap water due to absence of ions creating high concentration gradient. Previous studies showed that during static conditions the solution would reach saturation quite early delaying and preventing further ion release which was not observed for this PCN glass composition. Suggesting that the ions

released during this research was released in lower amounts and was not excessive. Dynamic conditions showed greater weight loss in tap water than static conditions, the consistent flow of water removing ions to maintain constant ion concentration of tap water. Whilst static tap water unlike deionised water has large amounts of ions already present allowing faster saturation of ions slowing down diffusion and degradation. Phosphate ion released showed $P_3O_9^{3-}$ being the most abundant ion followed by PO_4^{3-}, $P_3O_{10}^{6-}$ and $P_2O_7^{4-}$. The scale inhibition results carried out with humidifiers first mentioned in this thesis can be comparable to static and immersed all the time in tap water. As $P_3O_9^{3-}$ release in deionised water is more than 7000% than in tap water, it shows phosphate does not need to be released excessively amounts in order to achieve anti scaling. Degradation was faster in lower pH and hence increase in phosphate concentrations were observed. This confirmed previous research showing identical results explained by the higher concentration of protons at lower pH disrupting phosphate chains leading to accelerated dissolution and phosphate release. In future studies this thesis would like to explore into other phosphate ions to see if they have similar properties and research deeper into how and why different phosphate give different results.

Weathering and durability tests were performed on glass discs to understand how the conditions in which they were kept in will affect the degradation and ion release. Showing negligible physical difference at 20 and 30 °C. At higher temperatures and humidity, the glass surface formed white precipitates owing to absorption of moisture from air. Degradation tests showed comparable phosphate releases with the freshly prepared glass discs with difference of

delayed degradation due to surface of glass being dry causing slower hydration layer formation. Durability tests showed that this glass composition has the potential to be stored without deterioration of its properties making an attractive material that can be used in most living conditions.

Copper doping into the anti scaling PCN to achieve antimicrobial dual property was studied first with degradation. As CuO mol% increased the degradation rate decreased. Owing to the smaller ionic radius and with larger electronegativity of 1.90 in Cu than 1.00 in Ca by Pauling scale, possibly forming stronger interaction with hydroxyl ion from the solution within the structure. This was also observed with ^{31}P NMR showing chemical shifts forming and increasing in percentage with increasing addition of cooper, at the expense of Q^2 peaks. With addition of copper, $P_3O_9^{3-}$ release decreases by 87% from PCN to Cu20 in 7 day immersion but showed 212% increase of $P_3O_{10}^{6-}$. $P_3O_{10}^{6-}$ phosphate being well known to drive anti scaling the addition of copper showed more even phosphate release for all phsophates. Cu20 glass showed phosphate release in concentrations which we know that is effective in anti scaling. The more even release of polyphosphates with decrease in overall phosphate release is also positive as it reduces excessive release whilst increasing the anti scaling efficiency with more $P_3O_{10}^{6-}$. Cu20 glass pulled into glass fibres was very effective at killing pseudomonas aeruginosa, being an effective antimicrobial material due to Cu^{2+} ions released undergoing contact killing. Higher copper concentration showing more efficient antimicrobial effect as expected. With Cu20 we observed 2.9 times more Cu^{2+} released than Ca^{2+} when present in equal mol%. Possibly due to smaller size,

the migration of Cu^{2+} to the surface is easier which was also observed with XPS results showing migration of Cu as much as 30% more at the surface when compared to be before immersion. Sodium ions seemed to decrease at the surface which may be due to the faster speed of ion release and depletion as seen in previous studies. Phosphate and copper amount before and after immersion showed no noticeable difference up to 1000 nm into the bulk. It was also interesting to observed that the contact angle appeared to increase as copper concentration increase. This change in physical property is something that could be explored further in future studies to understand how the surface properties relate to dissolution. Future studies would also involve more detailed and extended antimicrobial study which was caught short due to COVID-19 restrictions. Incorporation of other antimicrobial metals into glass would also be informative in understanding effectiveness of contact killing and ion release properties. It would be interesting to study the how further increase if copper would effect phosphate release and it antimicrobial property.

Apart from glass disc, the glass fibre has wider potential applications, and it would be one of the next research that this thesis would like to conduct. Incorporation of effective glass fibres into air or water filters to see if it is able to achieve both antimicrobial and anti scaling property and how different physical form of the glass would impact the results. Research into phosphate glass and controlled degradation is a very attractive property currently not fully explored nor exploited commercially. This material has the potential to solve the hard water endemic with ease with the absence of complicated set-up and cost. Providing a cost effective and environmentally attractive solution.

Studying the glass on other appliances prone to scale attack would also be very interesting to see how it may perform on larger scale.

Expanding from the thesis research, metals not only have antimicrobial property. Essential metals such as iron for healthy blood and molybdenum for proteins and DNA are required in the body and this research, if possible, the research would like to also explore how these, and other essential metal ions may be released or even be delivered into the body in controlled amounts.

Bibliography

1. Semine Ras, H. & Ghizellaoui, S. Determination of anti-scale effect of hard water by test of electrodeposition. *Procedia Eng.* **33**, 357–365 (2012).

2. Baker, D. K. & Vliet, G. C. Identifying and reducing scaling problems in solar hot water systems. *J. Sol. Energy Eng. Trans. ASME* **125**, 61–66 (2003).

3. Glass, B. P. Glass: The Geologic Connection. *Int. J. Appl. Glas. Sci.* **7**, 435–445 (2016).

4. Aliprandi, G. *Glasses and the vitreous state*. *Materials Chemistry and Physics* vol. 30 (1992).

5. Paul, A. Glass Formation. *Chem. Glas.* 1–15 (1982) doi:10.1007/978-94-009-5918-7_1.

6. Martin, J. W. Glasses and ceramics. *Mater. Eng.* 133–158 (2006) doi:10.1533/9781845691608.2.133.

7. Karazi, S. M., Ahad, I. U. & Benyounis, K. Y. Laser Micromachining for Transparent Materials. *Ref. Modul. Mater. Sci. Mater. Eng.* 1–22 (2017) doi:10.1016/b978-0-12-803581-8.04149-7.

8. Plodinec, M. J. Borosilicate glasses for nuclear waste imobilisation. *Glas. Technol.* **41**, 186–192 (2000).

9. Hasanuzzaman, M., Rafferty, A., Sajjia, M. & Olabi, A.-G. *Properties of Glass Materials*. *Reference Module in Materials Science and Materials Engineering* (Elsevier Ltd., 2016). doi:10.1016/b978-0-12-803581-8.03998-9.

10. Ojovan, M. I., Lee, W. E. & Kalmykov, S. N. Immobilisation of Radioactive Wastes in Glass. *An Introd. to Nucl. Waste Immobil.* 319–368 (2019) doi:10.1016/b978-0-08-102702-8.00019-4.

11. Nevolina, L. A., Koroleva, O. N., Tyurnina, N. G. & Tyurnina, Z. G. Study of Alkaline Earth Borosilicate Glass by Raman Spectroscopy. *Glas. Phys. Chem.* **47**, 24–29 (2021).

12. ABE, T. The Structure of Borosilicate Glasses. *J. Ceram. Assoc. Japan* **59**, 474–481 (1951).

13. Nezafati, N., Moztarzadeh, F. & Hesaraki, S. Surface reactivity and in vitro biological evaluation of sol gel derived silver/calcium silicophosphate bioactive glass. *Biotechnol. Bioprocess Eng.* **17**, 746–754 (2012).

14. Hoppe, A. & Boccaccini, A. R. Biological Impact of Bioactive Glasses and Their Dissolution Products. *Front. Oral Biol.* **17**, 22–32 (2015).

15. Hudgens, J. J., Brow, R. K., Tallant, D. R. & Martin, S. W. Raman spectroscopy study of the structure of lithium and sodium

ultraphosphate glasses. *J. Non. Cryst. Solids* **223**, 21–31 (1998).

16. Ahmed, I., Lewis, M., Olsen, I. & Knowles, J. C. Phosphate glasses for tissue engineering: Part 1. Processing and characterisation of a ternary-based P2O5-CaO-Na 2O glass system. *Biomaterials* **25**, 491–499 (2004).

17. Richard K, B. Review: the structure of simple phosphate glasses. *J. Non. Cryst. Solids* **263**–**264**, 1–28 (2000).

18. Cruickshank, D. W. J. 1077. The rôle of 3d-orbitals in π-bonds between (a) silicon, phosphorus, sulphur, or chlorine and (b) oxygen or nitrogen. *J. Chem. Soc.* **0**, 5486–5504 (1961).

19. Mitchell, K. A. R. The use of outer d orbitals in bonding. *Chem. Rev.* **69**, 157–178 (1969).

20. Ahmed, I., Lewis, M., Olsen, I. & Knowles, J. C. Phosphate glasses for tissue engineering: Part 2. Processing and characterisation of a ternary-based P2O5-CaO-Na 2O glass fibre system. *Biomaterials* **25**, 501–507 (2004).

21. Salih, V. *et al.* Development of soluble glasses for biomedical use part II: The biological response of human osteoblast cell lines to phosphate-based soluble glasses. *J. Mater. Sci. Mater. Med.* **11**, 615–620 (2000).

22. Al Qaysi, M. *et al.* Strontium- and calcium-containing, titanium-stabilised phosphate-based glasses with prolonged degradation for orthopaedic tissue engineering. *J. Biomater. Appl.* **30**, 300–310 (2015).

23. Temperatures, M. *Introduction to Plastics Engineering Glass Transition Temperature*. *Rotational Molding Technology* (2002).

24. Paul, A. Phase Transformations in Glass. *Chem. Glas.* 16–50 (1982) doi:10.1007/978-94-009-5918-7_2.

25. Perera, G., Doremus, R. H. & Lanford, W. Dissolution Rates of Silicate Glasses in Water at pH 7. *J. Am. Ceram. Soc.* **74**, 1269–1274 (1991).

26. Tomozawa, M. & Capella, S. Microstructure in Hydrated Silicate Glasses. *J. Am. Ceram. Soc.* **66**, C-24-C-25 (1983).

27. Doremus, R. H. Diffusion-controlled reaction of water with glass. *J. Non. Cryst. Solids* **55**, 143–147 (1983).

28. European Commission. *Scientific Committee on Consumer Safety (SCCS)*. *Scientific Committees* (2021).

29. Doremus, R. H. & Turkalo, A. M. Phase separation in pyrex glass. *Science (80-.).* **164**, 418–419 (1969).

30. Gao, H., Tan, T. & Wang, D. Dissolution mechanism and release kinetics of phosphate controlled release glasses in aqueous medium.

J. Control. Release **96**, 29–36 (2004).

31. Bunker, B. C., Arnold, G. W. & Wilder, J. A. Phosphate glass dissolution in aqueous solutions. *J. Non. Cryst. Solids* **64**, 291–316 (1984).

32. Q.X. Liu, X.M. Chen, X. L. The hydrolysis of Na2O.CaO.2P2O5 bioglass. *J. Wuhan Univ. Technol.* **18**, 26–29 (1996).

33. LS Hou, Y. T. Y. Z. The chemical durability of Nd-phosphate glasses. *J. Chinese Silic.* **8**, 1980-undefined (1980).

34. WHO, G. Guidelines for drinking-water quality. *World Heal. Organ.* **216**, 303–304 (2011).

35. Ayoob, S. & Gupta, A. K. *Fluoride in drinking water: A review on the status and stress effects*. *Critical Reviews in Environmental Science and Technology* vol. 36 (2006).

36. Bouchard, M. F. *et al.* Intellectual impairment in school-age children exposed to manganese from drinking water. *Environ. Health Perspect.* **119**, 138–143 (2011).

37. Payment, P. *et al.* A prospective epidemiological study of gastrointestinal health effects due to the consumption of drinking water. *Int. J. Environ. Health Res.* **7**, 5–31 (1997).

38. Chaumont, A., Voisin, C., Sardella, A. & Bernard, A. Interactions between domestic water hardness, infant swimming and atopy in the development of childhood eczema. *Environ. Res.* **116**, 52–57 (2012).

39. Myers, J. T. The Relationship of Hard Water to Health : I . Hard Water as a Possible Factor in Urinary Concretion Formation Author (s): John T . Myers Source : The Journal of Infectious Diseases , Vol . 36 , No . 6 (Jun ., 1925), pp . 566-576 Published by : Oxford. *Oxford Journals* **36**, 566–576 (2019).

40. Myers, J. T. Relationship of Hard Water to Health : II . Effect of Hard Water on Growth , Appearance and General Well-Being Author (s): John T . Myers Published by : Oxford University Press Stable URL : https://www.jstor.org/stable/30101768. *Oxford Journals* **37**, 13–34 (2019).

41. Klevay, L. M. Some bottled water may be salubrious. *J. Trace Elem. Med. Biol.* **48**, 188–189 (2018).

42. Cotruvo, J. A., Costello, R. & Weglicki, W. B. Magnesium, Hard Water, and Health. *J. Am. Water Works Assoc.* **109**, 62–68 (2017).

43. Rapant, S. *et al.* Hard water, more elastic arteries: A case study from Krupina District, Slovakia. *Int. J. Environ. Res. Public Health* **16**, 1–14 (2019).

44. BRANDS, H. J. *Treatment of water*. (1971). doi:10.1002/j.1551-8833.1928.tb17744.x.

45. Cooper, K. G., Hanlon, L. G., Smart, G. M. & Talbot, R. E. The threshold scale inhibition phenomenon. *Desalination* **31**, 257–266 (1979).

46. Tadier, S., Rokidi, S., Rey, C., Combes, C. & Koutsoukos, P. G. Crystal growth of aragonite in the presence of phosphate Open Archive TOULOUSE Archive Ouverte (OATAO) Crystal growth of aragonite in the presence of phosphate. *J. Cryst. Growth* **458**, 44–52 (2017).

47. Lin, Y. P. & Singer, P. C. Inhibition of calcite crystal growth by polyphosphates. *Water Res.* **39**, 4835–4843 (2005).

48. Lin, Y. P. & Singer, P. C. Inhibition of calcite precipitation by orthophosphate: Speciation and thermodynamic considerations. *Geochim. Cosmochim. Acta* **70**, 2530–2539 (2006).

49. Brett, S. W., Gaterell, M. R., Morse, G. K. & Lester, J. N. A cost comparison of potable water softening technologies. *Environ. Technol. (United Kingdom)* **20**, 1009–1018 (1999).

50. Ostovar, M. & Amiri, M. A Novel Eco-Friendly Technique for Efficient Control of Lime Water Softening Process. *Water Environ. Res.* **85**, 2285–2293 (2013).

51. Roalson, S. R., Kweon, J., Lawler, D. F. & Speitel, G. E. Enhanced softening: Effects of lime dose and chemical additions. *J. / Am. Water Work. Assoc.* **95**, 97–109 (2003).

52. Eleni, G., Georgios, P., Konstantina, K. & Alexandros, B. Ca2+ removal from water by the use of Na-palygorskite for potential water softening. *Water Supply* **00**, 1–14 (2021).

53. Cinar, S. & Beler-Baykal, B. Ion exchange with natural zeolites: An alternative for water softening? *Water Sci. Technol.* **51**, 71–77 (2005).

54. Entezari, M. H. & Tahmasbi, M. Water softening by combination of ultrasound and ion exchange. *Ultrason. Sonochem.* **16**, 356–360 (2009).

55. Raistrick, B. _. *Discuss. Faraday Soc.* **234**, (1949).

56. Elliot, M. N. _. *Desalination* **8**, (1970).

57. A. Glasner and S. Skurnik. _. *Isr. J. Chem.* **6**, (1968).

58. Ayers, R. F. R. and A. D. _. *J.A.C.S.* **69**, (1947).

59. Parfitt, R. L., Thomas, A. D., Atkinson, R. J. & Smart, R. S. C. Adsorption of phosphate on imogolite. *Clays Clay Miner.* **22**, 455–456 (1974).

60. Suzuki, T., Inomata, S. & Sawada, K. Adsorption of phosphate on calcite. *J. Chem. Soc. Faraday Trans. I* **82**, 1733–1743 (1986).

61. Sawada, G. H. N. and K. _. *J. Pet. Tech.,* **645**, (1982).

62. Ayers, J. C. & Watson, E. B. Solubility of apatite , monazite , zircon , and rutile in supercritical aqueous fluids with implications for subduction zone geochemistry. *Philos. Trans. R. Soc. London* (1991) doi:10.1098/rsta.1991.0052.

63. Boels, L., Keesman, K. J. & Witkamp, G. J. Adsorption of phosphonate antiscalant from reverse osmosis membrane concentrate onto granular ferric hydroxide. *Environ. Sci. Technol.* **46**, 9638–9645 (2012).

64. Carpenter, S. R. Eutrophication of aquatic ecosystems: Bistability and soil phosphorus. *Proc. Natl. Acad. Sci. U. S. A.* **102**, 10002–10005 (2005).

65. Marshall, J. P. & Wilcox, H. How Green and Does it Clean. in *Developments in Surface Contamination and Cleaning* (eds. Kohli, R. & Mittal, K. L.) 1–69 (William Andrew Publishing, 2015). doi:10.1016/b978-0-323-29961-9.00001-6.

66. Yang, Q., Liu, Y., Gu, A., Ding, J. & Shen, Z. Investigation of calcium carbonate scaling inhibition and scale morphology by AFM. *J. Colloid Interface Sci.* **240**, 608–621 (2001).

67. Tang, Y. *et al.* Investigation of CaCO3 scale inhibition by PAA, ATMP and PAPEMP. *Desalination* **228**, 55–60 (2008).

68. Nowack, B. Environmental chemistry of phosphonates. *Water Res.* **37**, 2533–2546 (2003).

69. Jonasson, R. G., Rispler, K., Wiwchar, B. & Gunter, W. D. Effect of phosphonate inhibitors on calcite nucleation kinetics as a function of temperature using light scattering in an autoclave. *Chem. Geol.* **132**, 215–225 (1996).

70. Nowack, B. & Stone, A. T. Adsorption of phosphonates onto the Goethite-Water interface. *J. Colloid Interface Sci.* **214**, 20–30 (1999).

71. Bharadishettar, N. Coating Technologies for Copper Based Antimicrobial Active Surfaces : A Perspective Review. *Metals (Basel).* **11**, (2021).

72. Grass, G., Rensing, C. & Solioz, M. Metallic copper as an antimicrobial surface. *Appl. Environ. Microbiol.* **77**, 1541–1547 (2011).

73. Wang, P. *et al.* Surface touch network structure determines bacterial contamination spread on surfaces and occupant exposure. *J. Hazard. Mater.* **416**, 126137 (2021).

74. Dollwet, H. H. A. & Sorenson, J. R. J. Historic uses of copper

compounds in medicine. *Trace Elem. Med.* **2**, 80–87 (1985).

75. Rutala, W. A. & Weber, D. J. Disinfection and sterilization: An overview. *Am. J. Infect. Control* **41**, S2-5 (2013).

76. Kochare, T. and B. T. Assessment of Dairy Feeds for Heavy Metals. *Am. Sci. Res. J. Eng.* **11**, 20–31 (2015).

77. Fosmire, G. J. Zinc toxicity. *Am. J. Clin. Nutr.* **51**, 225–227 (1990).

78. Disease, W. Direct Determination of Non-Cerulo- plasmin-Bound Copper in Plasma A worldwide yearly survey of new data in adverse drug reactions. (2019).

79. Service, U. S. P. H. Toxicololgy profile for silver. *Agency Toxic Subst. Dis. Regist.* (1990).

80. Yazdankhah, S., Skjerve, E. & Wasteson, Y. Antimicrobial resistance due to the content of potentially toxic metals in soil and fertilizing products. *Microb. Ecol. Health Dis.* **29**, 1548248 (2018).

81. Vimbela, G. V., Ngo, S. M., Fraze, C., Yang, L. & Stout, D. A. Antibacterial properties and toxicity from metallic nanomaterials. *Int. J. Nanomedicine* **12**, 3941–3965 (2017).

82. Azam, A. *et al.* Antimicrobial activity of metal oxide nanoparticles against Gram-positive and Gram-negative bacteria: A comparative study. *Int. J. Nanomedicine* **7**, 6003–6009 (2012).

83. Bilian, X. Intrauterine devices. *Best Pract. Res. Clin. Obstet. Gynaecol.* **16**, 155–168 (2002).

84. Grass, G., Rensing, C. & Solioz, M. Metallic copper as an antimicrobial surface. *Applied and Environmental Microbiology* vol. 77 1541–1547 (2011).

85. Vincent, M., Duval, R. E., Hartemann, P. & Engels-Deutsch, M. Contact killing and antimicrobial properties of copper. *J. Appl. Microbiol.* **124**, 1032–1046 (2018).

86. Usman, M. S. *et al.* Synthesis, characterization, and antimicrobial properties of copper nanoparticles. *Int. J. Nanomedicine* **8**, 4467–4479 (2013).

87. Raffi, M. *et al.* Investigations into the antibacterial behavior of copper nanoparticles against Escherichia coli. *Ann. Microbiol.* **60**, 75–80 (2010).

88. Warnes, S. L. & Keevil, C. W. Inactivation of Norovirus on Dry Copper Alloy Surfaces. *PLoS One* **8**, (2013).

89. Borkow, G., Lara, H. H., Covington, C. Y., Nyamathi, A. & Gabbay, J. Deactivation of human immunodeficiency virus type 1 in medium by

copper oxide-containing filters. *Antimicrob. Agents Chemother.* **52**, 518–525 (2008).

90. Borkow, G., Zhou, S. S., Page, T. & Gabbay, J. A novel anti-influenza copper oxide containing respiratory face mask. *PLoS One* **5**, (2010).

91. Borkow, G. & Gabbay, J. 0005C.pdf. *Curr. Med. Chem.* **12**, 2163–2175 (2005).

92. Warnes, S. L., Caves, V. & Keevil, C. W. Mechanism of copper surface toxicity in Escherichia coli O157:H7 and Salmonella involves immediate membrane depolarization followed by slower rate of DNA destruction which differs from that observed for Gram-positive bacteria. *Environ. Microbiol.* **14**, 1730–1743 (2012).

93. Santo, C. E. *et al.* Bacterial killing by dry metallic copper surfaces. *Appl. Environ. Microbiol.* **77**, 794–802 (2011).

94. Ben-Sasson, M. *et al.* Surface functionalization of thin-film composite membranes with copper nanoparticles for antimicrobial surface properties. *Environ. Sci. Technol.* **48**, 384–393 (2014).

95. Wu, C. *et al.* Copper-containing mesoporous bioactive glass scaffolds with multifunctional properties of angiogenesis capacity, osteostimulation and antibacterial activity. *Biomaterials* **34**, 422–433 (2013).

96. Yahya, M. T. *et al.* Disinfection of bacteria in water systems by using electrolytically generated copper:silver and reduced levels of free chlorine. *Can. J. Microbiol.* **36**, 109–116 (1990).

97. Mijnendonckx, K., Leys, N., Mahillon, J., Silver, S. & Van Houdt, R. Antimicrobial silver: Uses, toxicity and potential for resistance. *BioMetals* **26**, 609–621 (2013).

98. Lok, C. N. *et al.* Silver nanoparticles: Partial oxidation and antibacterial activities. *J. Biol. Inorg. Chem.* **12**, 527–534 (2007).

99. Shrivastava, S. *et al.* Characterization of enhanced antibacterial effects of novel silver nanoparticles. *Nanotechnology* **18**, (2007).

100. Xiu, Z. M., Zhang, Q. B., Puppala, H. L., Colvin, V. L. & Alvarez, P. J. J. Negligible particle-specific antibacterial activity of silver nanoparticles. *Nano Lett.* **12**, 4271–4275 (2012).

101. Gordon, O. *et al.* Silver coordination polymers for prevention of implant infection: Thiol interaction, impact on respiratory chain enzymes, and hydroxyl radical induction. *Antimicrob. Agents Chemother.* **54**, 4208–4218 (2010).

102. Russell, A. D. & Hugo, W. B. Antimicrobial activity and action of silver. *Prog. Med. Chem.* **31**, 351–370 (1994).

103. Pal, S., Tak, Y. K. & Song, J. M. Does the antibacterial activity of silver nanoparticles depend on the shape of the nanoparticle? A study of the gram-negative bacterium Escherichia coli. *Appl. Environ. Microbiol.* **73**, 1712–1720 (2007).

104. Morones, J. R. *et al.* The bactericidal effect of silver nanoparticles. *Nanotechnology* **16**, 2346–2353 (2005).

105. Kawashita, M. *et al.* Antibacterial silver-containing silica glass prepared by sol-gel method. *Biomaterials* **21**, 393–398 (2000).

106. Ahmed, A. A., Ali, A. A., Mahmoud, D. A. R. & El-Fiqi, A. M. Study on the preparation and properties of silver-doped phosphate antibacterial glasses (Part I). *Solid State Sci.* **13**, 981–992 (2011).

107. Seil, J. T. & Webster, T. J. Antimicrobial applications of nanotechnology: Methods and literature. *Int. J. Nanomedicine* **7**, 2767–2781 (2012).

108. Li, M. *et al.* Elastin Blends for Tissue Engineering Scaffolds. *J. Biomed. Mater. Res. Part A* **79**, 963–73 (2006).

109. Sirelkhatim, A. *et al.* Review on zinc oxide nanoparticles: Antibacterial activity and toxicity mechanism. *Nano-Micro Lett.* **7**, 219–242 (2015).

110. Raghupathi, K. R., Koodali, R. T. & Manna, A. C. Size-dependent bacterial growth inhibition and mechanism of antibacterial activity of zinc oxide nanoparticles. *Langmuir* **27**, 4020–4028 (2011).

111. Espitia, P. J. P. *et al.* Zinc Oxide Nanoparticles: Synthesis, Antimicrobial Activity and Food Packaging Applications. *Food Bioprocess Technol.* **5**, 1447–1464 (2012).

112. J. Bae, J. Cha, D. Kim, Y. K. and B. R. Structure and Antibacterial Property of ZnO-B2O3-P2O5 Glasses. *J. Korean Ceram. Soc.* **55**, 4325–4330 (2018).

113. Nies, D. H. Microbial heavy-metal resistance. *Appl. Microbiol. Biotechnol.* **51**, 730–750 (1999).

114. National Research Council (US) Committe on Copper in Drinking Water. *Health Effects of Excess Copper*. *Copper in Drinking Water* (2000).

115. Ahmed, I., Lewis, M. P., Nazhat, S. N. & Knowles, J. C. Quantification of anion and cation release from a range of ternary phosphate-based glasses with fixed 45 mol% P2O5. *J. Biomater. Appl.* **20**, 65–80 (2005).

116. Delahaye, F., Montagne, L., Palavit, G., Touray, J. C. & Baillif, P. Acid dissolution of sodium-calcium metaphosphate glasses. *J. Non. Cryst. Solids* **242**, 25–32 (1998).

117. Bj, L., Wang, X. & Hupa, L. Dissolution of Bioactive Glasses in Acidic

Solutions with the Focus on Lactic Acid. *Int. J. Appl. Glas. Sci.* **7**, 154–163 (2016).

118. Luo, L. *et al.* Slow release of phosphate glass and its applications in the lead-contaminated soil remediation. *Toxicoloical Environ. Chem.* **98**, 518–529 (2016).

119. Massera, J. *et al.* Journal of Physics and Chemistry of Solids Effect of the glass composition on the chemical durability of zinc-phosphate-based glasses in aqueous solutions. *J. Phys. Chem. Solids* **74**, 121–127 (2013).

120. Greenspan, L. *Humidity Fixed Points of Binary Saturated Aqueous Solutions*. *JOURNAL OF RESEARCH of the National Bureau of Standards-A. Phys ics and Chemistry* vol. 81.

121. Samickannian, A., Venkatachalam, R., Nallaiyan, R. & Abubakkar, N. B. Structural and Textural Modifications of Ternary Phosphate Glasses by Thermal Treatment. *Int. J. Appl. Glas. Sci.* **2**, 222–234 (2011).

122. Kang, H. K. L. and W. H. Dissolution Properties of Phosphate Glasses with Trace Elements.pdf. *J. Korean Ceram. Soc.* **42**, 371–376 (2005).

123. Parsons, A. J., Burling, L. D., Scotchford, C. A., Walker, G. S. & Rudd, C. D. Properties of Sodium-Based Ternary Phosphate Glasses Produced From Properties of sodium-based ternary phosphate glasses produced from readily available phosphate salts. *J. Non. Cryst. Solids* **352**, 5309–5317 (2006).

124. Law, K. Y. Definitions for hydrophilicity, hydrophobicity, and superhydrophobicity: Getting the basics right. *J. Phys. Chem. Lett.* **5**, 686–688 (2014).

125. M. F. Barba, P. Callejas, J. O. Arzabe, J. M. V. Surface dissolution of calcium phosphate glass ceramics in dilute acid conditions. *J. Eur. Ceram. Soc.* **23**, 2893–2896 (2003).

126. Lina Ma, Richard K. Brow, M. E. S. Dissolution behaviour of Na2O-F2O-Fe2O3-P2O5 glasses. *J. Non. Cryst. Solids* **463**, 90–101 (2017).

127. Vincent, M., Hartemann, P. & Engels-Deutsch, M. Antimicrobial applications of copper. *Int. J. Hyg. Environ. Health* **219**, 585–591 (2016).

128. Yasuyuki, M. *et al.* Antibacterial properties of nine pure metals: A laboratory study using Staphylococcus aureus and Escherichia coli. *Biofouling* **26**, 851–858 (2010).

129. Champagne, V., Sundberg, K. & Helfritch, D. Kinetically deposited copper antimicrobial surfaces. *Coatings* **9**, 1–9 (2019).

130. Foroutan, F. *et al.* Antibacterial Copper-Doped Calcium Phosphate Glasses for Bone Tissue Regeneration. *ACS Biomater. Sci. Eng.* **5**,

6054–6062 (2019).

131. Abou Neel, E. A., Ahmed, I., Pratten, J., Nazhat, S. N. & Knowles, J. C. Characterisation of antibacterial copper releasing degradable phosphate glass fibres. *Biomaterials* **26**, 2247–2254 (2005).

132. Abou Neel, E. A., Pickup, D. M., Valappil, S. P., Newport, R. J. & Knowles, J. C. Bioactive functional materials: A perspective on phosphate-based glasses. *J. Mater. Chem.* **19**, 690–701 (2009).

133. Döhler, F., Mandlule, A., Van Wüllen, L., Friedrich, M. & Brauer, D. S. 31P NMR characterisation of phosphate fragments during dissolution of calcium sodium phosphate glasses. *J. Mater. Chem. B* **3**, 1125–1134 (2015).

134. Brady, G. W. Structure of sodium metaphosphate glass. *J. Chem. Phys.* **28**, 48–50 (1958).

135. Mathew, R. *et al.* Solid-state 31P and 1H NMR investigations of amorphous and crystalline calcium phosphates grown biomimetically from a mesoporous bioactive glass. *J. Phys. Chem. C* **115**, 20572–20582 (2011).

136. Jiménez-Holguín, J., Sánchez-Salcedo, S., Vallet-Regí, M. & Salinas, A. J. Development and evaluation of copper-containing mesoporous bioactive glasses for bone defects therapy. *Microporous Mesoporous Mater.* **308**, (2020).

137. Shih, P. Y., Ding, J. Y. & Lee, S. Y. 31P MAS-NMR and FTIR analyses on the structure of CuO-containing sodium poly- and meta-phosphate glasses. *Mater. Chem. Phys.* **80**, 391–396 (2003).

138. Santo, C. E., Quaranta, D. & Grass, G. Antimicrobial metallic copper surfaces kill Staphylococcus haemolyticus via membrane damage. *Microbiologyopen* **1**, 46–52 (2012).

139. Wei, X., Yang, Z., Wang, Y., Tay, S. L. & Gao, W. Polymer antimicrobial coatings with embedded fine Cu and Cu salt particles. *Appl. Microbiol. Biotechnol.* **98**, 6265–6274 (2014).

Appendix

Differential Thermal Alaysis

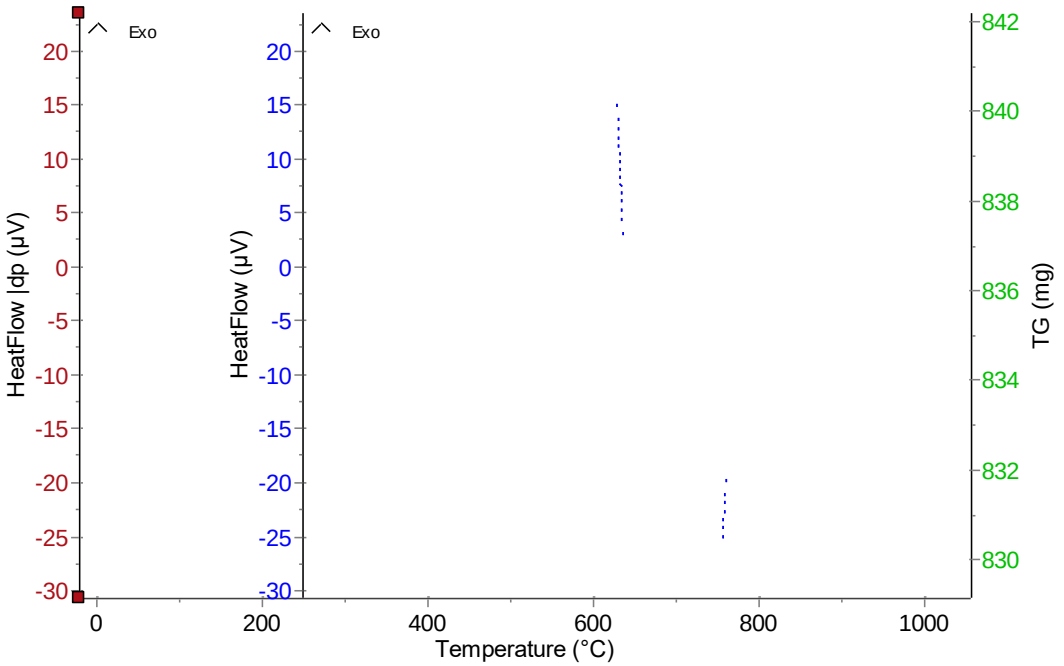

Figure 88. A plot given as result after running differential thermal analysis on P50Ca39Na10Cu1

Raman spectroscopy for glass

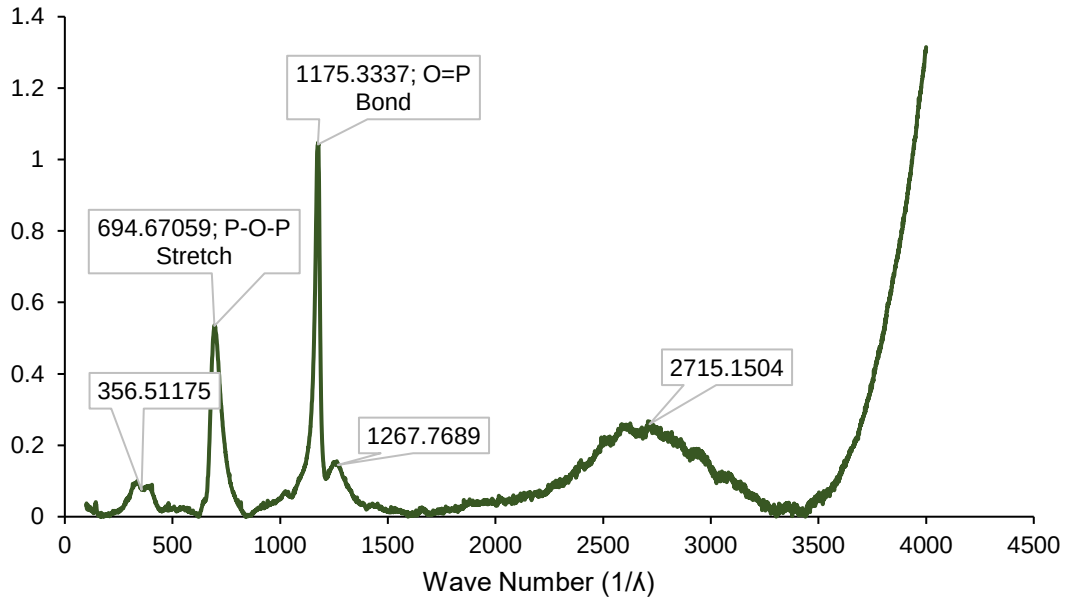

Figure 89. Raman spectroscopy for blank P50Ca40Na10 glass.

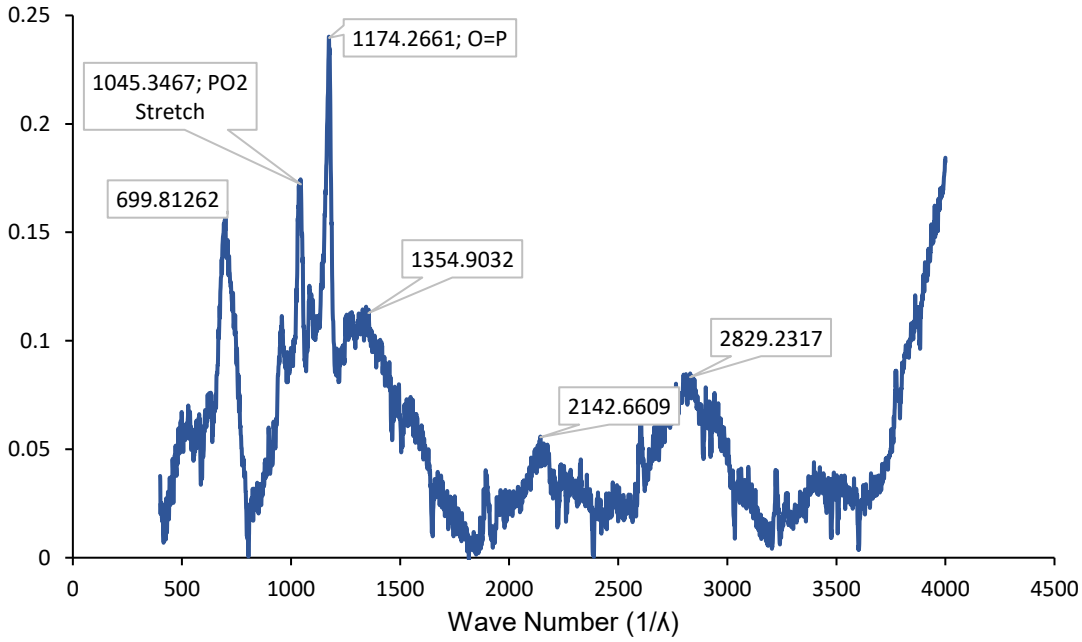

Figure 90. Raman spectroscopy for static and immersed all the time P50Ca40Na10 glass.

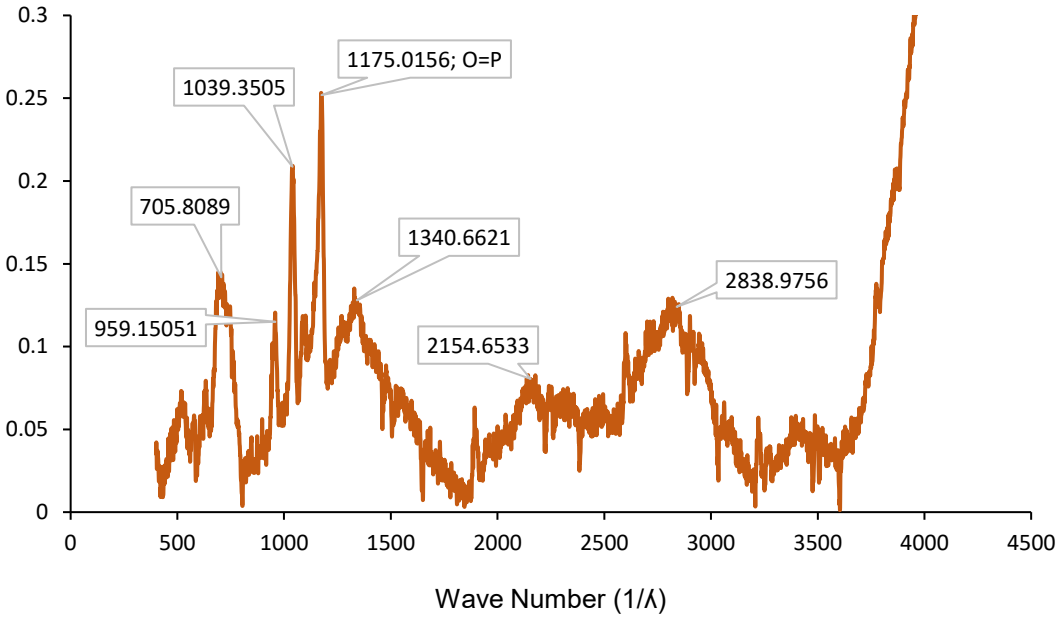

Figure 91. Raman spectroscopy for dynamic and immersed all the time P50Ca40Na10 glass.

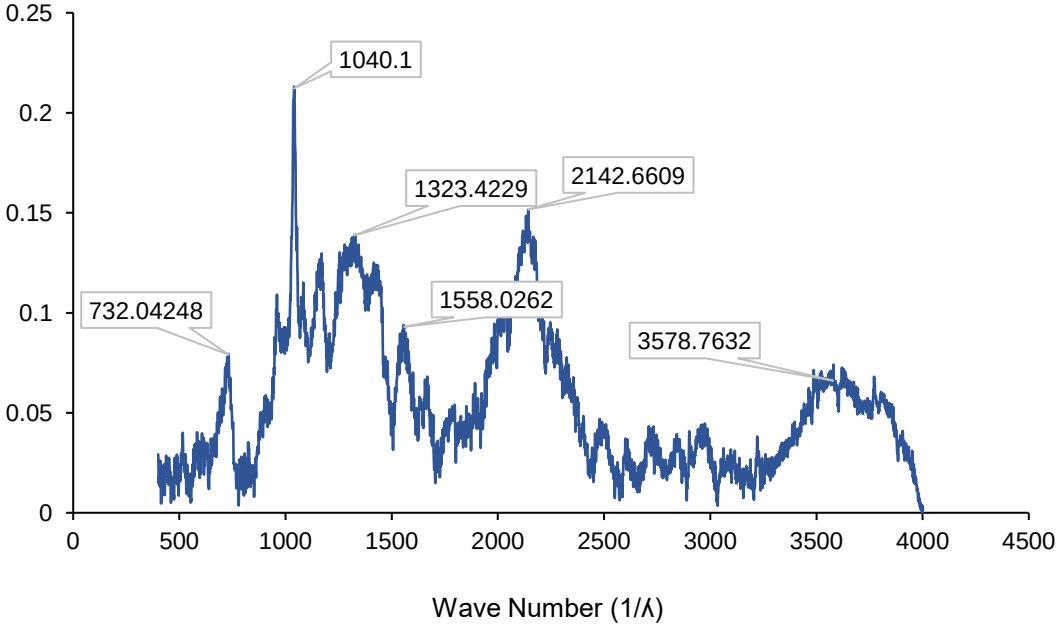

Figure 92. Raman spectroscopy for static and dried when not in used P50Ca40Na10 glass.

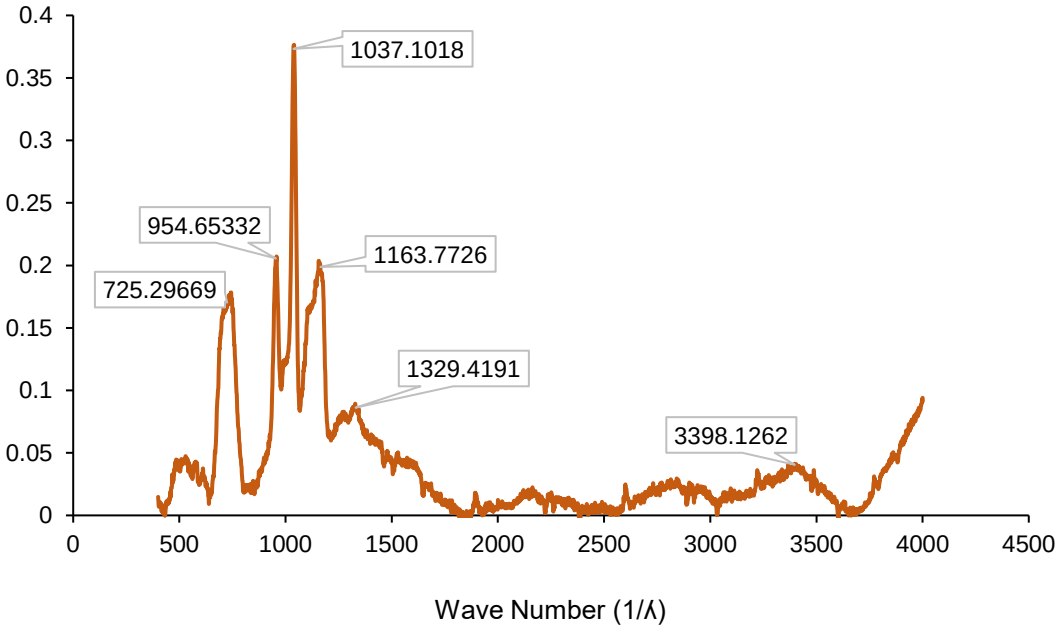

Figure 93. Raman spectroscopy for dynamic and dried when not in used P50Ca40Na10 glass.

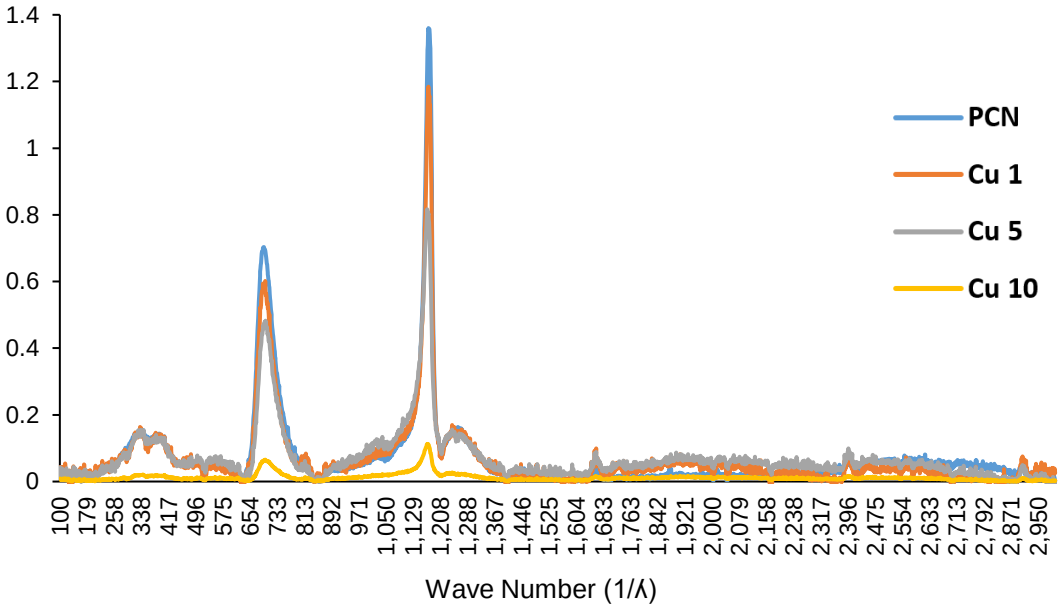

Figure 94. Raman spectroscopy for blank glass.

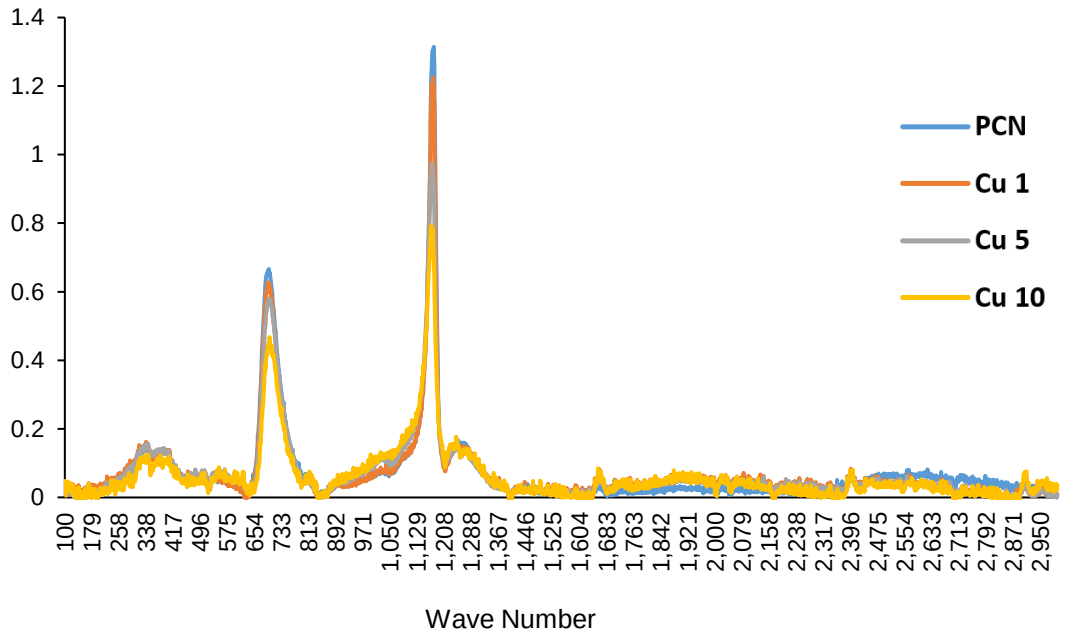

Figure 95. Raman spectroscopy for 3 day static immersed in DI glass.

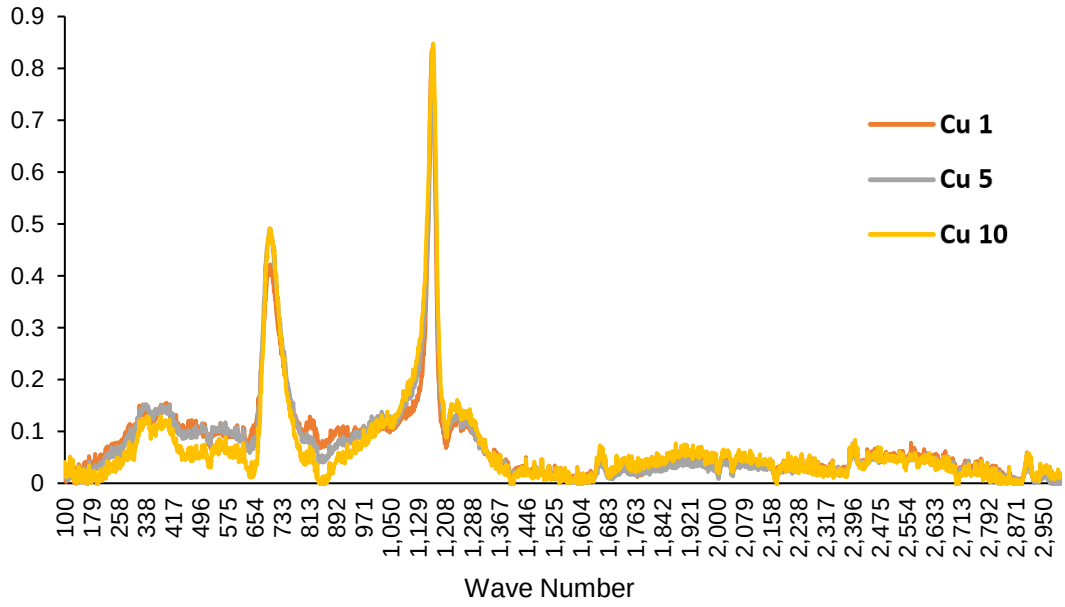

Figure 96. Raman spectroscopy for 7 day static immersed in DI glass.

P31 NMR Results

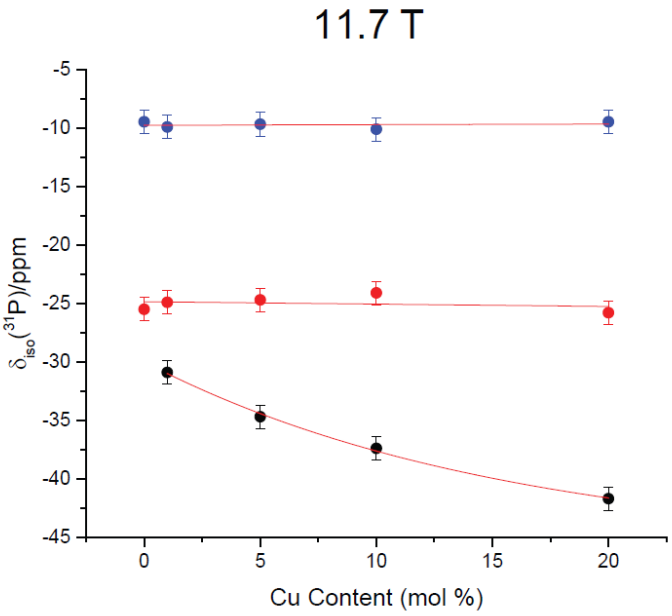

Figure 97. The change in chemical shift with increasing Cu content, $v_r = 20\ kHz, B_0 = 11.7\ T$.

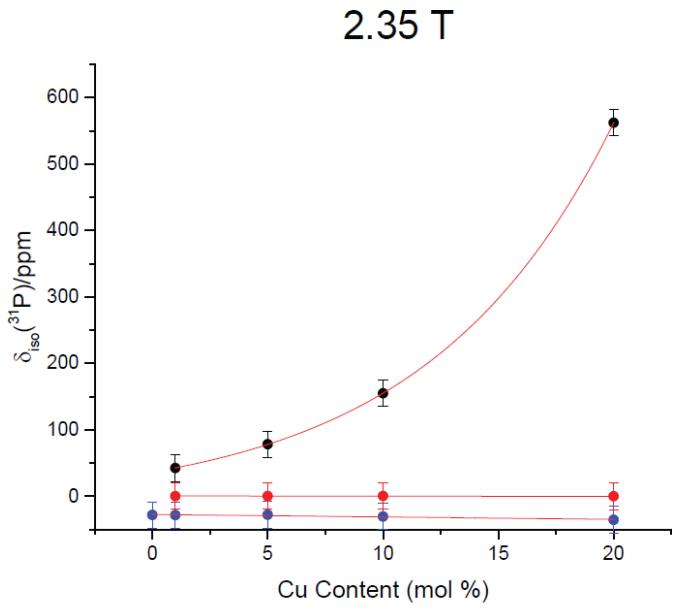

Figure 98. The change in chemical shift with increasing Cu content, $v_r = 60\ kHz, B_0 = 2.35\ T$.

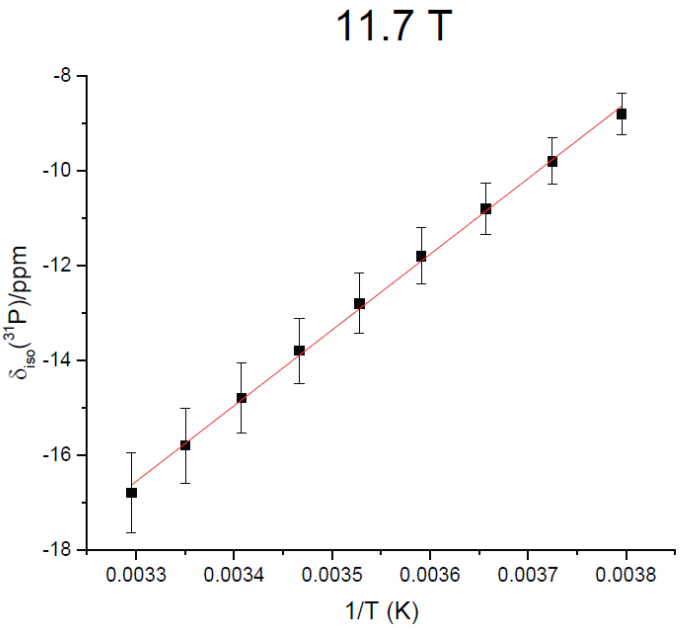

Figure 99. The change in chemical shift with increasing temperature, $v_r = 20\ kHz, B_0 = 11.7\ T$ for 20% Cu content.

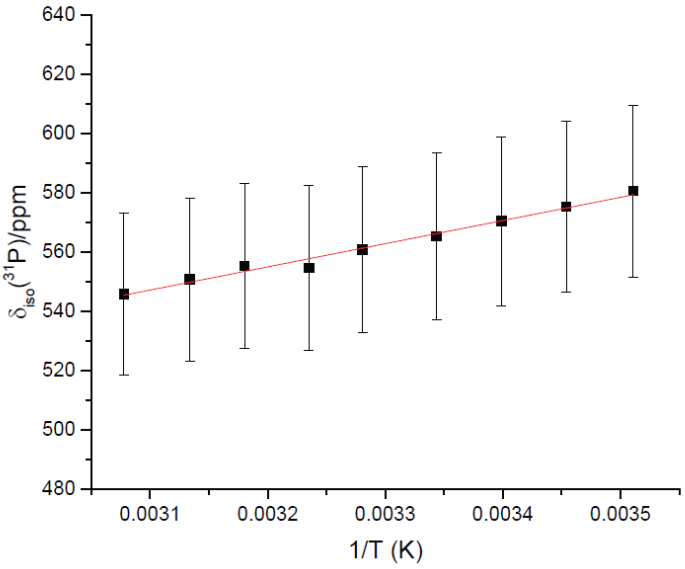

Figure 100. The change in chemical shift with increasing temperature, $v_r = 60\ kHz, B_0 = 2.35\ T$ for the broad component in 20% Cu.

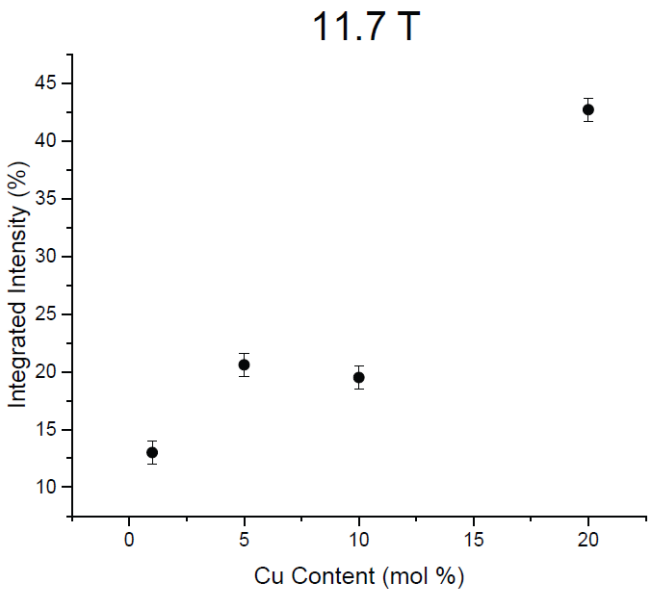

Figure 101. The change in integrated intensity (%) of the component at -30—40 ppm, $v_r = 20\ kHz, B_0 = 11.7\ T$.

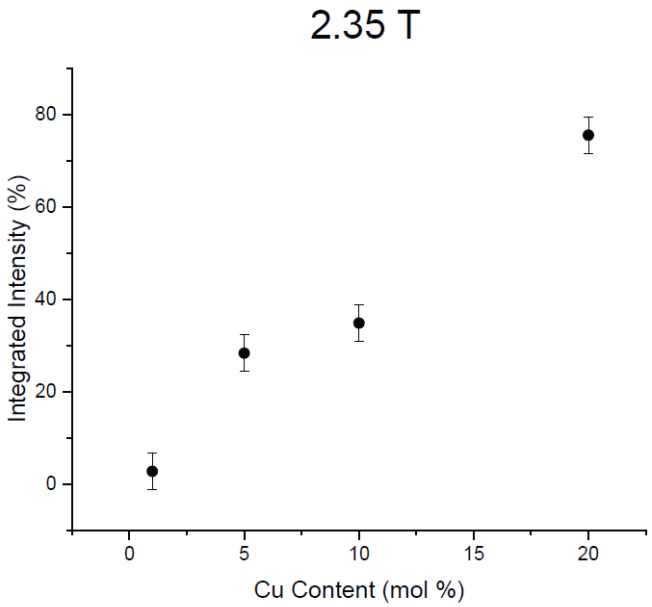

Figure 102. The change in integrated intensity (%) of the broad component at 100-600 ppm, $v_r = 60\ kHz, B_0 = 2.35\ T$.

Cation release of glass discs after 3 day static immersion test in DI for $50P_2O_5.10Na_2O.CaO.SrO$ composition.

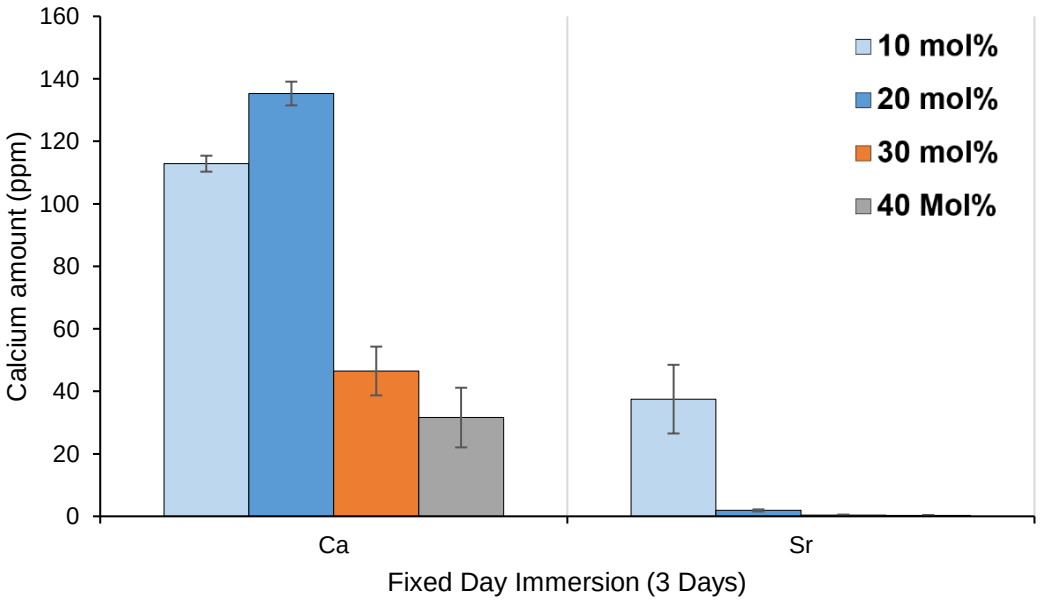

Figure 103. Calcium ion released after 3 day immersion in glass discs with either CaO or SrO.

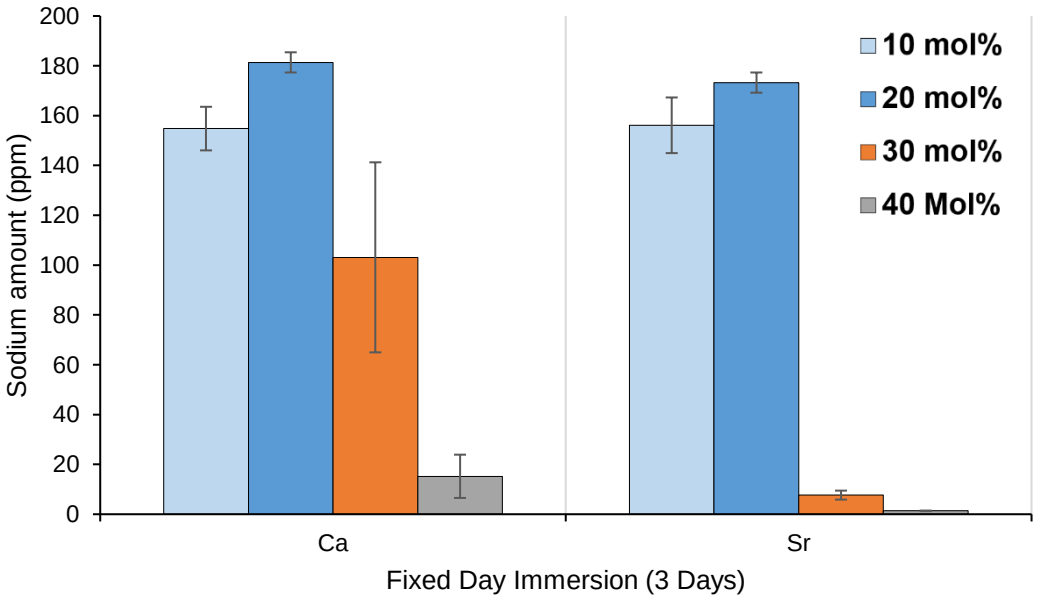

Figure 104. Sodium ion released after 3 day immersion in glass discs with either CaO or SrO.

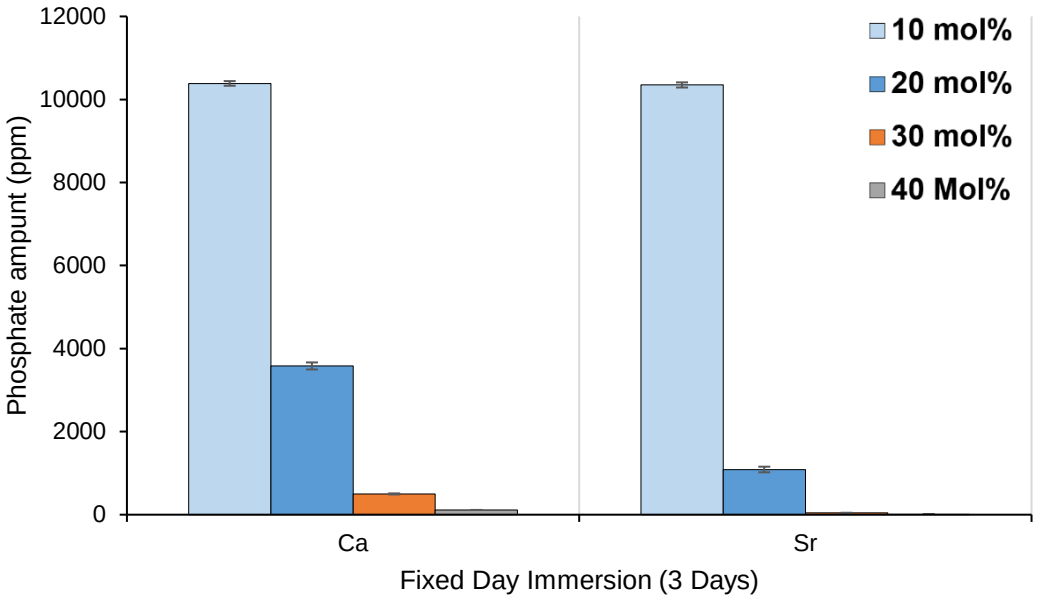

Figure 105. Phosphate ion released after 3 day immersion in glass discs with either CaO or SrO.

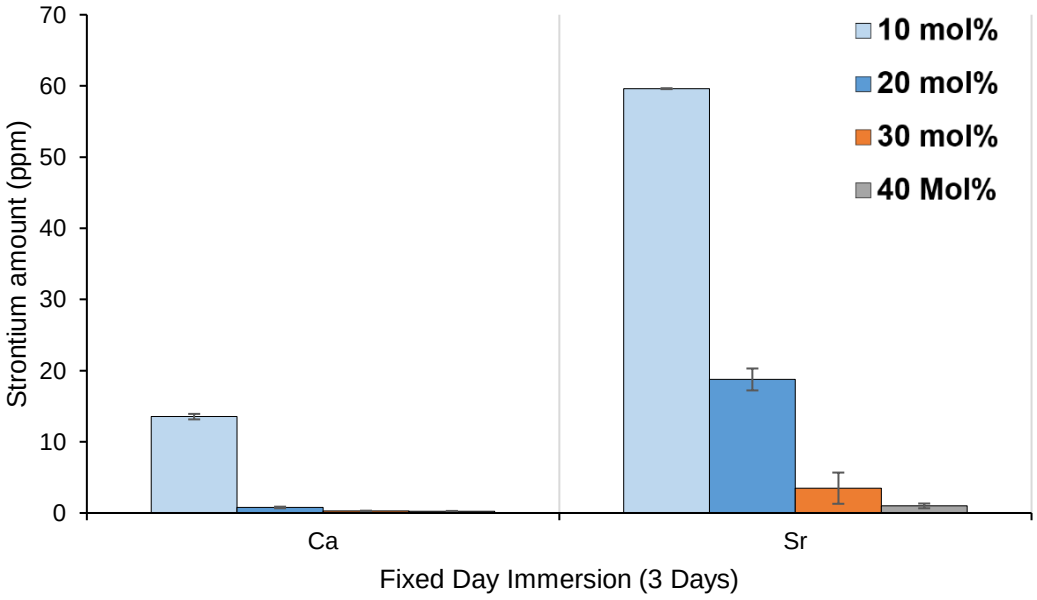

Figure 106. Strontium ion released after 3 day immersion in glass discs with either CaO or SrO.